AN ANALYSIS OF SMECTITE CLAY FRACTURE DENSITIES

AND HOW THEY AFFECT INFILTRATION

IN TRAVIS COUNTY, TEXAS 2004

THESIS

Presented to the Graduate Council
of Texas State University-San Marcos
in Partial Fulfillment
of the Requirements

for the Degree

Master of SCIENCE

by

Miriam Akselrod Scoulios, B.S.

San Marcos, Texas
May 2005

For my husband Tom,
who kept me sane and
always listened….even halfway across the globe

ACKNOWLEDGEMENTS

I would like to give my thanks to my husband Tom, my sister Sharon, brother Dan, and parents Gus and Ursula, for their support and encouragement throughout this long process.

I would like to thank my committee members for all their feedback and helpful pointers that made this project a success. I am especially grateful to Dr. Matthew Uliana. Without his foresight, guidance, ideas, and time, this project would not have become a reality. I would also like to thank Dr. Curran for her unfailing support and encouragement. And finally, I thank Dr. Earl for his wisdom and kind words.

I would also like to thank Vaughn Brock of the Brock Consulting Group and his Austin Community Foundation for their support. Without the use of this property, I would still be hunting for the perfect piece of land to conduct my experiments.

This manuscript was submitted on May 5, 2005.

TABLE OF CONTENTS

LIST OF TABLES

LIST OF FIGURES

CHAPTER 1

INTRODUCTION

Groundwater modeling of aquifers has been a top priority for water management officials for many years. These models are essential to sustainable management of the water resources in the future. One of the more difficult model parameters to quantify is the rate of recharge to the aquifer. Recharge is frequently controlled by soil types, and in areas covered by soils with high clay contents, the low-permeability of the soils can limit recharge. Clay soils can also impede the movement of contaminants, such as pesticides and runoff from pavements, into the subsurface.

Clay soils are common throughout Central Texas, including Travis County (Young 1977). In many parts of Travis County, the soils contain high amounts of smectite clays. This clay is known for its ability to absorb water and swell during rain events, creating an almost impermeable barrier above the aquifer. During dry times, however, this clay will shrink, creating fractures that become pathways into the ground. These cracks develop because shrinkage creates tensile forces acting in the horizontal plane (Baer and Anderson 1997). While it seems obvious that these fractures must affect infiltration and movement of contaminants in the soil zone, the degree to which these fractures affect infiltration has not been quantified.

The overall objective of this study is to determine the effects of desiccation fractures in high-smectite soils on infiltration rates. More specific objectives of this study are to develop methods for quantitatively characterizing fracture parameters (i.e., density, depth, aperture, and longevity), determine empirical correlations between fracture parameters and moisture contents, and measure infiltration rates at various moisture contents. This study focuses on clay soils in Travis County, Texas through a 6-month period covering the spring, summer, and fall months of 2004. I will develop a general relationship between soil moisture content and fracture development that will lead to a more quantitative understanding of recharge rates in clay soils in Central Texas.

Statement of Research Problem

Infiltration rates and recharge estimates are very difficult to quantify for use in groundwater models. This is especially true in areas like Travis County, Texas, where smectite clays can impede or expedite the flow of water into underlying aquifers. Clays absorb water like a sponge, causing the individual crystals to swell and restrict the movement of water through the clay layer Saturated clays create an impermeable barrier that impedes infiltration into the subsurface. Crack healing (mending) is a dynamic process that depends on the interaction of shear stress, temperature, fluid chemistry and initial geometry of the crack (Renard et al. 2000). Little or no infiltration because of closure means less recharge for the underlying aquifer. Unsaturated smectite clay layers act differently when saturated. Drying of clay layers creates desiccation fractures which can drastically increase permeability and infiltration rates to the subsurface. D'Astous et al. (1989) and Ruland et al. (1991) found that clay soils with fracture depths of 4-6 meters had hydraulic conductivity values 2 to 3 times greater in magnitude than unfractured clay soils. The difficulty arises when quantifying the magnitude of the effect that these fractures have on increasing recharge. This problem is critical for understanding infiltration recharge rates through smectitic soils. A better understanding of the relationship between fracture formation and infiltration rates in high-smectite soils will help modelers develop better and more realistic estimates of recharge, resulting in models that produce more effective management strategies in the future. At this date, the variability of infiltration rates in smectite clay soils has not been quantified.

The specific factors that can affect infiltration rates in smectite soils are fracture density (defined as the total length of fractures per unit area of soil), fracture depth, and fracture aperture (width). Clays containing only a few fractures will not support fluid flow. Connectivity of fractures promotes flow into the subsoil and aquifer, and the fracture density required to sustain advective flow is called the percolation threshold, which Vance (2004) calculated at 0.3 NL_F^2, where N is fracture density and L_F is equal to fracture length times $\pi/2$. Once this threshold is exceeded, water flows through these fractures unimpeded. Fracture aperture is also an important variable. Apertures are very difficult to measure in the field because they are very sensitive to disturbance. There are ways to indirectly measure apertures based on the hydraulic conductivity and fracture spacing (McKay, Cherry, and Gillham 1993). Hydraulic conductivity is measured using piezometers, which monitor pore water head. Measuring fracture spacing occurs by counting each fracture and measuring the distance between each fracture. The drawback to this method is that tiny fractures can be overlooked and not counted.

The depths of fracture penetration are another important aspect of these fractures that will be studied. The depth to which these clay fractures penetrate varies depending on thickness of the clay, hydraulic gradient, and diffusion properties of the clayey soil (Harrison, Sudicky, and Cherry 1992). Smectite clay has a low permeability and a high absorption capacity that slows the travel time of water and contaminants into the subsurface. In effect, saturated clay soils protect the underlying aquifer from contamination originating at the soil surface (Oostindie and Bronswijk 1994). Fractures fully penetrating the clay layer can act as conduits for flow, enabling vertical migration of contaminants to an underlying aquifer (McKay, Cherry, and Gillham 1993). Thus, clay soils filled with deep fractures lose the ability to protect against water contamination. Establishing the maximum depth at which these fractures exist can help determine more accurate rates of infiltration and contaminant transport. The depth of these fissures is particularly important west of the Balcones Escarpment where the depth to highly permeable bedrock is often less than one meter (Soil Conservation Service 1974).

Theoretical Framework

Clays are members of the phyllosilicate family of minerals, consisting of layers in which planes of oxygen atoms coordinate to cations like Si^{2+}, Al^{3+}, Mg^{2+}, Fe^{2+}, and Fe^{3+} to form two-dimensional sheets (Kloprogge, Komarneni, and Amonette 1999). The substitution of these cations between sheets leads to charge imbalances on the surface of the layers. This results in high total porosity, but low effective porosity which determines the maximum amount of fluid flow through a soil. One method to calculate porous media flow is thorough the use of Darcy's law. For this law, flow is considered to be macroscopic and is written as:

$$Q = KA\frac{dh}{dl} \qquad (1)$$

where Q is volumetric discharge, $\frac{dh}{dl}$ is hydraulic gradient, K is the hydraulic conductivity, and A is the cross-sectional area (Mesri and Olson 1971). The hydraulic conductivity (K) describes the relationship between total discharge of a fluid and the hydraulic gradient. This method is macroscopic because it is primarily used to determine flow over large areas, such as in an aquifer. This law is not necessarily suitable for media with very low values of hydraulic gradient in low permeability materials, such as clays (Lamont-Doherty Earth Observatory 2003).

Swelling clay soils are characterized by two subsystems of cracks: seasonal or interblock cracks, which widen significantly in the summer months, and intrablock or capillary cracks with widths in the micrometers that do not vary from season to season (Chertkov and Ravina 2001, 1245). One method of calculating fluid flow through both types of cracks is the cubic law. This law states that the magnitude of flow through local fracture voids is proportional to the cube of the local aperture (Brush and Thomson 2003, SBH 5-2). Even so, the cubic law assumes flow to be laminar, as if flowing through two smooth plates. Unfortunately, fractures do not necessarily behave as smooth plates, so the cubic law in not always appropriate.

According to Brush and Thomson (2003) and Oron and Berkowitz (1998) another method for characterizing flow through fractures is the Navier-Stokes equation. This mathematical model describes complex flow behavior, taking into account tortuosity of flow, differing aperture widths, and roughness of a crack wall. This is especially useful when identifying flow paths at the local scale because fracture walls exhibit more complexity locally than globally.

In addition to flow through primary pores, shrinkage and cracking of clay creates conduits for water flow into the subsurface. Most of the water penetrating a typical clay layer flows through fractures created by desiccation, and rates of infiltration and flow through these fractures are dependent upon fracture density per unit area at the surface, fracture apertures, and fracture depths. Smectite clays have four distinct shrinkage phases: (1) structural shrinkage where saturated soil dries without a change in volume, (2) normal shrinkage where water loss is equal to variations in volume, (3) residual shrinkage where the variation in volume is less than the water loss and air penetrates the aggregate, and (4) zero shrinkage when the soil particles reach their maximum configuration density (Haines 1923; Keen 1931; Stirk 1954). The isotropic geometry of a cube of clay soil can be described mathematically. Bronswijk (1991, 1221) determined the soil profile crack volume per area (V_{cr}) from measurements of vertical soil movement.

$$v_{cr} = \Delta v - \Delta z \qquad (2)$$

and

$$\Delta v = [1 - (1 - \frac{\Delta z}{z})^{r_s}]z \qquad (3)$$

where v_{cr} is crack volume per unit area; Δv is the change in soil volume per unit area; Δz is change in soil layer thickness; z is the fully swollen soil layer thickness; and r_s is a dimensionless geometry factor. For an isotropic shrinkage, r_s is set at 3. Yule and Ritchie (1980, 1287) simplified this equation and included structural shrinkage in their analysis and suggested:

$$\Delta v = 3\Delta z - 3\frac{\Delta z^2}{z} \qquad (4)$$

and

$$\Delta W = S + \Delta v \qquad (5)$$

where S is the water loss in the structural shrinkage phase. In order to include residual, zero, and anisoptropic shrinkage, these equations were extended to (Bronswijk 1991, 1221):

$$\Delta w = S + \Delta v + \frac{[e(\vartheta]z}{1 + e_s} \qquad (6)$$

where v is now moisture ratio; $e(\vartheta)$ is void ratio at moisture ratio v; and e_s is saturated void ratio.

These equations explain the process of shrinking in a quantitative way that takes the phase of shrinkage into account. The shrinkage geometry theory is important because correctly quantifying the volume of clay fractures depends on using the most precise information available. Used together with equations 2-6, these theories give the most complete picture on how fracture densities and depth affect infiltration through a clay layer.

Connections to the Problem Statement

All these variables, such as density, aperture width, fracture depth, and grain size distribution, are important in some respect to understanding the mechanics of infiltration through smectite clay. However, there is still considerable uncertainty concerning which of these variables has the most significant control on infiltration and flow. This study will provide a more detailed picture of how fractures develop and how they control infiltration through clay soils.

Literature Review

Geomorphology of Field Site

The field site is located in the Blackland Prairie District of the western Gulf of Mexico Section of the Atlantic and Gulf Coastal Plain Physiographic Province (Fenneman 1938). The site is underlain by the Taylor Marl and the Navarro Group which were deposited in the late Cretaceous (Young 1977). The Taylor Marl is made up of the Bergstrom Clay, the Pecan Gap Chalk, and the Sprinkle Clay and is about 213 meters (700 feet) thick.

The Kemp Clay and Corsicana Marl make up the Navarro Group with a total thickness of 152 meters (500 feet) (Soil Conservation Service 1974). These beds consist of calcareous clays, chalky marls, and silty clays.

The climate of this area is on the drier, subhumid margin of the humid subtropical climate region (Koppen Cfa) and has a bimodal precipitation regime. Koppen refers to Wladimir Köppen a German botanist who created the Köppen system of classification for the climates of the Earth. The "C" in Cfa represents the "mild mid-latitude" category, the letter "f" stands for moist from the German word feucht, and the third letter "a" signifies that the average temperature of the warmest month is above 22°C (72°F) (Rosenberg 2005). Maximum precipitation falls in the early spring and early fall. Minimum precipitation falls during the height of summer (August) (US National Climate Data Center 2004). The following table depicts the 1971-2000 average precipitation and temperatures for Austin.

Table 1. Temperature and Precipitation of Travis County in 2003

Month	**Average Precipitation**		**Average Temperature**	
	Inches	mm	°F	°C
January	1.89	10.1	50.2	48
February	1.99	12.6	54.6	51
March	2.15	16.5	61.7	55
April	2.51	20.2	68.3	64
May	5.09	23.9	75.1	129
June	3.81	27.2	81.0	97
July	1.95	29.0	84.2	50
August	2.31	29.2	84.5	59
September	2.91	26.4	79.5	74
October	3.97	21.4	70.6	101
November	2.68	15.4	59.7	68
December	2.44	11.2	52.1	62
Total	33.70	20.3	68.5	856

Source: US National Climate Data Center 2004

Soils at the site are mapped and classified as Houston Black clay, Lewisville silty clay, and Burleson gravelly clay (Soil Conservation Service 1974). The Houston Black series consists of deep, moderately drained clay soils. The type found at the field site has slopes of 1 to 5 percent. The moderate slope means that erosion is moderately severe, but the soils can be suited to farming if erosion controls are established (Soil Conservation Service 1974). The addition or subtraction of water can cause these clays to swell or shrink, causing large changes in volume. This volume change can cause large amounts of damage to structures built on or with this type of soil because of the shrink-swell potential inherent in this soil. The Houston Black clay also tends to have pH values that limit the types of vegetation.

The Lewisville series consists of gently sloping, well-drained, silty clays (Soil Conservation Service 1974). With moderate permeability, the soils can be easily plowed and have a high water capacity. The soils found at the field site have 1 to 2 percent slopes, with the soil thickness measuring 58 to 71 centimeters (23 to 28 inches). Erosion can be moderate, but the soil is suited to farming for hay or as improved pasture. The Lewisville silty clay also has high shrink-swell potential, and is not suitable for construction.

The Burleson series consists of deep, moderately drained clay soils (Soil Conservation Service 1974). The color profile of this series is dark gray at the surface, to a grayish brown, and a yellowish brown at 152 centimeters (60 inches) of depth. The soil at the field site is Burleson gravelly clay with gravel making up 40 percent of the surface layer. This soil is suited for range or improved pasture. The shrink-swell potential of this soil is high as well, so construction is not recommended. The following table shows the classification of these soils in relation to some of the other soil series found in the county.

Table 2. Classification of Soil Series

Series	Family	Subgroup	Order
Austin	Fine-silty, carbonatic, thermic	Typic Calciustolls	Mollisols
Bergstrom	Fine-silty, mixed, thermic	Cumulic Haplustolls	Mollisols
Burleson	**Fine, montmorillonitic, thermic**	**Udic Pellusterts**	**Vertisols**
Dougherty	Loamy, mixed, thermic	Arenic Haplustolls	Alfisols
Houston Black	**Fine, montmorillonitic, thermic**	**Udic Pellusterts**	**Vertisols**
Lewisville	**Fine-silty, carbonatic, thermic**	**Typic Haplustolls**	**Mollisols**
Miller	Fine, mixed, thermic	Vertic Haplustolls	Mollisols
Travis	Fine, mixed, thermic	Ultic Paleustalfs	Alfistols
Volente	Fine, mixed, thermic	Pachic Haplustolls	Mollisols

Source: Soil Conservation Service 1974

The vegetation at the field site is classified as Live Oak, Mesquite, and Ashe Juniper Parks (savannah) (McMahon, Fry, and Brown 1984). This type of vegetation is found on level or gently rolling uplands and also on the Edwards Plateau. These hardy plants are well suited for growth in the shrink swell soils found at the site.

Trends in Area of Interest

The infiltration rates of different types of fractures have been studied to see how they affect water flow in soils (Beven and Germann 1982; Zhou 2001; Snow 1969). All types of fractures were shown to contribute to infiltration into the subsoil with some having larger rates of infiltration than others. For instance, those fractures not dependent on the degree of saturation (such as granite fractures) tended to have greater infiltration rates because they do not swell shut over a period of time (Bouma et al. 1977). These studies are important because differences in infiltration rates will affect the recharge rate of an aquifer.

Transport of contaminants through subsurface clay fractures has been investigated to see how fractures that are not visible on the ground may affect groundwater contamination. Harrison, Sudicky, and Cherry (1992, 525) investigated how contaminants from a waste disposal site were found in the underlying aquifer despite the presence of a clay lining with no evidence of fracturing. They found that a few, fully penetrating, vertical fractures provided flow for contaminants when the fracture apertures had a minimum width of 10 μm. The results agree with previous studies conducted by D'Astous et al. (1989) and Ruland, Cherry, and Feenstra (1991) in showing that fractures typically penetrate below the superficial weathered zone. Clay liners do not fully protect the subsoil from contamination, and fractures do not need to be visible in order to transmit contaminants to an aquifer.

Tracking evaporation rates from clay fractures has also been a subject of previous research, particularly in the farming and ranching industries. Crop type has a significant impact on evaporation rates, as does the width of clay cracks at the surface (Adams and Hanks 1964). These studies confirm the earlier findings of Holmes, Greacen, and Gurr (1960) and Johnston and Hill (1945).

All these studies improve upon the research already conducted concerning the effects of clay soil on fracture formation and development, contaminant flow, and crop growth;

however, none of the above studies cover the issue of fracture characteristics and flow rates through factures. This research will quantify water flow through smectite fractures and identify which fracture characteristics are important for infiltration through this type of clay.

Review of the Literature

Other studies focused on infiltration through clay soils, more specifically how water flows through fractures (Blake, Schlichting, and Zimmermann 1973; Bouma and Dekker 1978; Bouma et al. 1977; Bouma, Jongerius, and Schoonderbeek 1979; Bouma and Wösten 1979; Ritchie, Kissel, and Burnett 1972). Some of these studies determined water movement by using chemical tracers (dyes) to track flow patterns. Bouma, Jongerius, and Schoonderbeek (1979) and Blake, Schlichting, and Zimmermann (1973) found that tracers were most prevalent on the sides of the large cracks at depth and at the boundary between cracked clay and an undisturbed clay layer. These results show that fractures are a major path for flow through clays, and also give information on flow movement between large and small cracks. Bouma and Dekker (1978) agree, noting that most water flows through large (>2mm) vertical pores. These studies greatly increase the knowledge about how water flows through clay cracks, but the inherent methodology of these studies disturb the soil, increasing the chance for error. With this in mind, Bouma and Wösten (1979) used chloride breakthrough curves to identify pore continuity patterns and to show that only a fraction of the soil volume is used as water flows through fractures. This technique not only defines the pattern of flow but does so in a nondestructive way.

Early studies used soil cores to determine water movement through fractures.

Hydraulic conductivity (flow) through the cores was measured in the lab and the results extrapolated to the field setting (van Schilfgaarde 1970). Taking soil cores can lead to large errors during analysis because of edge effects and other disturbances inherent in taking a core out of the ground (Ritchie, Kissel, and Burnett 1972). Mason, Lutz, and Petersen (1957) found that hydraulic conductivities varied so much that conductivities obtained from five core samples could be placed into each of three classes: slow, moderate, and fast, with a 95 percent probability of being correct. The effectiveness of using soil cores in determining flow through fractures has questionable value and subsequent studies have used in-situ field experiments in order to reduce errors (McKay, Cherry, and Gillham 1993; Reynolds et al. 2000).

Fracture aperture (width) is an important variable that has not received much attention. According to McKay, Cherry, and Gillham (1993, 1149), fracture apertures are very hard to measure in the field because they are very sensitive to disturbance. An early method of measuring apertures was based on fluid flow between two smooth plates, using the cubic law to calculate fracture aperture indirectly (Snow 1969, 1275). The major drawback to this method is that it assumes a constant fracture width and roughness with depth. Brown (1987) and Tsang (1984) suggested models that include width and roughness variability into flow representations, but a lack of data has hampered their efforts. D'Astous et al. (1989, 51) used tracer tests and the Navier-Stokes equation to calculate values for fracture apertures of 0.026mm and 0.032mm in the weathered zones of the Sarnia Clay Plain in Ontario, Canada. Their method was replicated in Mexico City by Rudolf, Cherry, and Farvolden (1991) and showed agreement with the previous study. While these two studies show that measuring fracture aperture is not impossible, many studies still use a spatially uniform value for the sake of simplicity (Harrison, Sudicky, and Cherry 1992).

Fracture depth and density have been examined to a limited extent. McKay, Cherry, and Gillham (1993, 1153) and Ruland, Cherry, and Feenstra (1991, 406) used test pits to determine both depth and density of fractures. Density was calculated by counting the number of fractures intersecting a horizontal mapping line. Depth of fractures has not been as widely studied, but Moriari and Knisel (1997) calculated the depths of fractures by adding together the thickness of the cracked layers to reach an estimated depth. Depth was also measured by direct observation of vertical fractures. There are inherent weaknesses in measuring the fracture characteristics using trenches. First, digging trenches disturbs the soil layers and can collapse small fractures, increasing the chance of omitting some fractures. Second, smearing of clay along the trench wall is unavoidable and disturbs the original fracture face, creating the need to remove this smeared clay by hand. Third, the test pits might not reach the full depth of the fractures so depth data may be incorrect. D'Astous et al. (1989, 46?) found the depth of fractures using tritium tracers while investigating the age of modern groundwater. Piezometers analyzed high levels of tritium in subsoil deposits, which indicate where the fractures ended and the water penetrates the matrix. This technique is superior to the previous one because it does not disturb the soil. Unfortunately, it does not confirm that all fractures in the test area were part of the flow, so errors in measuring depth are possible.

Other research used models to predict flow through fracturing clay soils. These models were developed using the GLEAMS-CF code, the FLOCR code, and the FLOWEX code. They assess the effects of changes in water management on a number of soil utilization properties (Bronswijk 1988, 199). For instance, most models consider the soil as a porous, homogenous medium and adopt Darcy's equation to describe moisture flow (Morari and Knisel 1997). To correct this error, the GLEAMS (Groundwater Loading Effects of Agricultural Management Systems) code was modified to simulate the movement of water and solutes through cracks. Morari and Knisel (1997) found that the modified code, GLEAMS-CF, did a reasonable job predicting macropore flow through cracking clays. Prior to this experiment, only a few models considered macropore flow in cracking clays. One such previous model, used by Bouma and de Laat (1981), accounted for the effects of cracks on infiltration by reducing the rainfall that infiltrates into the matrix by 10-20 percent, according to the time of year. Unfortunately, this technique was never validated with field results. Hoogmoed and Bouma (1980) combined two existing models to predict vertical and horizontal infiltration into cracked clay soil. Their model reliably predicted short circuiting (preferential movement of free water) and found that it increased with higher initial soil moisture content and that vertical infiltration was more important than horizontal infiltration (Bouma and Dekker 1978). Another type of simulation code, FLOCR (FLOw in CRacking soils), computes unsaturated vertical water flow in cracking clay soils. Oostindie and Bronswijk (1994) used this model to determine residence times of contaminants in the unsaturated zones of cracking clay soils. A major weakness of this model is the difficulty in validating the results. Validation for the model requires long-term monitoring of water transport that is usually not feasible for most studies. Bronswijk (1991) adapted the simulation code FLOWEX (transient moisture flow in soils) to model water balance, cracking, and subsidence of clay soils. This model satisfactorily calculated subsidence and cracking, but due to limitations in the model, agreement between field measurements and model calculations of top layer wetness were not accurate. Another weakness is that it assumed soil volume change to be isotropic, which is disputed by Baer and Anderson (1997). Even with their weaknesses, these models are a vital component in measuring infiltration through clay fractures because they can be used to predict future rates of flow and changes in clay layers.

Research Method to Operationalize Problem Statement

Hypotheses

Central Texas has a growing population with an insatiable appetite for the shrinking stores of water in its aquifers. Water resource managers use models to monitor groundwater availability. In order to provide the most accurate information, these models need accurate and precise recharge inputs that distinguish between the different soil properties found in the recharge zones. My study will look at how fracture characteristics affect infiltration into the subsurface. In particular

> Which fracture characteristics affect infiltration rates the most?
>
> What is the minimum level of desiccation needed to promote smectite clay fracture growth?
>
> What mixture of sand, silt, or pebbles will alter the time smectite clay takes to form fractures?
>
> How long will it take for the test area to reach maximum fracture density?

Because my research is quantitative in nature, I will need to analyze the data statistically. Using multiple linear regression, my statistical null hypothesis is:

> Smectite clay fracture characteristics do not affect infiltration rates into the subsoil.

The questions I present here are the focus for my study. I hope to provide the information necessary for groundwater models to accurately portray infiltration through smectite clays in Travis County, Texas. In order to accomplish this goal, I have acquired permission to use a parcel of land in Travis County, Texas to collect my research data.

Field Site and Spatial Management

The field site for my study is in South Austin, one mile east of IH-35 and one-half mile south of Highway 71 (Figure 1).

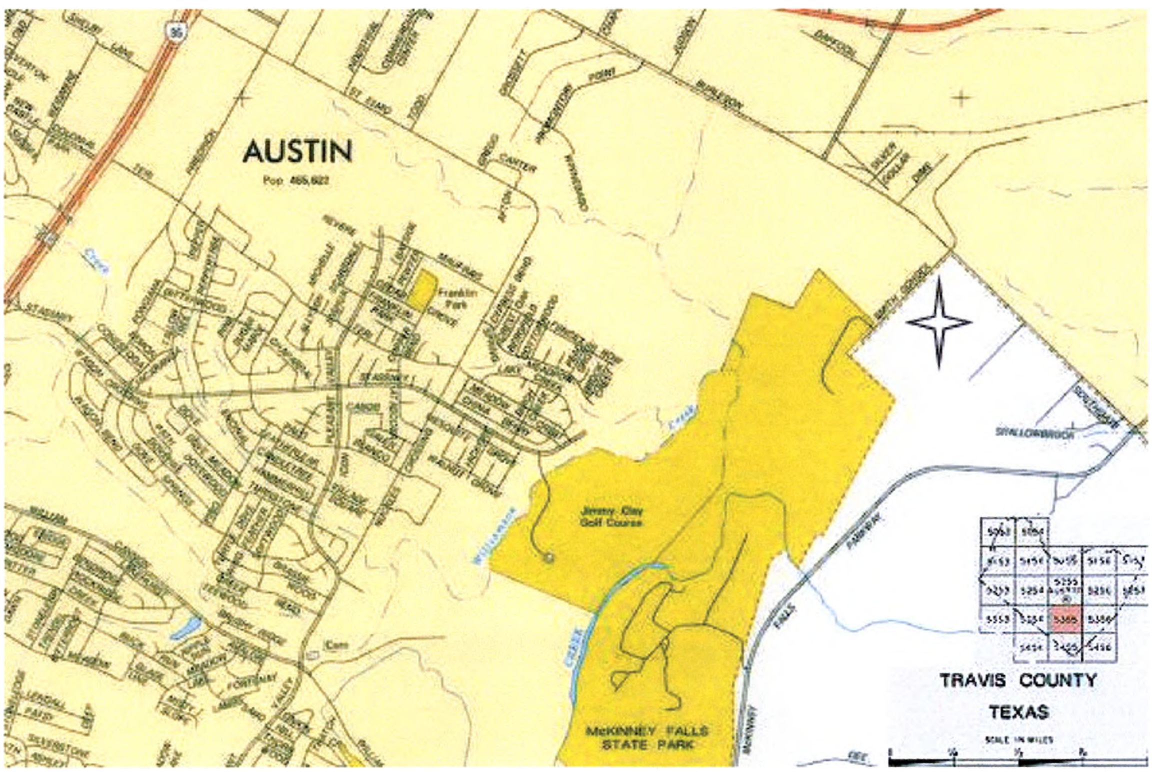

Figure 1. Location of Field Site in Travis County, Texas
Source: Texas Department of Transportation 1996

The property is an undeveloped plot covering ten acres. I chose this site for my study because it is a good representation of the high smectite clay soils typically found in central Texas. The north side of the property is composed of a grassy, high area with little change in elevation. This area gives way to a ravine area containing a stream that bisects the land in an East-West direction. This ravine area houses a large intermittent wetland area to the south of the actual stream. East of the wetland area is a region that is slightly higher in elevation, has a greater variety of vegetation present, and more hummocky soils. To the south of the wetland region is a large expanse of upper slope grassy area. This area differs slightly from the northern section. It has more relief, sporadic pockets of dense vegetation, and exhibits greater fracture density. Each of these soil regions can be found in many parts of central Texas. I chose sampling sites that encompass the range of variable conditions in the study area (Figure 2).

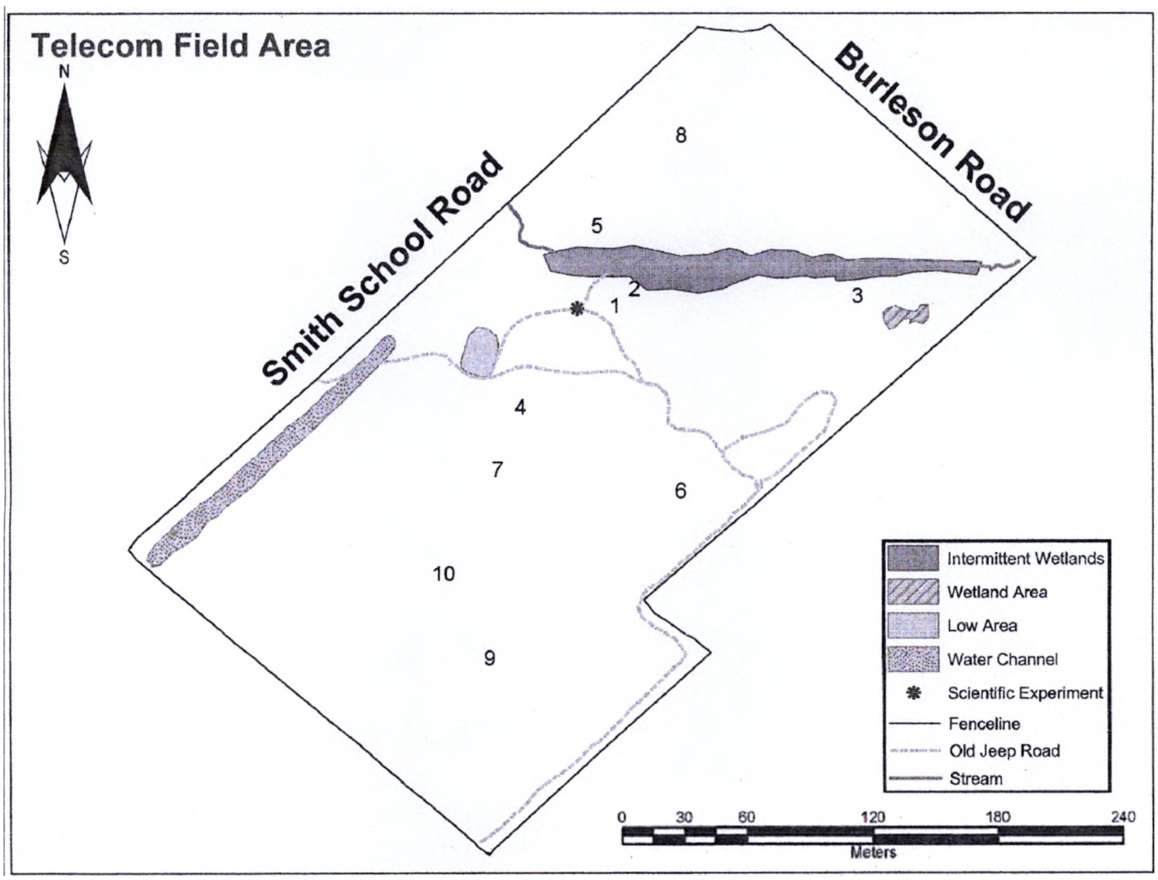

Figure 2. Location of Individual Sites

I chose ten plots based on land and soil characteristics including slope, amount of vegetation, and the amount of sand or limestone grains mixed into the clay layer. I chose various surface slope angles to determine if clay fracture development depends on slope. Slight changes in the soil characteristics can influence the shrink and swell potential of a clay layer, so testing an assortment of compositions will give more information about fracture growth potential. Detailed characteristics of the individual sample plots are given in Table 3.

Table 3. Description of Individual Field Sites

Site Number	Color	Vegetation	Observed Soil Composition	Slope
One	Light brown/tan	None	Clays	0
Two	Black	None	Clays	0
Three	Dark brown	Mesquite	Organics/Clays/Gravel	1-5%
Four	Light brown	Tall grasses	Clays/Gravel	1-5%
Five	Black/dark grey	Ashe Juniper	Clay/Silt	5-10%
Six	Brown	Mesquite/Grass	Clays/Gravel	1-5%
Seven	Grey to brown	Tall grasses	Clays/Gravel	1-5%
Eight	Dark brown	Tall grasses	Clay	1-5%
Nine	Dark brown	Tall grasses	Clay/Silt	1-5%
Ten	Grey to light tan	Tall grasses	Clay/Silt	1-5%

Temporal Framework

My study took place between April and September of 2004. As stated earlier, the field site experiences a bimodal precipitation regime. These extremes in both temperature and precipitation provided a broad range of conditions for studying fracture growth and fluid flow through these fractures. For a 12-week period, I sampled each plot once a week, and after each storm that generated more than 2.54 centimeters (one inch) of rain (Baer and Anderson 1997; Blake, Schlichting, and Zimmermann 1973; Bronswijk 1991; Jamison and Thompson 1967).

I expect to find that soil moisture content is the dominant independent parameter controlling smectite clay fracture growth. I also believe that aperture width and fracture depth will correlate with each other, such that fractures with the greatest aperture widths will also be the deepest fractures. I also anticipate that maximum infiltration through these fractures will occur when the fractures are at peak growth, during a summer rainstorm, before the clay has a chance to begin swelling. This study will try to determine which soil characteristics and fracture properties have the greatest affect on infiltration through smectite clay fractures.

CHAPTER 2

PROCEDURES FOR DATA ANALYSIS

Every week for five months I performed a variety of procedures to measure fracture density, aperture width, fracture depth, grain size distribution, and infiltration. Each experiment had several parts until an end result was reached. Some of these steps did not produce reliable information in the early stages of the project and were subsequently discarded. Other methods were used in multiple experiments, producing reliable and useful results. The next few pages outline each step of each procedure.

Fracture Density and Aperture Data

Measuring fracture density is a main component of my project. The first step in acquiring these data consisted of taking a digital photo of the site each week. These pictures included a numbered card with a small ruler for matching the picture to the correct site and for establishing scale.

Figure 3. Example of Numbered Card with Ruler

I used a digital camera set to take 2048 by 1536 pixel photos at a resolution of 72 dpi in jpeg format. This resolution allowed me to view fractures down to apertures of less than 0.5 mm. Each week I took between two and four pictures of the sites and then downloaded the images onto my computer. Next, I imported the best picture of each site into the graphic software program Macromedia Freehand 10. This program was used to digitize the fracture traces in the photos.

After importing the image into Macromedia Freehand 10, I set the image scale by zooming in on the ruler in the image, drawing a line along the length of the scale with the pen tool, recording the length at the bottom of the image, and locking the line into a separate layer within the software program. Next, I defined an area of the photo that contained visible fractures and that would serve as the analysis area. Next, a grid was superimposed over the image, separating the image into individual squares. I then used the pen tool to outline the analysis area using the grid as a guide to define an area that is free of vegetation and that clearly shows the fractures. Once this analysis area was defined, I recorded the number of squares in the area and locked the layer. A third layer in the program was used to trace fractures. Within this layer, I zoomed into the image until I could see an adequate amount of detail without compromising the resolution of the fractures. I traced each fracture using the pen tool, creating short, straight line segments that define the center-line of the fractures. Once each fracture within the analysis area was traced, I locked the layer.

After locking this layer, I traced aperture widths in a separate layer. I drew several scanlines across the photo, and zoomed in on the photo until I reached the closest view without compromising the resolution. I then used the pen tool to draw short, straight line segments perpendicular to the walls of each fracture at each point where the fracture intersected a scanline. Once all fracture apertures at scanline intersections were traced, I locked this layer and prepared the file for export.

After these steps were completed, I exported each layer as an Encapsulated Post Script (EPS) file. First, I locked all the layers, and then unlocked the layer containing the scale. I selected the scale line, selected Export as EPS format, and saved the file. I repeated this process with the fracture trace layer and with the aperture trace layer, so that I ended up with three separate files containing the scale, fracture trace, and aperture trace data. These exported files could now be imported into Microsoft Excel for analysis.

I acquired a template for Microsoft Excel that enabled me to import the data from these layers and calculate fracture density and fracture aperture distribution at each site for each day I took a photo. I opened the Scale layer in a text editor (Microsoft Wordpad) and copied the x-y coordinates of the scale line into the spreadsheet. The spreadsheet used the length of this line to determine the image scale, and then used the scale and the total number of grid squares in the analysis area to determine the total area of the analysis area. Next, I opened my fracture trace file in a text editor, deleted everything but the x-y coordinates of my fracture tracings, and saved this file as a text file. I then opened this new text file in Microsoft Excel, copied it into the new spreadsheet, and formatted and filtered the raw data so that I was left with the x,y coordinates that define each line segment tracing the fractures. These x,y coordinates are made up of fractures composed of a series of straight-line segments defined by nodal points. For example, line segment AB is defined by points A and B which are composed of coordinates $x_1 y_1$ and $x_2 y_2$, respectively. The line segment length, L, is:

$$L = \sqrt{(\Delta x)^2 + (\Delta y)^2} \qquad (7)$$

where $\Delta x = x_2 - x_1$ and $\Delta y = y_2 - y_1$. The tangent of angle a is equal to the length of the opposite side (Δx) divided by the length of the adjacent side (Δy), so:

$$\alpha = \left(\frac{|\Delta x|}{|\Delta y|} \right) \qquad (8)$$

where $\alpha = 0$ if $x_1 = x_2$, and, if $y_1 = y_2$, then $\alpha = 90$. Angle Q represents the azimuth orientation of the fracture trace from 0 to 179 degrees and is calculated as Q=90-a (when $y_1 < y_2$), Q=90+a (when $y_1 > y_2$), or Q=a (when $x_1 = x_2$ and $y_1 = y_2$). The total length of the fracture trace is represented by the length L. This process determined the length of the line segments, added these segments together, and divided the total length by the total analysis area as specified by the x-y coordinates of the scale. The result is a single fracture density value that characterizes the overall density of fractures in the image. The aperture data were also imported into the same Excel workbook and processed so that the length of each aperture line was calculated. A frequency histogram of all fracture apertures was created in the same Excel workbook.

I also used manual methods to calculate aperture width. At the field site, I placed two perpendicular scanlines across the site. I measured the aperture width of each fracture that crossed each scanline using a ruler with millimeter marks. I recorded my observations and later transcribed the data into the appropriate Excel workbook. These data were compared to the data calculated by the Excel spreadsheet. If the data acquired manually was not similar, I discarded the results. If the data was comparable, I incorporated the manually acquired data with the computed data and incorporated those data into the frequency histogram.

Fracture Depth Data

Fracture depth is probably the most difficult variable to acquire. No matter which method is used, disturbance of the fracture is a real possibility. I measured fracture depth two different ways. The first procedure consisted of measuring fracture depth in situ at each field site. I began by laying out two perpendicular scanlines across each plot. After measuring the aperture widths of those fractures that intersected the plumb line, I measured the depths of these same fractures. I inserted a thin, straight rod into the fracture. As soon as I felt resistance, I stopped pushing the rod down. I drew a tick mark on the rod with a marker at the point where the rod was level with the ground, and then withdrew the rod and measured the length that was inserted into the fracture.

The second method was done in the laboratory. First, I extracted a 0.4 m by 0.25 m by 0.2 m thick piece of intact soil from a location between plots 01 and 02 at the field site and placed the piece intact into a clear plastic container with several small drain holes at the bottom of the container. I brought this container back to the lab, saturated the soil, and placed a 120-watt heat lamp approximately 0.15 m from the surface of the soil. After a few days the soil started to fracture. Once the soil started to fracture I measured the depth of these fractures using the same method used to measure depths in the field. I measured the same fractures everyday until the soil reached maximum desiccation after about five days. These measurements were then entered onto an Excel spreadsheet, and could then be compared to those depth measurements recorded in the field.

These measurements recorded the depth of the fracture at the top one to two centimeters. The true depth of the fracture cannot be measured with this method. Also, if a fracture curved at depth, this manual method could not penetrate past the curvature. To measure the true depth of a fracture without disturbing the structure, I had intended to create a mold of the fracture networks by pouring a watered down cement or an epoxy into the fracture network. After the cement/epoxy dried, I could dig the mold up and get an idea of how deep the fractures penetrated at that point in time. Unfortunately, before I could initiate this experiment, my field site was overrun by a herd of cows that destroyed any possible sites for making molds. The soil horizons were also trampled into an unrecognizable mess, making future field work impossible. I was able to use the previously collected depth data to investigate and establish relationships between fracture depth, aperture, and density.

Moisture Content Data

I also measured moisture content of the soil each time I visited the site and collected fracture measurement data. I tried several methods to get the best information possible. Two of these procedures did not produce the desired result and were discarded after two weeks. One of these methods involved the use of a tensiometer. A tensiometer measures soil suction at depth, and is an indirect measure of the degree of saturation in the subsurface (Reynolds et al 2000). I initially attempted to use a portable QuickDraw tensiometer to measure moisture contents in the subsurface, and I collected measurements at the site throughout the first four weeks of the study. Unfortunately, this method produced values that were not reliable. The clay particles clogged the tube's port of entry, making an accurate estimate of soil suction impossible. After four weeks of testing, this method was discarded in favor of other procedures.

The other method that was later discarded consisted of using a soil auger to get a soil core of the site. In addition to getting a sample to use for moisture content, this core could have established the clay thickness of each site and the grain size distribution. Two problems became apparent almost immediately. First, wet clay, even slightly wet, does not core well. Auguring into the wet clay would compact the soil in the soil tube so that calculating soil thickness became impossible. Also, much of the wet clay did not stay in the soil tube as the auger was extracted from the ground, making it impossible to analyze for grain size distribution. When the clay soil was extremely dry the soil auger could not penetrate deeply enough into the hard ground to get sufficient samples for grain size analysis.

To overcome this predicament, I switched from using an auger with soil tubes to using 6 oz. steel soil sample cans. I collected each sample by turning the can upside down and stepping on it until the bottom of the can was even with the ground. I then carefully extracted the soil sample by digging a hole next to the can and placing my hand underneath the soil sample to keep the soil inside the can as I withdrew it. Next, I labeled the soil sample with the date and number of the field site. Later the same day I went to the lab where I weighed each can using a digital scale. I recorded this initial weight into an Excel spreadsheet. Next, I took the lid off the can, placed it under its respective sample, and then placed each sample into a drying oven heated to 71° Celsius (160° Fahrenheit) for one week. After one week, I took the samples out and reweighed each one. I recorded these dry weights in the same spreadsheet and set aside the samples for grain size distribution analysis. Once both wet and dry samples were recorded, a water weight was calculated by subtracting the weight of the moist sample from the weight of the dried sample. Finally, the gravimetric moisture content for each soil sample was calculated by dividing the water weight of the sample by its desiccated weight. These data were compared to the temperature and precipitation data for the area as well as to the fracture density of each site for each date.

Grain Size Distribution

Grain size distribution is another important part of my research and was measured for each soil sample. After the soil samples were dried and the moisture contents recorded, I took two soil samples from each site into a separate lab containing a shaker. I chose six sieves for soil separation and grain size analysis. The largest sieve, placed at the top of the stack, trapped particles between 2.4 mm or larger in size. The next size smaller trapped grains with sizes between 1.2 mm and 2.39 mm. The third sieve held particles that were between 0.6 mm and 1.19 mm in size. The fourth sieve contained mesh that trapped grains between 0.3 mm and 0.59 mm in size. Grain sizes between 0.15 mm and 0.29 mm were trapped in the next sieve down. The last sieve in the stack trapped particles between 0.07 mm and 0.149 mm. The remaining particles, ones less than 0.07 mm in size, were caught in the bottom pan. Once I picked out the sizes of my sieves, I weighed each one and recorded their weights. I was then ready to perform the grain size distribution analysis on my samples.

The drying process caused many of the clay particles to interlock together, and I needed to separate these clumps in order to determine an accurate grain size distribution. First, I took a soil can and placed a portion of its contents onto a clean piece of white paper. I then used the handle of a heavy wrench as a mortar to separate the clay clumps for easier passage through sieve shaker. Once I separated the clay particles, I stacked the sieves and placed the soil in the shaker. I then repeated the separation process with the rest of the soil in the can. When all the soil from the one sample can was placed in the shaker, I turned the shaker on for five minutes. After five minutes, I removed the top four sieves, carefully emptied the soil onto the same piece of paper, and repeated the separation procedure. Once I felt the clumps were separated satisfactorily, I dumped the soil back into the sieve shaker. I ran the machine for another five minutes, and carefully separated each sieve from one another. Next, I weighed each sieve with the soil and recorded the weights. Each sieve weight was subtracted from the soil and sieve weight, and then this number was entered into an Excel spreadsheet for analysis. Once these values were in the spreadsheet, I was able to calculate the average grain sizes at the cumulative percent retained by weight for d_{20}, d_{50}, and d_{80} for all sites.

Infiltration Data

Understanding how soil characteristics affect infiltration rates in smectite clay is one purpose of my study. In order to fully understand this relationship, I needed to acquire data on infiltration. To that end, I performed several experiments and procedures to fully understand the movement of water through smectite clay.

I used an improvised infiltration ring, a pressure transducer, and an electric data logger to record infiltration rates. First, I picked a space near site number four that exhibited large, polygonal fracturing. Once the site was chosen, I placed the infiltration ring (a five gallon bucket with one centimeter demarcations on its side and with its bottom cut out) into the ground to a depth of one inch. I then placed a pressure transducer attached to a data logger at the bottom of the bucker. After equilibrating the transducer, I filled the bucket about two-thirds full. As I was recording the drop in water level manually, the pressure transducer transmitted the data to the logger, which then electronically recorded water infiltration. I initially wanted to do this experiment several times in different locations, but my field site was compromised by a herd of cattle. Even so, this experiment did provide enough information to determine the point at which threshold values change.

Since my field site was rendered useless, I shifted my focus into the laboratory. I used the plastic containers of soil, initially used to measure fracture depths, to perform several infiltration experiments. First, I took digital pictures of the soil in order to measure the fracture density and aperture width of the fractures. I then manually measured the fracture depth and aperture width of a number of fractures. Next, I punctured small symmetrical holes in the bottom of a one gallon water jug, then punched a hole in the lid of the jug and attached one end of a plastic tube to a faucet and stuck the other end in the hole in the lid. I filled the jug to about half full of water, and held the jug over the container of soil to simulate rainfall on the surface of the soil. I timed how long it took the fractures to close once the 'rain' started falling, as well as the length of time until water started ponding on the surface of the soil. Once the water started ponding on top of the soil, I stopped watering. I continued to measure the amount of time it took the water to infiltrate through the soil and begin to drain out of the bottom of the bucket. Once this data was recorded, I set a 120 watt heat lamp about 0.15 m from the surface of the soil and checked back every few days to see how many fractures had formed in the clay. Once I felt the fractures had reached maximum growth (no increases in aperture width or fracture density), I redid the experiment multiple times in order to verify my data.

CHAPTER 3

RESULTS AND DISCUSSION

The goal of this study is to determine the effect of desiccation fractures on infiltration rates through smectite clay soils. Specifically, I want to understand the mechanisms that alter fractures in these soils and ultimately change infiltration rates through these soils. I have identified some fracture characteristics and soil properties that might create changes in infiltration rates. The following pages outline the results and discuss the meaning of these results.

Fracture Density

Understanding fracture density is an important part of my study. A greater density of fractures in a clay soil suggests faster infiltration to the subsurface that will slow as the fractures heal. There are several variables that affect the fracture density in a clay soil. These variables are air and soil temperature, precipitation, gravimetric moisture content, and grain size distribution. I have analyzed the data to answer the questions of which variables dominate affects of fracture density and in what ways these variables affect fracture density.

The first variable I analyzed against fracture density was air temperature. There are two locations in Austin, Texas, that record daily air temperature and precipitation for the US National Climate Data Center. I took the high temperature and low temperature recorded at the location closest to my field site and averaged them together to provide a single value that characterizes the temperature during fracture formation.

Figure 04, showing temperature versus fracture density for site 01, illustrates a significant drop in fracture density subsequent to a large drop in temperature between March twentieth and April twentieth. There is a rise in fracture density as temperature increases, as illustrated on the twenty-first of May and just after the twenty-second of July. The figure also shows length of time without any increase or decrease in fracture density, although temperatures ranged between 24°and 29° C (75°and 85° F). This suggests that a different variable is controlling fracture density at this time. There is no pattern in fracture density from August through September, further indicating that temperature is not the main variable controlling for fracture density at site 01.

Figure 05 shows temperature versus fracture density at site 02. There is a general increase in fracture density after temperatures increase. The same holds true for decreases in temperature and fracture density. There is about a four day delay between the rise or fall in temperature and the increase or decrease in fracture density. There are also three instances where the temperature plots in a fairly high range yet the fracture density is zero, meaning no fractures are visible. Conversely, in mid July the fracture density shows a dramatic increase, yet temperature values are consistently high. These irregularities suggest that temperature is not the main variable affecting the density.

Figures 06 through 13 (corresponding to sites 03 through 10) follow the same general pattern - high densities are found slightly after higher temperatures and lower densities behind lower temperatures. The exception is when the fracture densities are zero and the temperatures are relatively high. This again suggests that a different variable, most likely precipitation, is affecting fracture densities at these times.

Figure 14 shows all the field sites on one graph for easy comparison. This graph clearly demonstrates that higher fracture densities are associated with higher temperatures. However, this graph does not explain why each site experiences zero fracture density during periods of high temperature.

The next set of graphs depicts fracture density versus precipitation. Each one of these graphs clearly illustrates that high densities correspond to low or no precipitation while low to no fracture densities occur immediately after precipitation events. The one inconsistency appears after the June sixth through eleventh rain event, when many sites show an increase in fracture density even with an influx of over 12.7 centimeters (5 inches) of rain. This increase is more likely caused by a temperature increase of 6° C (10° F) during the same period. Nonetheless, an inverse relationship between precipitation and fracture density holds largely true for most sites.

Figures 15 and 16, depicting sites 01 and 02, show a slight deviation from this inverse relationship. These two sites are situated in a low spot which sometimes retains water on the surface after heavy rain events, creating ponding on the soil surface. This standing water retarded these sites' ability to form fractures until the water either infiltrated or evaporated. Both sites 01 and 02 (figures 15 and 16) show an increase in fracture density once this standing water has disappeared.

Figure 17 (site 03) shows zero fracture density from April fifth through May nineteenth. Low fracture densities during this time are not seen at any other site except for site 01 (figure 15). Site 03 is situated in a heavily wooded area just east of the wetland area. The soil found at the site contains more organic material and appeared to be actively re-worked by organisms throughout the early part of the study. Also, during this time average air temperatures were generally below 20° C (68° F). The combination of soil structure, precipitation, and low temperatures could have caused the soil to remain relatively moist and therefore devoid of fractures.

Both sites 02 and 04 (figures 16 and 18) exhibit increasing fracture density from April fourteenth through May nineteenth despite some precipitation events during this time. I believe this increase in density is caused by steady increases in temperature, as shown in figures 04 and 06. After May nineteenth, figure 16 follows the inverse pattern or has been previously explained. Site 04 (figure 18) follows the pattern quite well except on July twelfth which depicts a slight increase in density as well as a precipitation event on that day. This is probably due to the fact that I completed my field work in the morning before the precipitation event occurred, so the data does not reflect the precipitation event on that day.

Site 05 (figure 19) follows the same pattern, but experiences a slight deviation from the pattern on July twelfth. There is an increase in density corresponding to a precipitation event on that date. As in figure 18 (site 04), this data was collected just before the precipitation event, and is accurate.

At site 06 (figure 20), the fracture density closely follows the inverse relationship to precipitation. Sites 07 and 09 (figures 21 and 23) have almost identical responses to precipitation except for the day of June twenty-first. Site 07, in figure 21, shows a slight drop in fracture density, while site 09, seen in figure 23, shows a small increase in fracture density.

Site 08 (figure 22) follows the inverse pattern with a few exceptions. Fracture density from April thirtieth through June fourteenth shows a large increase despite precipitation events. This increase corresponds with the general increase in temperature over the time frame. Also, the figure depicts a decrease in density on August ninth, but no precipitation event. In fact, this drop is seen in figures 15, 20, 21, and 24 (corresponding to sites 01, 06, 07, and 10, respectively) as well. This drop is probably explained by temperature variations as it follows a 4° C (7° F) drop in average temperature. This was enough of a decrease to affect the fracture densities at these five field sites.

Site 10, seen in figure 24, also follows the inverse relationship pattern closely. The one exception occurs after August twenty-second. A precipitation event occurred over a five day period, yet site 10, as well as sites 02 and 06 (figures 16 and 20), shows an increase in fracture density. This increase happens to correspond to a 3° C (6° F) increase in average temperature. In this instance, temperature seems to have contributed more to forming fractures than precipitation did to heal them. Finally, figure 25 shows all ten sites along with precipitation for comparison purposes. This graph clearly shows the inverse relationship between precipitation and fracture density. It also illustrates the close resemblance that most sites have with each other.

Both temperature and precipitation affect fracture density. Fracture densities show slight changes with the increase or decrease in average temperature, while precipitation events cause large variations in fracture densities. Increases in average temperatures usually lead to a drop in air moisture. This drier air creates an imbalance between soil moisture and ambient air moisture that leads to drier soil and a greater tendency to form fractures. Cooler temperatures slow down the evaporation process, inhibiting fracture formation. Slight changes in average temperatures cause soil to react by increasing fracture formation or by slowing this formation. This growth or lack of growth suggests that soils are very sensitive to even slight changes in the environment.

Precipitation inundates the soil with moisture. Heavy precipitation events can quickly heal all fractures in a soil and saturate the soil for extended periods. Three of these heavy precipitation events are illustrated in figures 15 through 25. Other precipitation events saturate the soil for a limited time, allowing the soil to dry out a little and create new fractures. A good example is shown on April thirtieth, when most of the values have decreased from the previous weeks sampling, but, despite numerous precipitation events, have not reached a fracture density of zero. The reason that some of these events affect fracture density more than other events depends on the duration of the event and the amount of rain associated with the event. A precipitation event that occurs over several days will increase soil moisture contents and decrease fracture densities more than a precipitation event with the same magnitude over a shorter time. The water from the longer precipitation event has a greater chance of saturating the soil. The short event will see a higher probability of surface runoff sooner because heavy rain over a short time can exceed the infiltration capacity of the soil, making it impossible for additional water to infiltrate. The higher moisture contents from the longer event lead to slower fracture growth over time.

Another reason for the correlations between fracture growth and precipitation events is the frequency of sampling and the time between rain events and sampling. For example, June eighth and ninth saw over seven centimeters (three inches) of rain, yet the soil on the next sampling date, June fourteenth, exhibited fractures at most sites. Soil sampled during or right after lesser precipitation events exhibited zero fracture densities. This discrepancy can be remedied by more frequent sampling and by sampling closer to precipitation dates. In summation, fracture densities are affected by precipitation based on duration, magnitude, and the length of time since a precipitation event.

The next variable I compared to fracture density was gravimetric moisture content. An increase in moisture content should lead to a decrease in fracture density and figures 26 through 36 follow this trend. Figures 28, 31, 33, 34, and 35, corresponding to sites 03, 06, 08, 09, and 10, do not support fractures above moisture contents of 0.22. This number is the point at which the soil can no longer support fracture growth at these sites.

Figures 26, 27, 29, 30, and 32, corresponding to sites 01, 02, 04, 05, and 07 do have one point above the 0.22 value. This point (except for site 05) occurs on April fifth at each site, when moisture contents were above 0.300. The fracture densities for these four sites range from 0.004 to 0.035 cm^{-1}. Site 05 (figure 30) has a fracture density of 0.005 cm^{-1} on August twenty-fourth, when its gravimetric moisture content was measured at 0.284. These fractures formed in soils with high gravimetric moisture contents because of slight increases in temperature in the days before sampling. The early days of April had an average temperature of 19° C (66° F), warmer than those seen at the end of March. These higher temperatures most likely dried the soil enough to allow for small fracture growth. Sites 08, 09, and 10, corresponding to figures 33, 34, and 35, had not been established until after April fourth, so fractures might have been found at moisture contents above 0.22 for those sites as well. Site 03 and site 06 (figures 28 and 31) had less sun exposure, so the higher temperatures probably did not support fracture growth in soils with such high moisture contents.

Despite these few anomalies, each site trends toward lower fracture densities with increasing gravimetric moisture content. This negative correlation is illustrated by the trendline in each figure. However, R^2 values associated with each trendline suggest that none of these relationships are completely linear. These R^2 values range from 0.0795 to 0.5132. Site 03, shown in figure 28, has the highest R^2 value of 0.5132 which is only a moderately linear relationship. Site 07, in figure 32, has the lowest R^2 value of 0.0795. This value indicates that fracture density and moisture content have a very weak relationship, and that other processes are affecting fracture density. The other sites all exhibit a weak relationship as well. The weakness of this relationship suggests that moisture content is not the main variable affecting fracture density in clay soils.

Another possible explanation for the weakness of the R^2 values may be the inclusion of data not collected on a weekly basis. These data were collected between April and mid-June. When these data are not included, the R^2 values for the data collected on a weekly basis increases, meaning that gravimetric moisture content and fracture density do in fact have a moderate to strong relationship. Figures 37 through 46 illustrate this stronger linear relationship. These graphs also show fracture densities supported only in soil of less than 0.025 gravimetric moisture contents, except for site 05 (figure 41). This value is the point at which the moisture content is too great to sustain fracture creation. Site 05 (figure 41) is the only place where fractures are found along with high moisture content. The fracture density, however, is very low, only 0.005 cm^{-1}. A fracture density this low implies that fracture growth was limited.

Gravimetric Moisture Content

One way to understand changes in fracture densities is through the changes in gravimetric moisture content. This soil property is affected by two variables, temperature and precipitation, by varying degrees. To better understand how fracture densities are dependent on moisture content, I needed to know which variable affected gravimetric moisture contents the most. Weekly sampling started in mid-June after a period of intermittent sampling.

Figure 47 summarizes the maximum, minimum, median, and average moisture contents throughout the whole study period for all ten sites. One interesting characteristic displayed is the variation in moisture content values on a weekly basis. Another notable characteristic is the height of the maximum moisture content values. Sites 01 and 02 are located in a low lying wetland area that sometimes holds standing water. These two sites are the reason the maximum moisture values are much higher than the other moisture content values and the reason why the average values are skewed towards the higher range. Despite this, the median and average moisture content values are very close, meaning that the distribution of moisture contents is centered around the average values.

Figures 48 through 58 depict daily temperature versus gravimetric moisture content values for sites 01 through 10. An increase in temperature should lead to a decrease in gravimetric moisture contents if temperature is the main control for gravimetric moisture content values. The daily temperature from mid-June through mid-August is relatively stable, between 24° C and 29° C (75° F and 85° F). All sites show large swings in moisture content values during this period. These large changes in moisture content usually occur during or just after a small drop in temperature. While these drops in temperature are not enough to create such large changes, the precipitation events associated with the temperature drops are able to cause these fluctuations. Even so, in periods of increasing temperature the graphs do show a trend toward decreasing gravimetric moisture content. From April fourteenth through May nineteenth, most of the figures, except for figures 50, 52, and 56 (corresponding to sites 03, 05, and 09), show a general decrease in moisture contents with increasing temperature. On the other hand, May nineteenth through June fourteenth depict an increase in temperature, yet most graphs, except figure 50 (site 03) and 52 (site 05), also show an increase in moisture content. This leads me to conclude that throughout the study period temperature was not a significant control over changes in soil moisture contents.

Figures 59 through 69 depict daily precipitation versus gravimetric moisture contents for each site. Each graph shows an increase in moisture content just after a precipitation event and a decrease in moisture contents after dry periods. This is especially evident starting in mid-June when sampling occurred on a weekly basis. However, there are some deviations from this pattern. For example, two separate precipitation episodes occurred between April sixth and eleventh. The first episode produced more than two centimeters (one inch) of rain, yet the field sites sampled after these two events show a marked decrease in gravimetric moisture content from the previous sample. Even more interesting is the fact that April seventh brought a 5° C (8° F) increase in temperature from the previous day, but April eleventh brought a 10° C (17° F) decrease in temperature from the day before (figures 48 through 58). The behavior in temperature during this time period and the number of dry days between sampling and the precipitation occurrences explain why the soil is drier than it was previously.

Figures 61, 63, and 67, corresponding to sites 03, 05, and 09, show an increase in moisture content values from mid-April to the end of April. These sites responded to an increase in precipitation from two separate rain events. It is interesting to note how the other sites did not respond to the precipitation and had lower gravimetric moisture contents. This decrease is in response to increases in average temperatures through this time period. Also, sites 03 (figure 61) and 05 (figure 63) are not in direct sunlight, which could inhibit the drying of the clay soil.

These figures show marked changes in moisture content corresponding to precipitation events. Rain episodes increase gravimetric moisture contents while periods of zero precipitation are followed by lower moisture contents in the soil. These changes suggest that precipitation is the main variable driving the increases and decreases in gravimetric moisture content. Small discrepancies in the major trend inform me that precipitation is not the only variable driving these changes. Average temperature also plays a small role in controlling how gravimetric moisture contents change over time.

Aperture Width and Fracture Depth

Fracture density is only one of the fracture properties that I am considering. The other two properties are aperture width and fracture depth. Both of these variables provide additional information for understanding infiltration rates into the soil. Before understanding this relationship, however, I needed to verify and quantify the relationship between aperture width and fracture depth. It is expected that aperture widths should correspond positively with fracture depths.

Figure 70 through 78 depict aperture widths versus fracture depths for sites 02 through 10. Site 01 was devoid of fractures during the acquisition period. Each graph shows a positive correlation between aperture width and fracture depth, corresponding with the expected relationship. The R^2 values for each site, however, suggest that this relationship is not directly linear. Site 03 (figure 71) has the strongest correlation, but its

R^2 value is only 0.4989, which is only moderately linear. Site 05 (figure 73) has the weakest correlation, with a R^2 value of 0.0012. These values tell me that many of the largest apertures do not correspond with the deeper fractures and vice versa. One explanation is that there are inherent problems with the data collection methods. This situation is quite possible since I used manual methods to acquire the data that do not take into account many of the variables that could affect this relationship such as the tortuosity of the fractures. The method I used was not able to compensate for potential curvatures in the fractures at depth, potentially underestimating the total fracture depth. Another potential complication involves the method of marking the depth of fracture on the measuring rod. Any movement of the rod could result in false depth readings, in turn weakening the width-depth relationship. Even with these limitations, however, these data support the hypothesis that aperture width is positively correlated with fracture depth.

I also calculated aperture distribution histograms from the data acquired through the digital photographs. These data tell me the frequency of the aperture widths found within a certain analysis area, whether each width is distributed equally throughout, or if there is a different distribution pattern. This information is important because differences in aperture width distributions can mean large fluctuations in infiltration rates.

Figures 79 through 89 illustrate aperture width versus frequency for sites 01 through 10, with one summary graph. A log normal distribution provides the best fit to the data for each graph. This distribution means that most of the values are clustered around the lower values, with fewer large apertures. The frequency of each aperture width depends on the total number of aperture widths I measured within each analysis area. The maximum frequencies range from 125 for site 07 (figure 85), to a low maximum of 28 for site 05 (figure 83). Also, aperture widths are most frequently between of 0.06 cm and 0.20 cm. Even so, each graph has its own unique spread of frequencies over aperture width. For example, figure 81 corresponding to site 03, has frequencies numbering greater than 10 spread over 34 different aperture widths. In contrast, site 01 illustrated in figure 79, has frequencies numbering greater than 10 distributed over 8 different aperture widths. A larger distribution of high frequencies enables more water to infiltrate into the subsurface at a faster rate before fracture healing occurs. All of these graphs provide a clearer picture of how aperture width and fracture depth affect infiltration.

Grain Size Distribution

Soil grain size distributions are important because differences in grain size distributions at each site could lead to disparities in fracture growth rates and therefore infiltration rates. Figures 90 through 99 and table 4 show the results of the soil grain size analyses.

Table 4 depicts the grain size distributions in millimeters for each sample at 20 percent, 50 percent, and 80 percent retention by weight. The table also shows the average size at these three percentages for each plot. D_{20} retains some of the larger grains in a sample while d_{80} is composed of much smaller grain sizes. The difference in grain size between each sample is very small. For example, the d_{80} averages range from a high of 0.328 mm for site 06 to a low of 0.120 mm for site 01. These variations are so small that there is not enough variation in grain size to identify any trends with confidence.

Each graph depicts the cumulative distribution of grain sizes in each sample. At least two separate samples were analyzed per site. For most sites, each sample follows similar distributions. The slope of the grain size distribution curves of each sample between 10 percent and 90 percent are almost identical for each site. The steep slopes indicate that grain sizes rapidly decrease as grain retention increases. Another similarity in most graphs is the size of the grains along this curve. Most of the graphs show similar sized grains retained at various percentages. In addition, most grains fall between 0.1 mm and 1 mm in size between 20 percent and 90 percent retention. Together, these observations indicate that most of the sites have a homogeneous grain size distribution.

There are a few exceptions, however. Site 01 (figure 90) has a sample from June fourth that does not quite match this pattern. In fact, this sample is shifted to the left, signifying that smaller grain sizes composed this sample than the sample of June twenty-eighth. Site 09, figure 98, also shows an irregularity. The sample for May nineteenth shows an almost vertical component in its steepness curve. It is also situated to the right of the other two samples. The vertical portion of the grain size distribution curve indicates that grain size did not decrease as the percent retained by weight increased. At 43 percent retention, the grain sizes start to decrease once again. The rightward shift of this sample means that the sample is composed of much larger grains than the other two samples.

There is one other glaring exception. Site 06, seen in figure 95, shows a wide disparity between the two samples in the amount of grains retained in the sieves. The sample collected on May nineteenth shows a regular logarithmic pattern seen in the other graphs. The June twenty-eighth sample, however, depicts an almost linear pattern. The first 30 percent of grains retained follows the regular pattern, but after this point, an increasing amount of grains is retained in the smaller sized mesh. This increase in grain retention is dependent on the method of grain separation. In Chapter 2, I described how the clay grains clumped together during the drying process. The method used for separating the clumped clay grains probably did not separate all of the smallest grains completely. The site 06 sample from June twenty-eighth shows an increased retention of these tiny grain sizes. This is due to successful separation of these grains from soil clusters. I believe that had the small grains separated as well as in the final sample, the other samples would have also followed this linear pattern.

Once I plotted these data, I computed the grain size distribution averages at d_{20}, d_{50}, and d_{80}, as shown in table 4. I then plotted these averages against fracture growth rate to see if grain size distribution affected fracture growth. Figures 100 through 103 depict grain size distribution versus fracture density growth rate from June through September. Fracture density growth rate is calculated by taking the difference in fracture densities on two separate dates. For example, site 04 had a fracture density of 0.050 on June fourteenth and a fracture density of 0.054 on June twenty-eighth, with the difference between the two being 0.004. This fracture density difference number is then divided by the number of days separating the two dates. The final number is the fracture density growth rate over the specified time period.

Each figure illustrates three separate grain size distribution averages- d_{20}, d_{50}, and d_{80}. These averages are compared to the fracture density growth rate of each site for a specified month. For example, figure 100 shows the grain size distribution averages versus density rate for the month of June. All these figures show the d_{20} average grouped within the largest grain sizes while the d_{80} average is grouped within the smallest grains. I expected that increased amounts of clay would signify that the soil is affected by the shrink swell properties of these clays to a greater degree than soils with larger grain inclusions. The fracture growth rate in a soil with a higher percentage of clay should therefore be greater than the growth rate in a soil without as much clay. I expect a negative correlation between fracture growth and the d_{20}, d_{50}, and d_{80} grain size averages since these averages contain grains that are much larger than clay mineral grains. In other words, larger d_{20}, d_{50}, and d_{80} values equate to less clay and in turn produce a slower fracture growth rate.

Figures 100 through 103 show the grain size distribution versus fracture density growth rate at all ten sites from June to September. Of the four graphs, only figure 101 (July) and figure 103 (September) depict a positive correlation between grain size distribution and fracture rate for all three grain averages. This positive trend is in contrast to the type of relationship that I hypothesized would occur. The other two figures, 100 and 103, have mixed correlation trends between grain size distribution and fracture density rate. The R^2 values for all the correlations are very revealing, though. The largest R^2 value is 0.4828, as shown in figure 101. This value indicates a weak to moderate relationship. All the other R^2 values are less than 0.100, which is a very weak relationship. These low values indicate that any correlations depicted in these graphs are not significant and should not be relied. The inconsistent correlations between grain size distribution and fracture density growth rate lead me to believe that no significant trends occur between fracture growth rate and grain size distribution.

Infiltration Data

One of my infiltration experiments was conducted in the field. This experiment used a pressure transducer and data logger to calculate the drop in water level over time, which corresponds with the amount of water infiltrating into the soil. Figure 104 presents the results of this experiment.

The graph shows a steady drop in water level for about 0.3 meters in the first four minutes of the experiment. Following this drop is a period of zero infiltration. This change in rate lasts about two minutes. The next minute then shows a surprising change. The water level in the bucket increases slightly. After this increase in water level, another period of zero infiltration transpires. Next, another period of steady infiltration is observed followed by a leveling off. Once again an increase in water level occurs, followed by a short period of no water movement. This cycle is repeated one more time until the water level in the bucket reaches zero, indicating that all the water has infiltrated into the soil. These cycles are caused by limitations in the pressure transducer and cannot be traced to any type of physical phenomenon. The results from the pressure transducer are not a reliable indicator of infiltration. Fortunately, I also manually recorded the infiltration information, and the results are found in figure 105.

I manually recorded that a water depth of 20 cm took fourteen minutes to completely infiltrate into the ground. Figure 105 depicts infiltration following an exponential curve. This curve shows faster infiltration decreasing over time. The calculated R^2 value is 0.9923 which means there is a strong relationship between infiltration and time. The density of fractures before infiltration was calculated at 0.007 cm^{-1}. Extrapolating this data to the other field sites, I believe that those sites with greater fracture density will infiltrate more water in the first minutes than those areas with less fracture density. Even so, I believe that all sites will follow this exponential curve pattern, meaning that infiltration will slowly decrease over time as fractures heal.

To check this idea, I performed a couple of infiltration experiments in the laboratory.

Using a plot of soil taken from the field, I calculated the fracture density of the soil, and then measured the amount of time it took 950 ml (32 fluid ounces or ¼ gallon) to infiltrate through the soil. On December third, 950 ml (32 fluid ounces) took six minutes and fifteen seconds to infiltrate through the sample plot (figure 106). The fracture density of the plot measured 0.025 cm^{-1} before the experiment. Figure 108 shows the fracture density reaching zero in forty-five seconds. On December fifteenth, the same amount of water took nine minutes to infiltrate through (figure 107). The fracture density before this experiment was calculated at 0.019cm^{-1} and was reduced to zero, one minute after infiltration commenced, as seen in figure 109. This difference in fracture density modifies the infiltration rate of water through the soil.

In order to verify these results, the data collected from these experiments were input into the SPSS 12.0 statistical program. I performed a multivariable linear regression with the data, with infiltration rate as my dependent variable. Fracture densities, as well as aperture width and fracture depth, were the independent variables in the regression. My goal was to find out which of these fracture characteristics influences infiltration rate the most. In Chapter 1, I stated the null hypothesis as smectite clay fracture characteristics do not affect infiltration rates into the subsoil. The results of the analysis are presented in tables 5 through 7.

Table 5, the model summary table, answers the question of which independent variables taken together explain the variation of the dependent variable. In this case, AR^2, or adjusted R^2, has a value of .984, which is a very strong relationship. My independent variables account for 98% of the infiltration rate's variability. The sum of squares regression line in table 6 also explains the variability in the infiltration rate.

More than 98% of the variability is explained by a combination fracture density, aperture width, and fracture depth. A very small portion of the variability is not explained by these variables. The high rate of explanation means that other factors are less likely to impact the infiltration rate than these three independent variables.

Table 6 also shows the significance level of the model. Earlier, I set my level of risk at 0.05. This table shows the model's significant at the 0.001 level which means that there is a 0 1% chance of rejecting the null hypothesis when it is actually true. This table also expresses the obtained F ratio as 124.70, or $F_{(3,3)}$= 124.70. At the 0.05 level of significance, the value needed for rejection of the null hypothesis is 9.28. The obtained value is more extreme than the critical value for rejection; therefore the null hypothesis cannot be accepted.

Table 7 reports the output of the separate variables. The Beta coefficients for each independent variable are negative. This means that a negative correlation exists between the rate of infiltration and each independent variable. For example, density of fractures has a Beta value of -0.702. The correlation is inversely related, so that as infiltration increases the density of fractures decreases. The value of this number is also important. The aperture width and fracture depth variables have Beta values below 0.4 which means that a weak relationship exists between infiltration rate and each of these variables. The density of fractures, however, has a value of 0.702 which correlates into a moderate to strong relationship with infiltration rate. Another important value to understand is the significance of each variable with infiltration rate. Density of fractures is significant at the 0.05 level, while fracture depth and aperture width are not significant at the 0.05 level. Fracture depth is significant at the 0.06 level, meaning that there is a 6% chance that the null hypothesis will be rejected incorrectly. Aperture width is significant at the 0.35 level, meaning that there is a 35% chance that the differences found are due to unknown reasons. In other words, fracture density is the only independent variable where chance alone cannot account for changes in infiltration rates. This significance level means that my research hypotheses are more favored as explanations than the null hypothesis.

The multiple regression analysis states that density of fractures does in fact affect infiltration rates. Fracture depth and aperture width have less probability of affecting infiltration rates than fracture density. The degree of the significance value for these two independent variables is important. Fracture depth is very near the level of risk I set for the analysis. Aperture width, on the other hand, is nowhere close to this preset risk level. This difference means that fracture depth has a greater chance of influencing infiltration rates while aperture width has no impact on infiltration rates. Of the three independent variables, fracture density exerts the most control over infiltration, fracture depth has some probability of affecting infiltration rates, and aperture width does not affect infiltration into the subsoil.

These results create a clear picture of which variables affect each other and ultimately affect infiltration into smectite clay soil. Smectite clay soil provides ample opportunity for infiltrating water to reach the subsurface. Areas with high fracture density provide the greatest opportunity for infiltration. Low soil moisture content and periods of zero precipitation enable the successful growth of clay fractures. The grain size distribution in this soil did not affect fracture growth as much as one might expect. Finally, out of all the fracture properties and soil characteristics, fracture density has the greatest effect on rates of infiltration. These outcomes provide insight into the mechanisms influencing recharge rate in Travis County, Texas.

DAILY TEMPERATURE VERSUS FRACTURE DENSITY

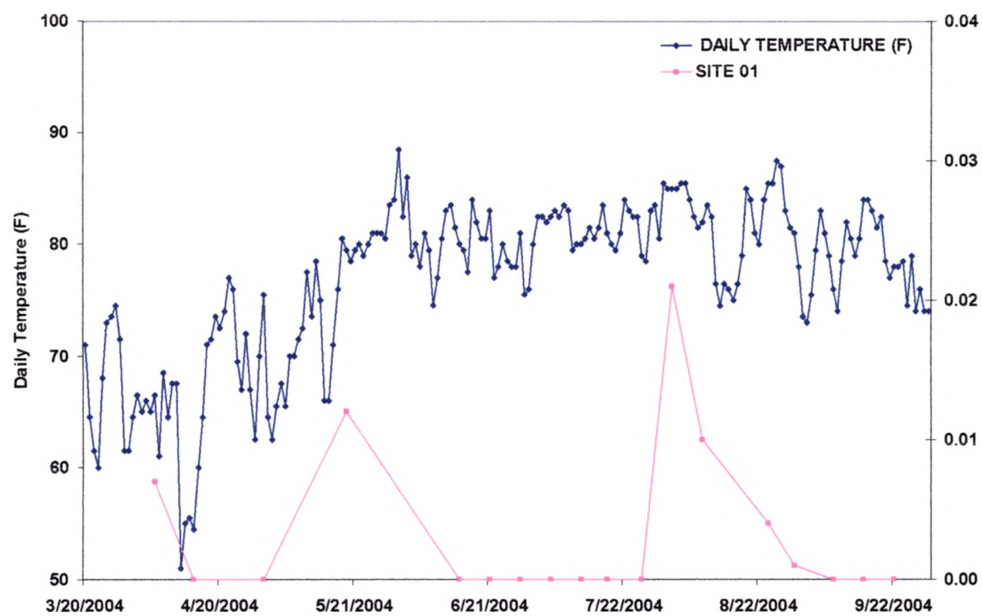

FIGURE 4. DAILY TEMPERATURE VERSUS FRACTURE DENSITY FOR SITE 01

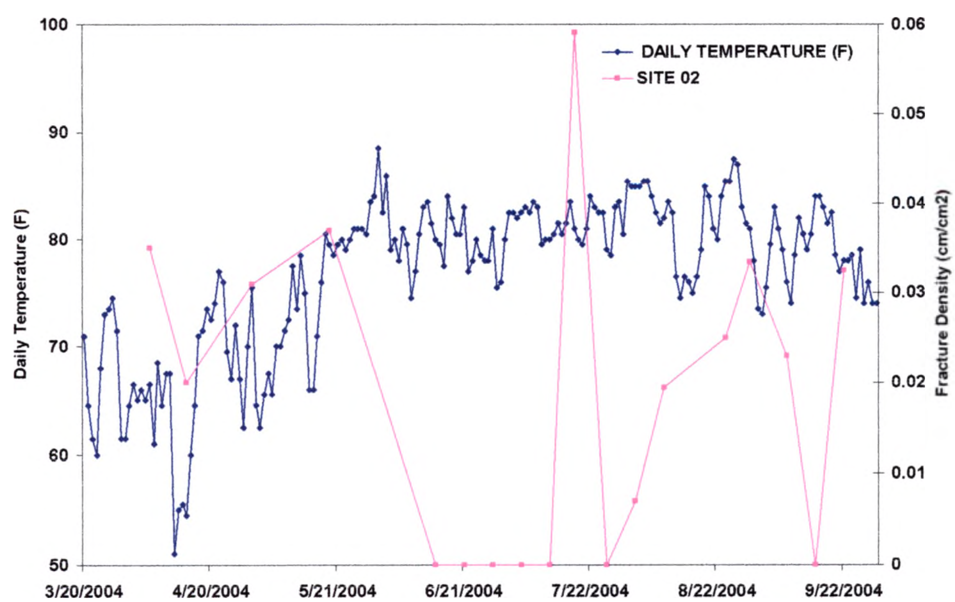

FIGURE 5. DAILY TEMPERATURE VERSUS FRACTURE DENSITY FOR SITE 02

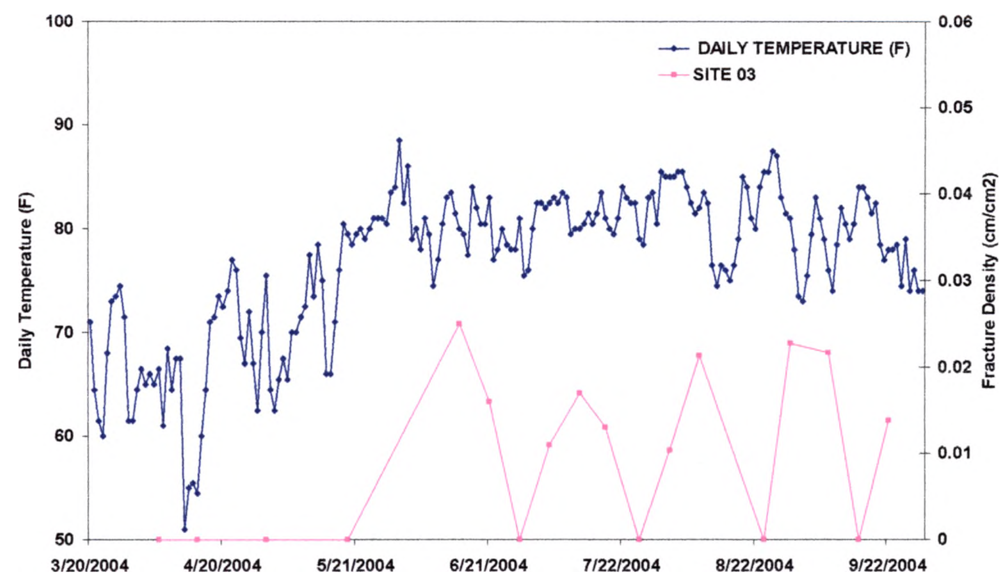

FIGURE 6. DAILY TEMPERATURE VERSUS FRACTURE DENSITY FOR SITE 03

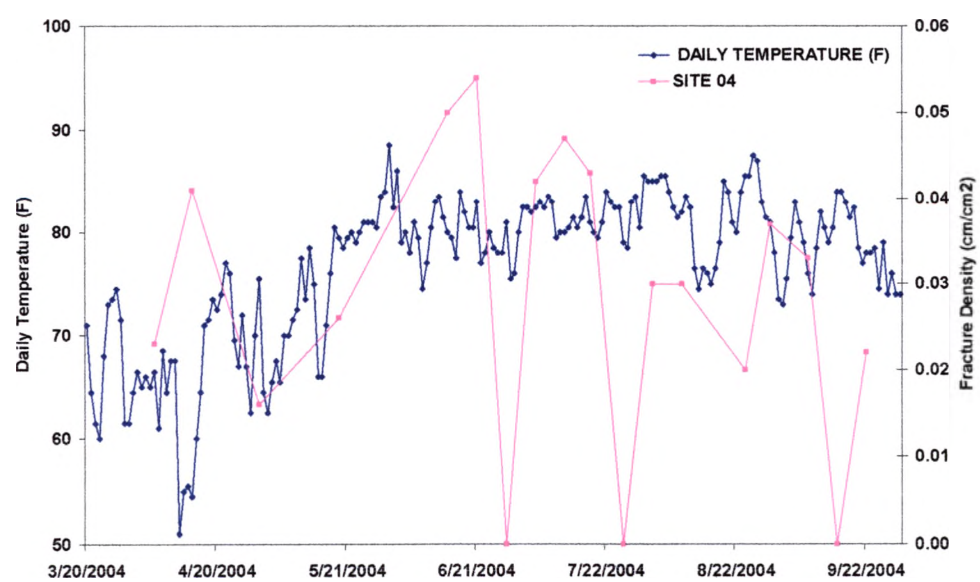

FIGURE 7. DAILY TEMPERATURE VERSUS FRACTURE DENSITY FOR SITE 04

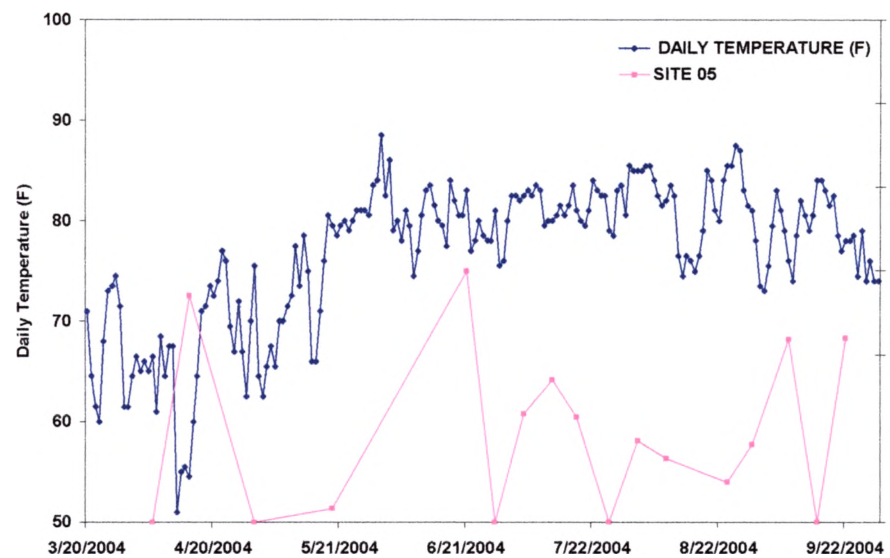

FIGURE 8. DAILY TEMPERATURE VERSUS FRACTURE DENSITY FOR SITE 05

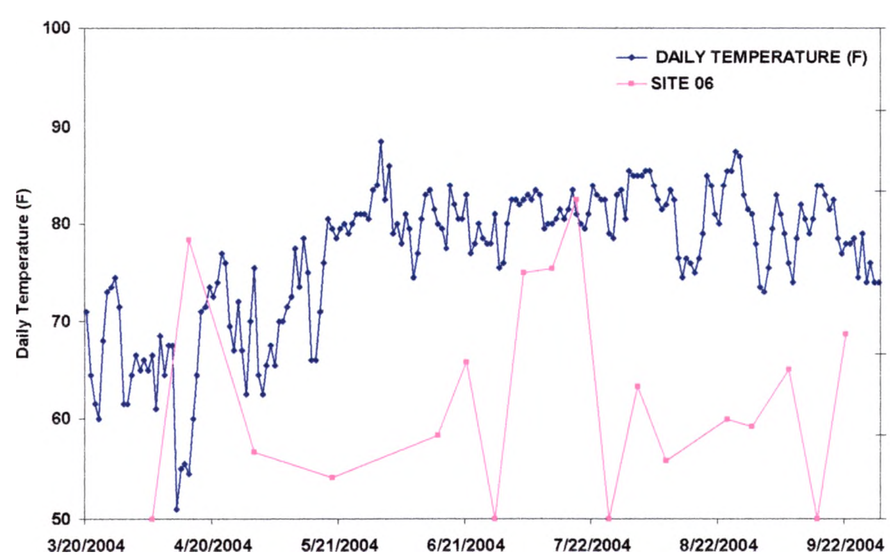

FIGURE 9. DAILY TEMPERATURE VERSUS FRACTURE DENSITY FOR SITE 06

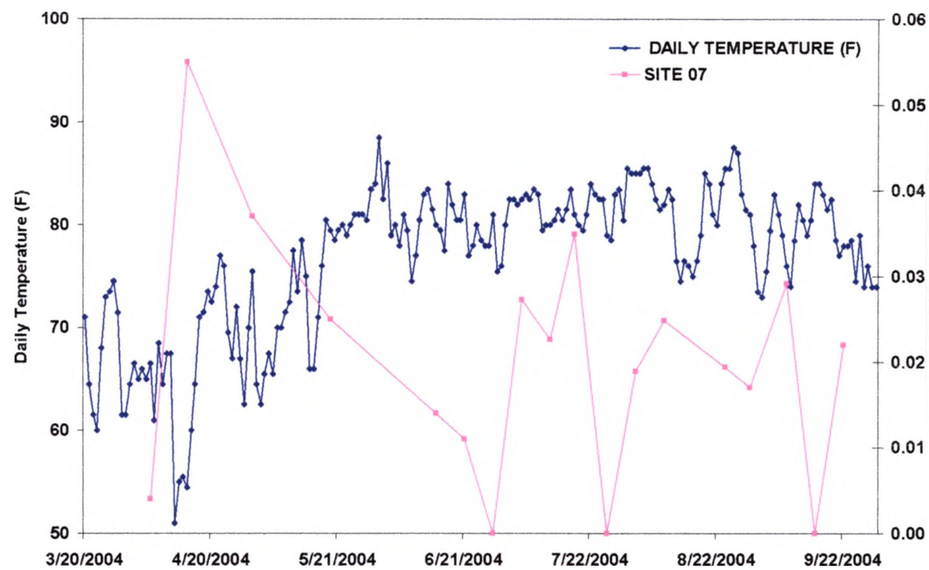

FIGURE 10. DAILY TEMPERATURE VERSUS FRACTURE DENSITY FOR SITE 07

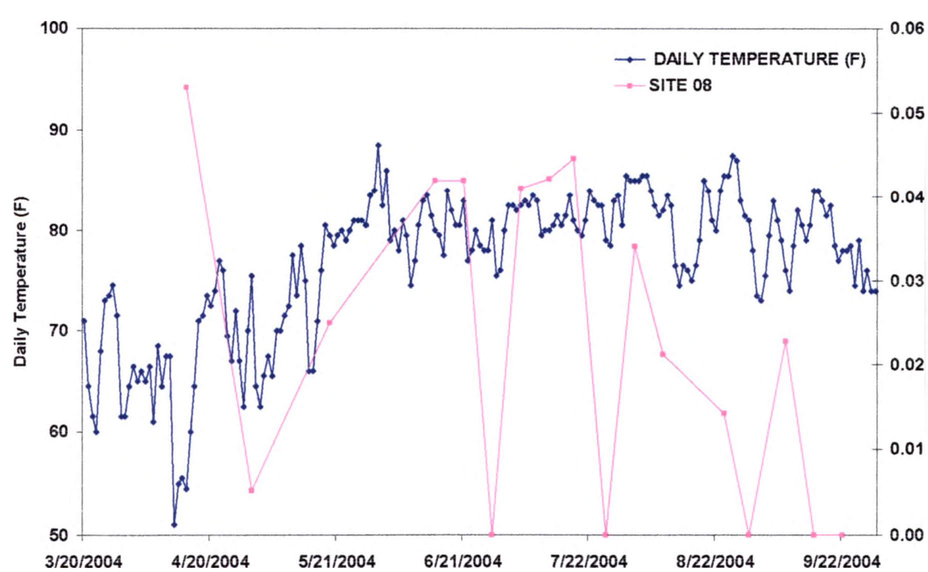

FIGURE 11. DAILY TEMPERATURE VERSUS FRACTURE DENSITY FOR SITE 08

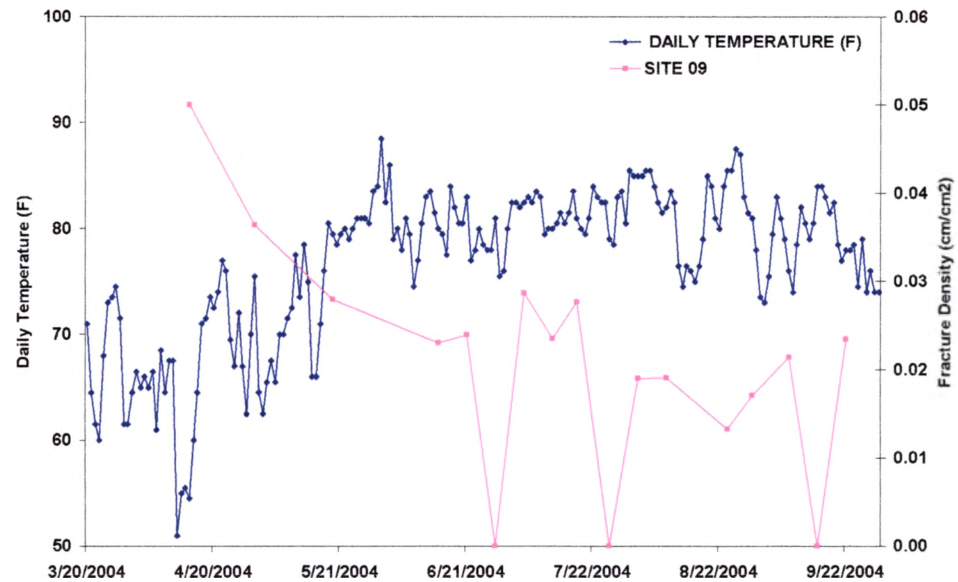

FIGURE 12. DAILY TEMPERATURE VERSUS FRACTURE DENSITY FOR SITE 09

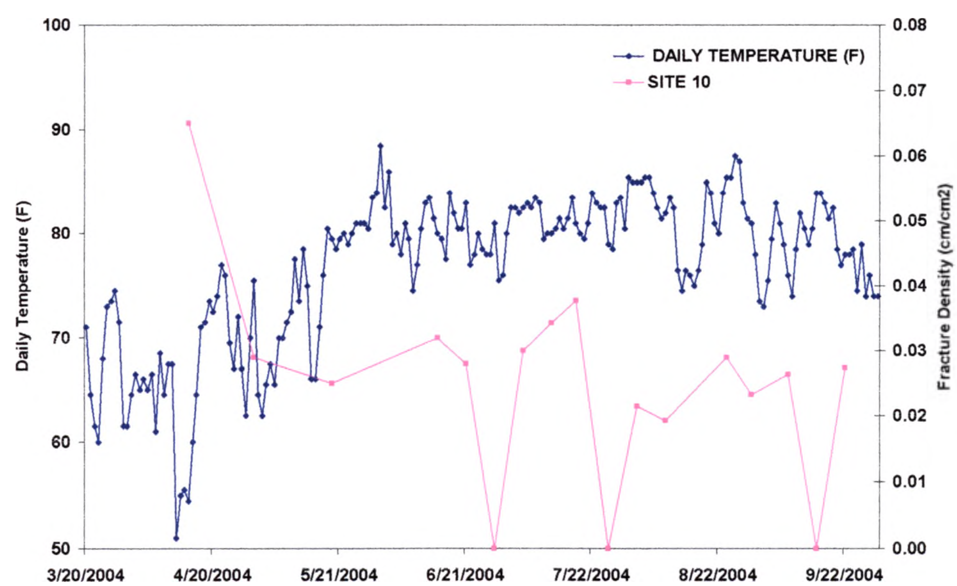

FIGURE 13. DAILY TEMPERATURE VERSUS FRACTURE DENSITY FOR SITE 10

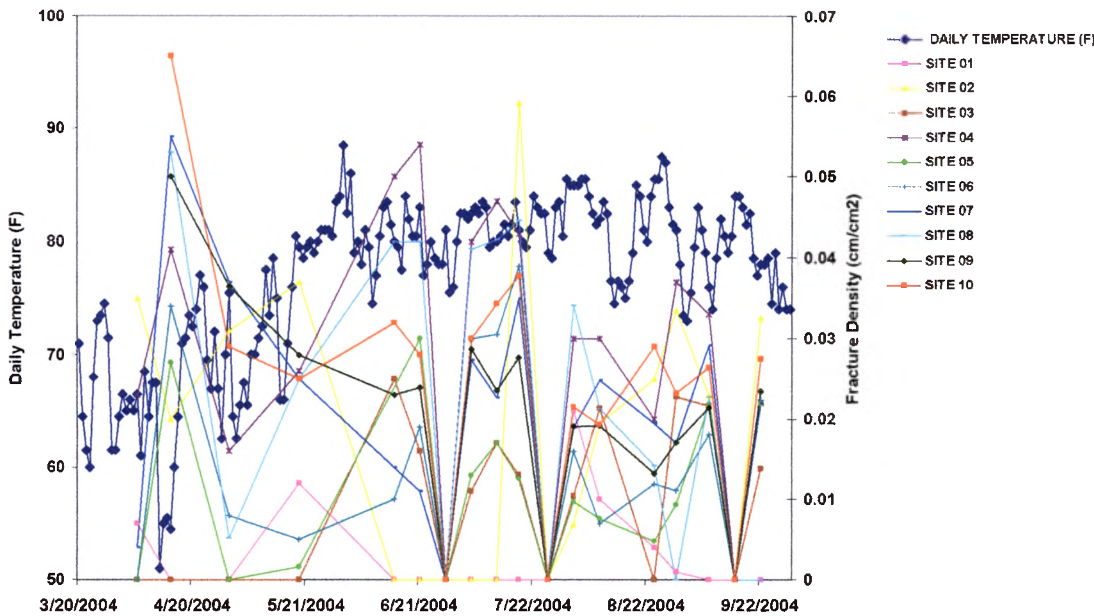

FIGURE 14. DAILY TEMPERATURE VERSUS FRACTURE DENSITY FOR ALL SITES

DAILY PRECIPITATION VERSUS FRACTURE DENSITY

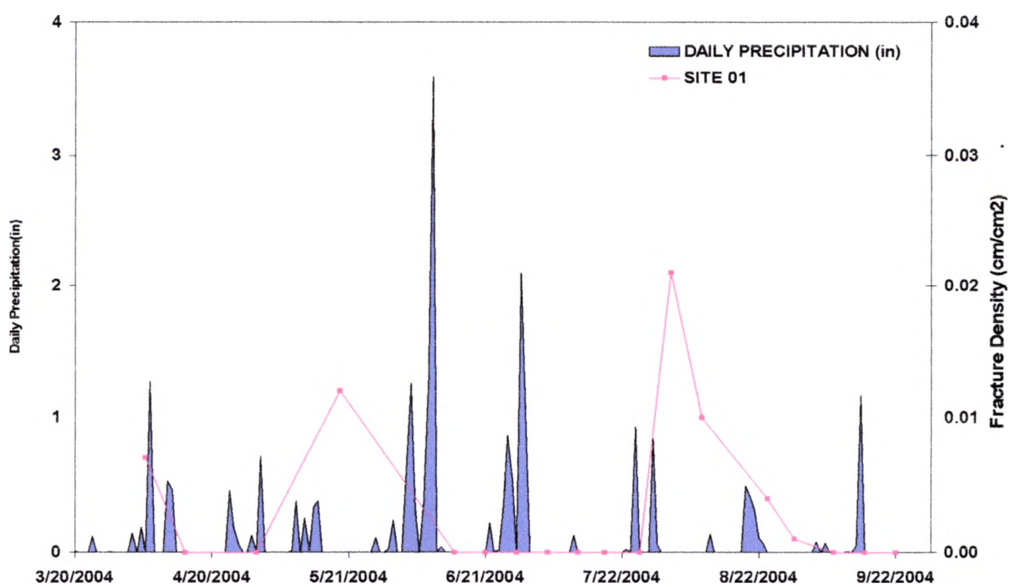

FIGURE 15. DAILY PRECIPITATION VERSUS FRACTURE DENSITY FOR SITE 01

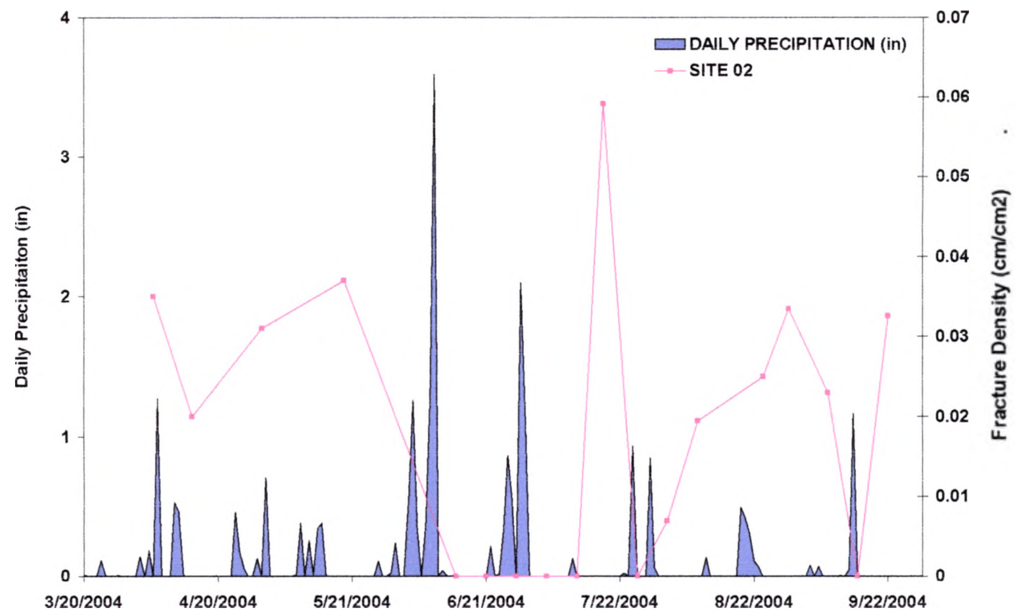

FIGURE 16. DAILY PRECIPITATION VERSUS FRACTURE DENSITY FOR SITE 02

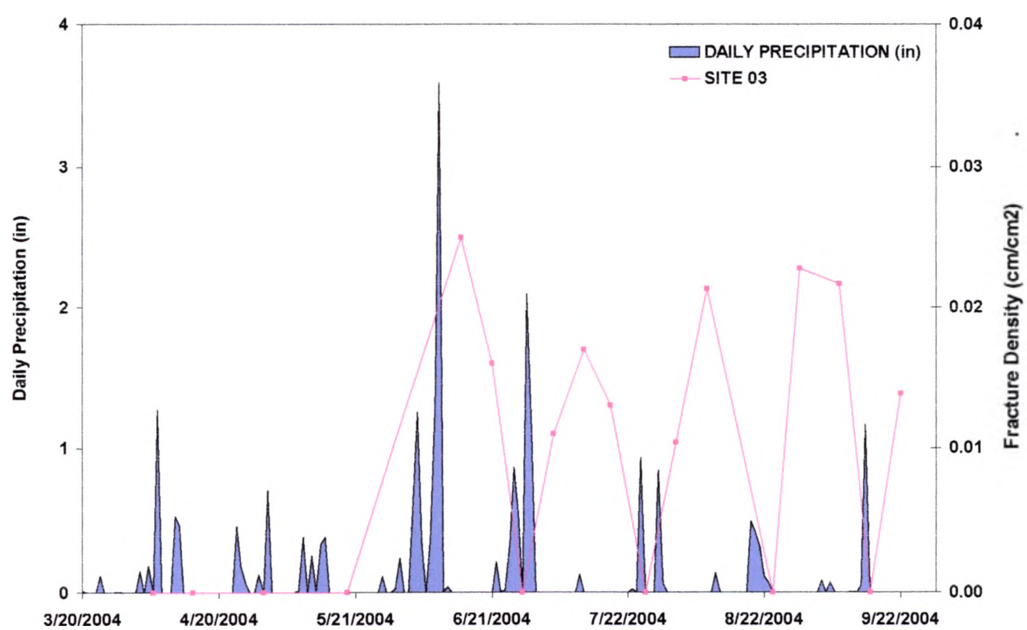

FIGURE 17. DAILY PRECIPITATION VERSUS FRACTURE DENSITY FOR SITE 03

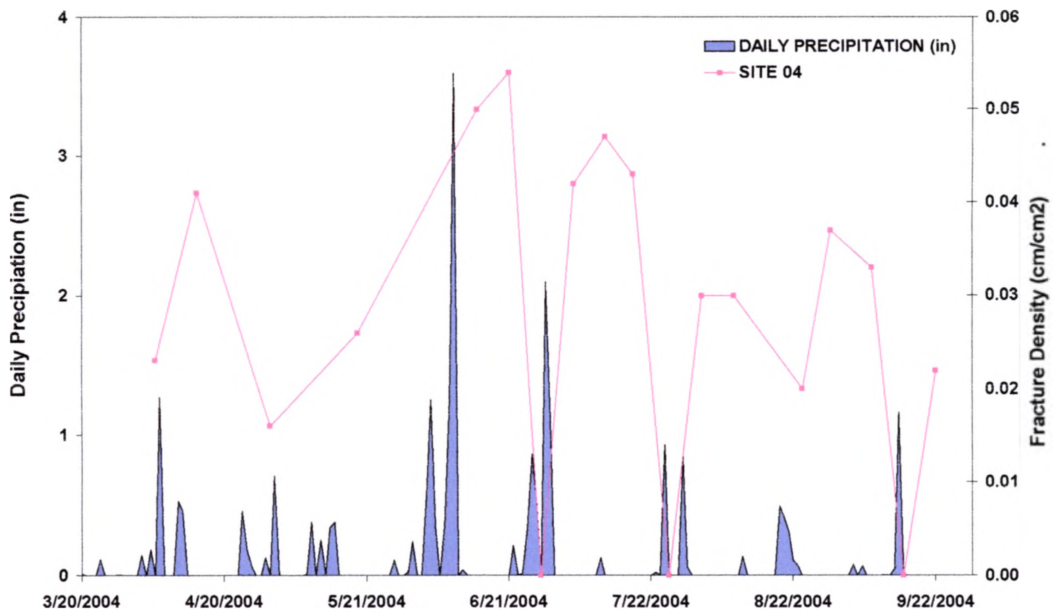

FIGURE 18. DAILY PRECIPITATION VERSUS FRACTURE DENSITY FOR SITE 04

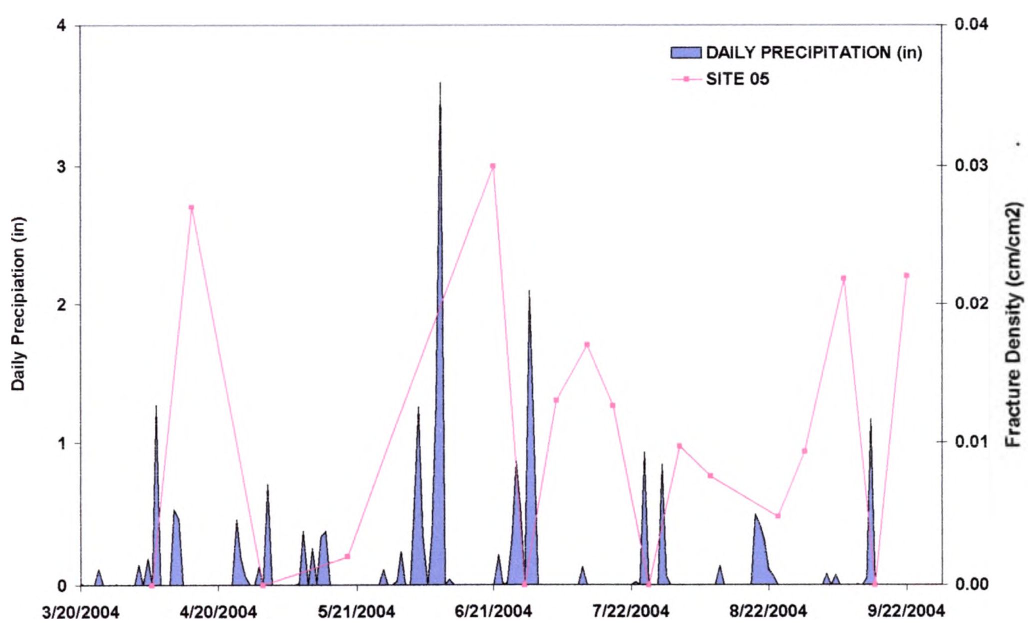

FIGURE 19. DAILY PRECIPITATION VERSUS FRACTURE DENSITY FOR SITE 05

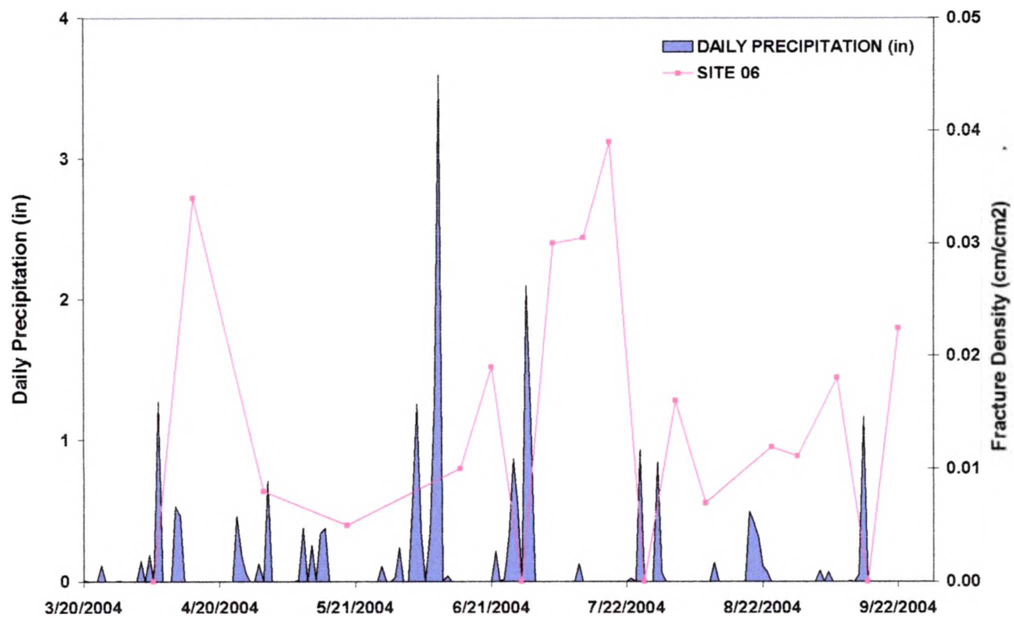

FIGURE 20. DAILY PRECIPITATION VERSUS FRACTURE DENSITY FOR SITE 06

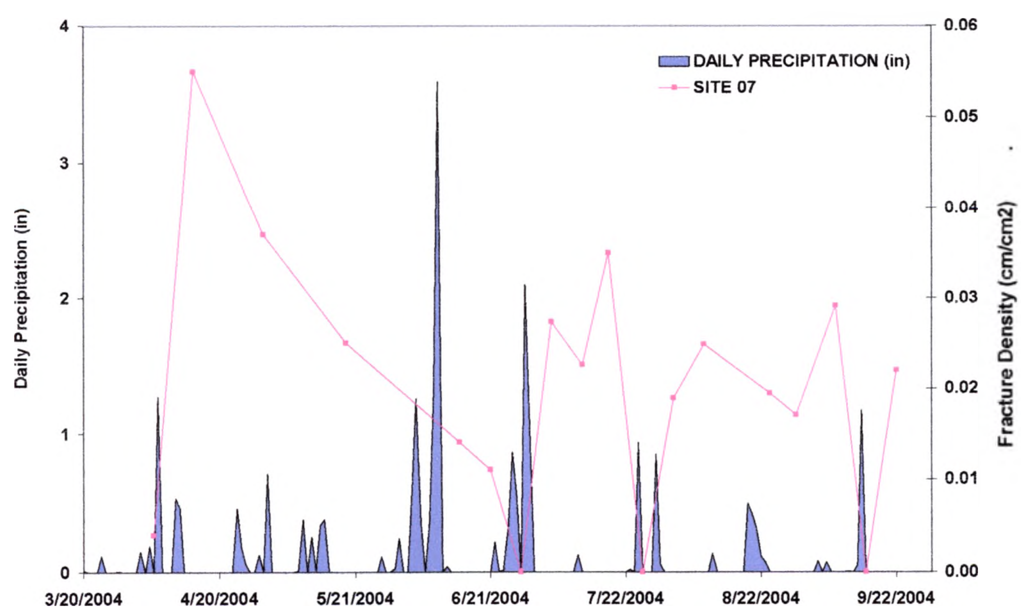

FIGURE 21. DAILY PRECIPITATION VERSUS FRACTURE DENSITY FOR SITE 07

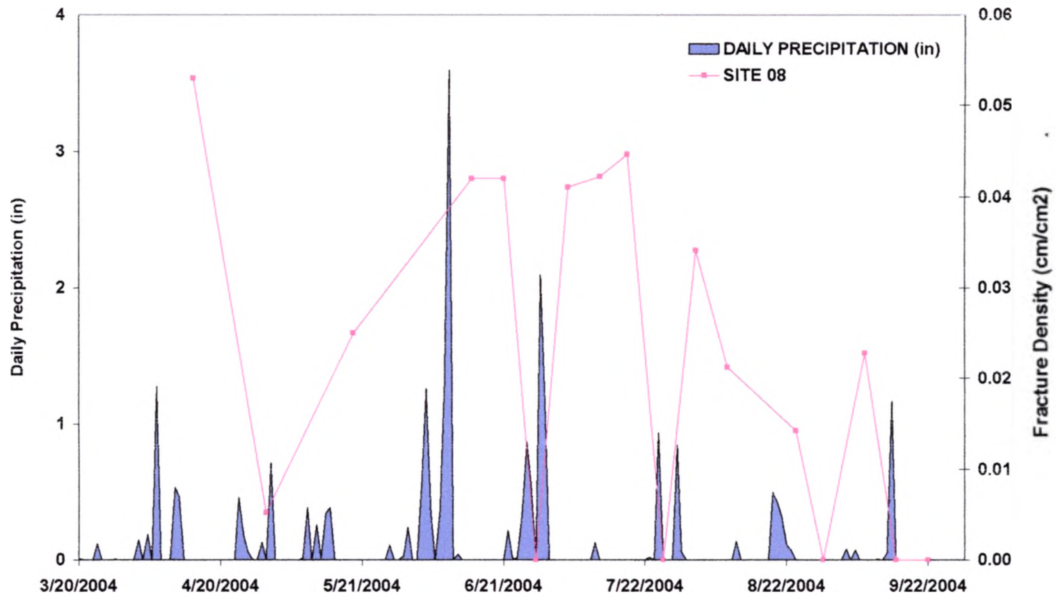

FIGURE 22. DAILY PRECIPITATION VERSUS FRACTURE DENSITY FOR SITE 08

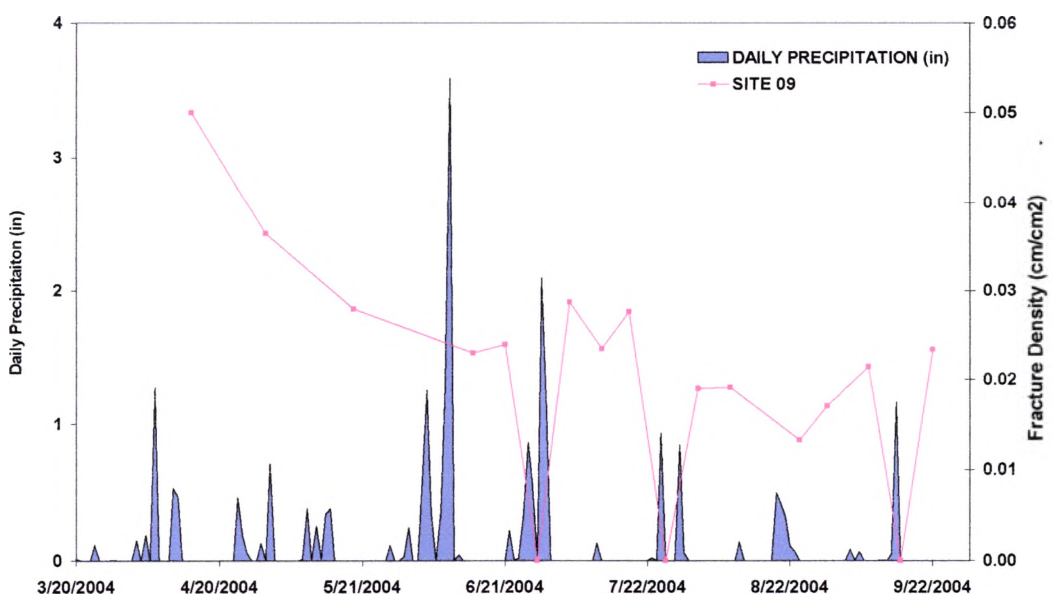

FIGURE 23. DAILY PRECIPITATION VERSUS FRACTURE DENSITY FOR SITE 09

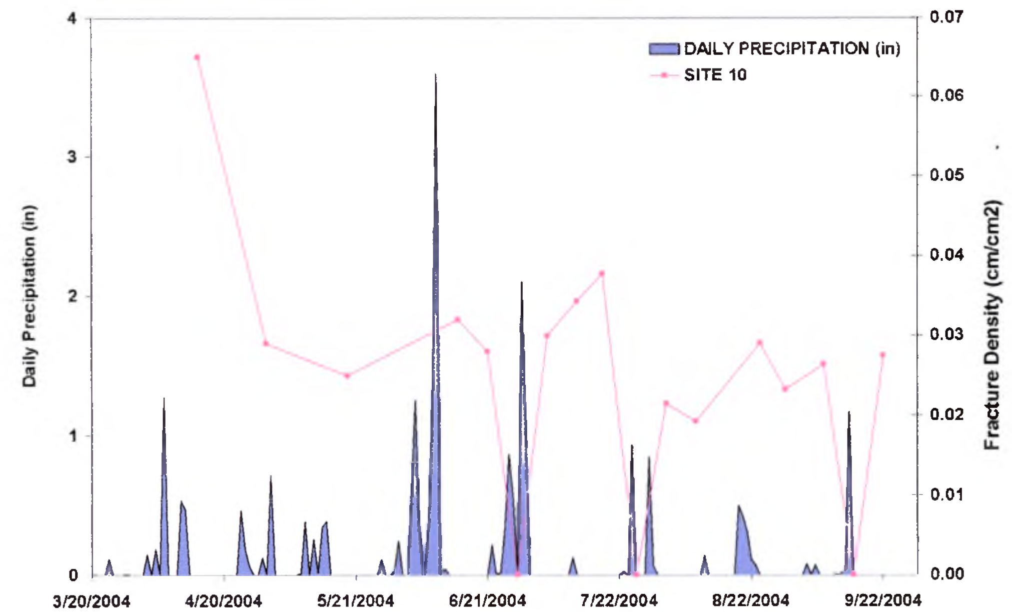

FIGURE 24. DAILY PRECIPITATION VERSUS FRACTURE DENSITY FOR SITE 10

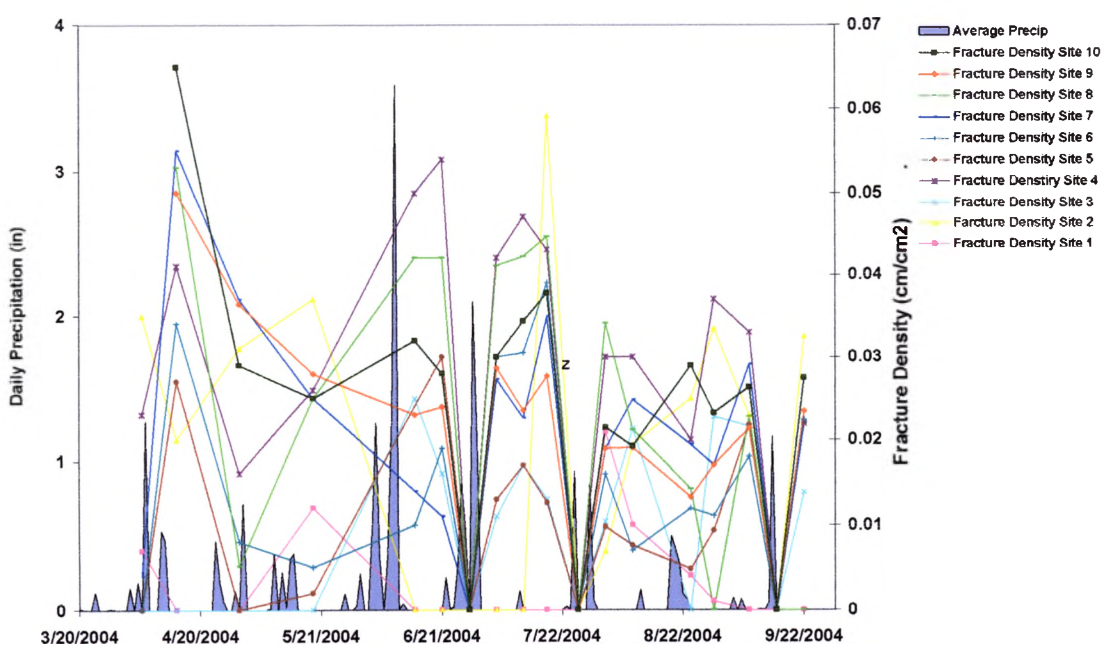

FIGURE 25. DAILY PRECIPITATION VERSUS FRACTURE DENSITY FOR ALL SITES

FRACTURE DENSITY VERSUS GRAVIMETRIC MOISTURE CONTENT

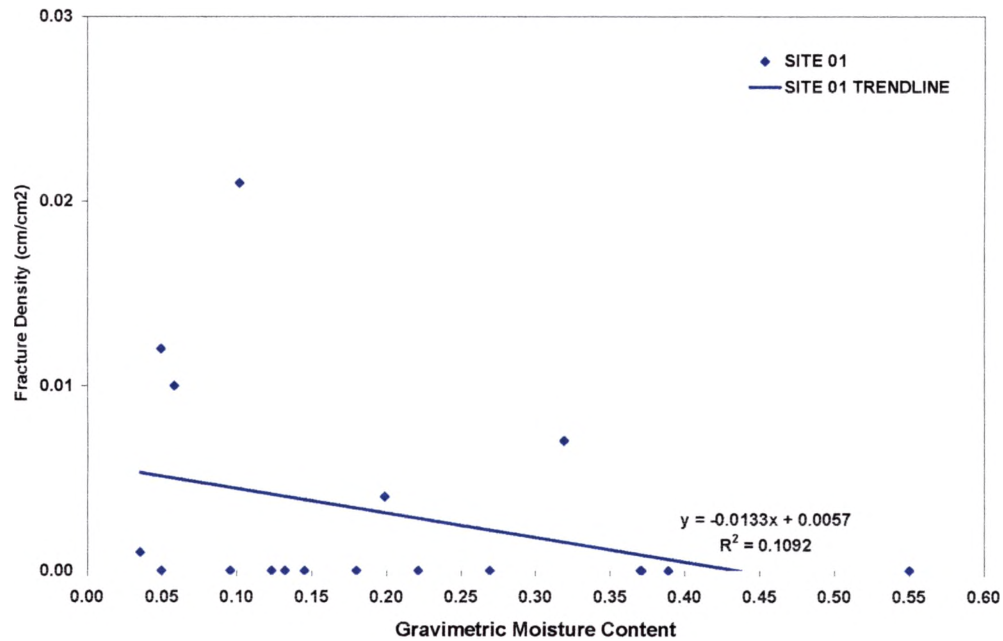

FIGURE 26. FRACTURE DENSITY VERSUS GRAVIMETRIC MOISTURE CONTENT FOR SITE 01

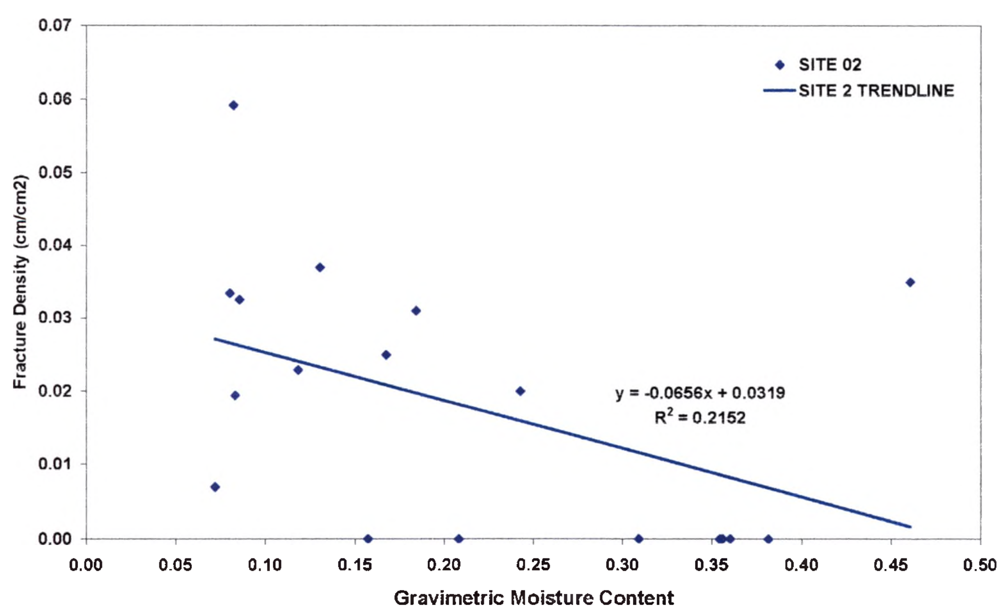

FIGURE 27. FRACTURE DENSITY VERSUS GRAVIMETRIC MOISTURE CONTENT FOR SITE 02

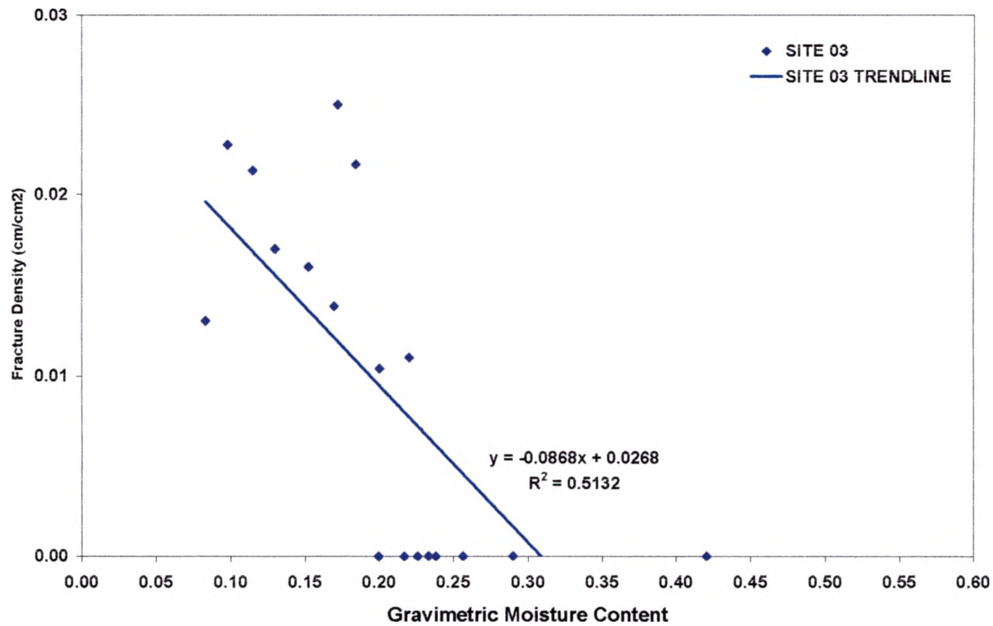

FIGURE 28. FRACTURE DENSITY VERSUS GRAVIMETRIC MOISTURE CONTENT FOR SITE 03

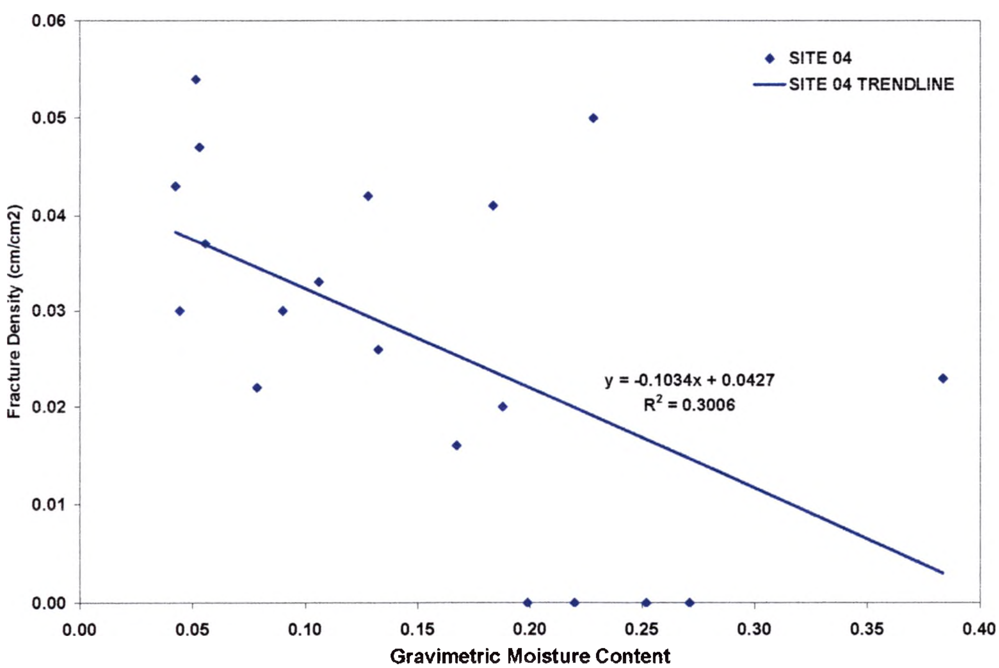

FIGURE 29. FRACTURE DENSITY VERSUS GRAVIMETRIC MOISTURE CONTENT FOR SITE 04

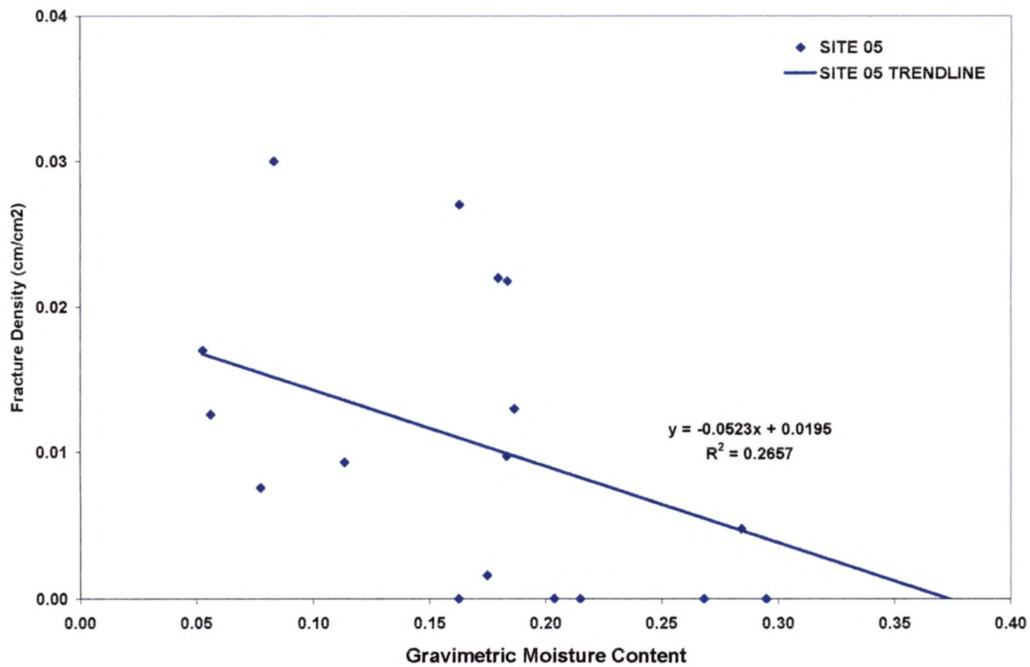

FIGURE 30. FRACTURE DENSITY VERSUS GRAVIMETRIC MOISTURE CONTENT FOR SITE 05

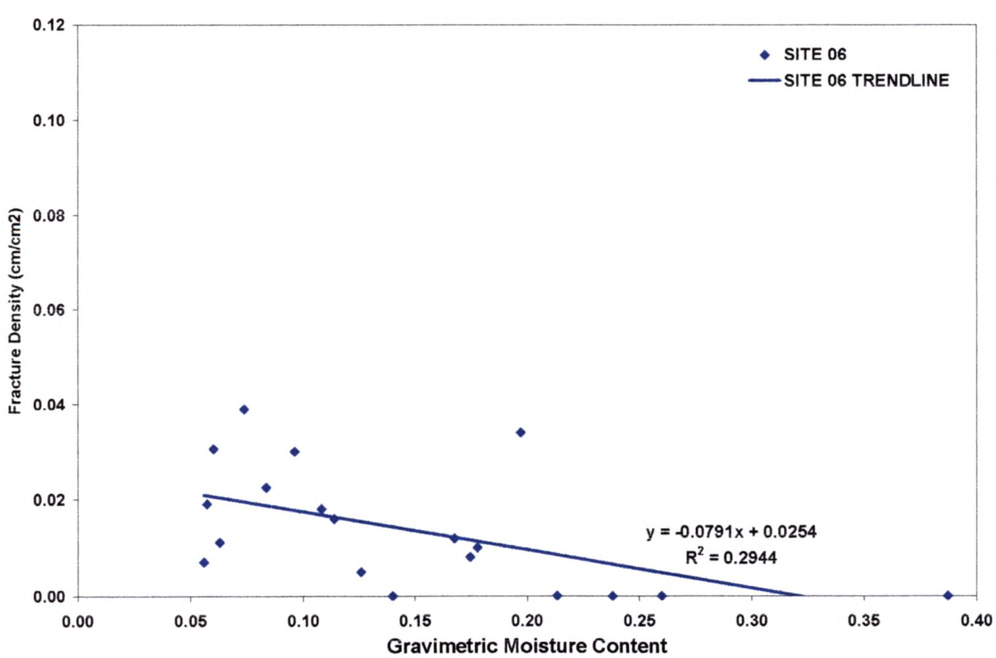

FIGURE 31. FRACTURE DENSITY VERSUS GRAVIMETRIC MOISTURE CONTENT FOR SITE 06

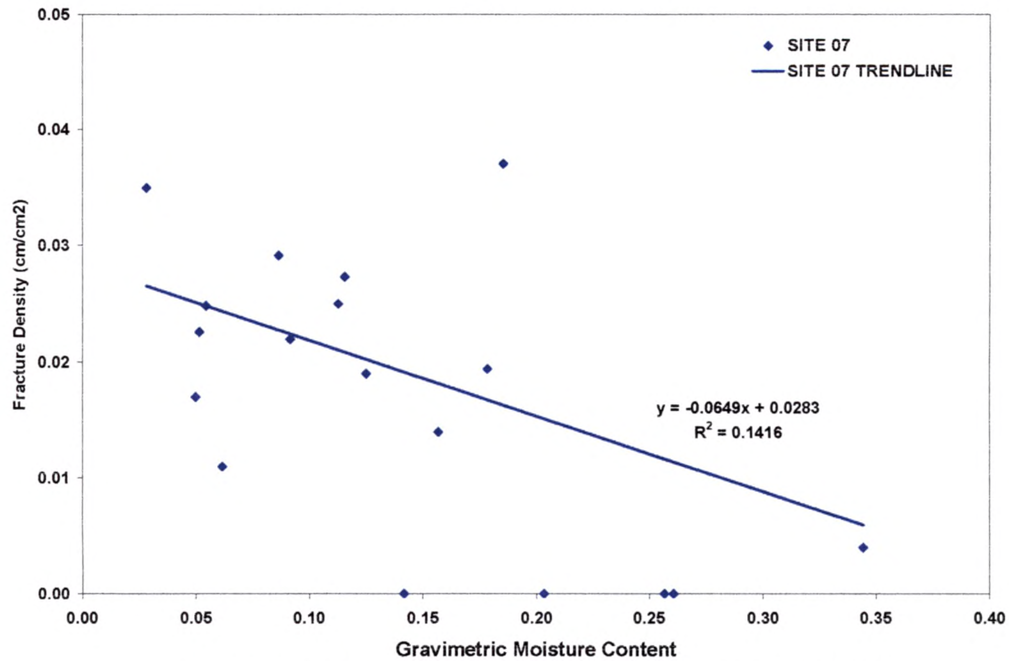

FIGURE 32. FRACTURE DENSITY VERSUS GRAVIMETRIC MOISTURE CONTENT FOR SITE 07

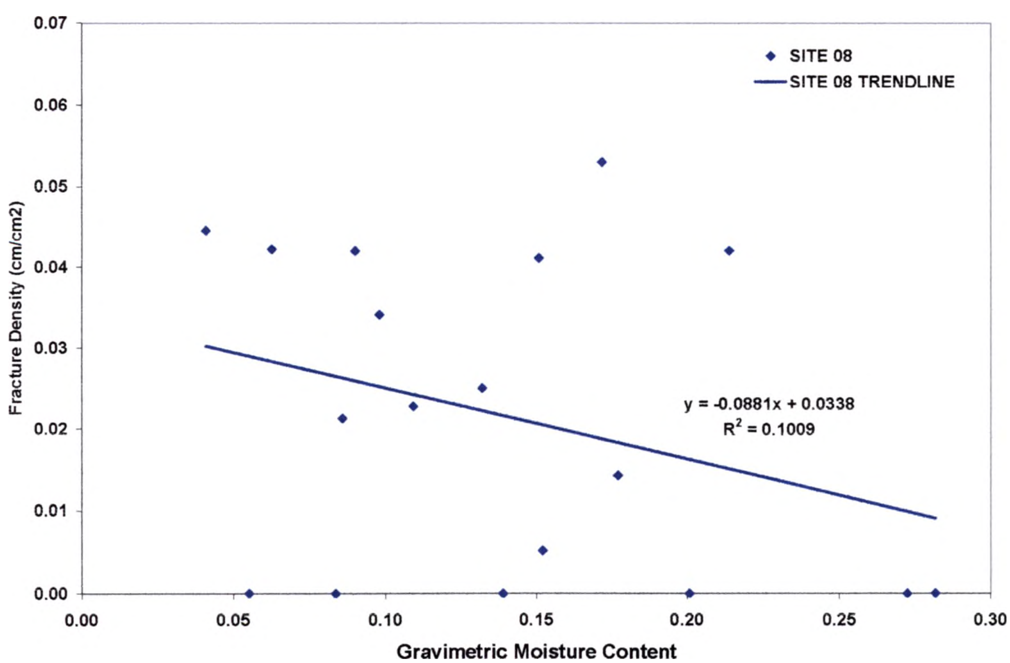

FIGURE 33. FRACTURE DENSITY VERSUS GRAVIMETRIC MOISTURE CONTENT FOR SITE 08

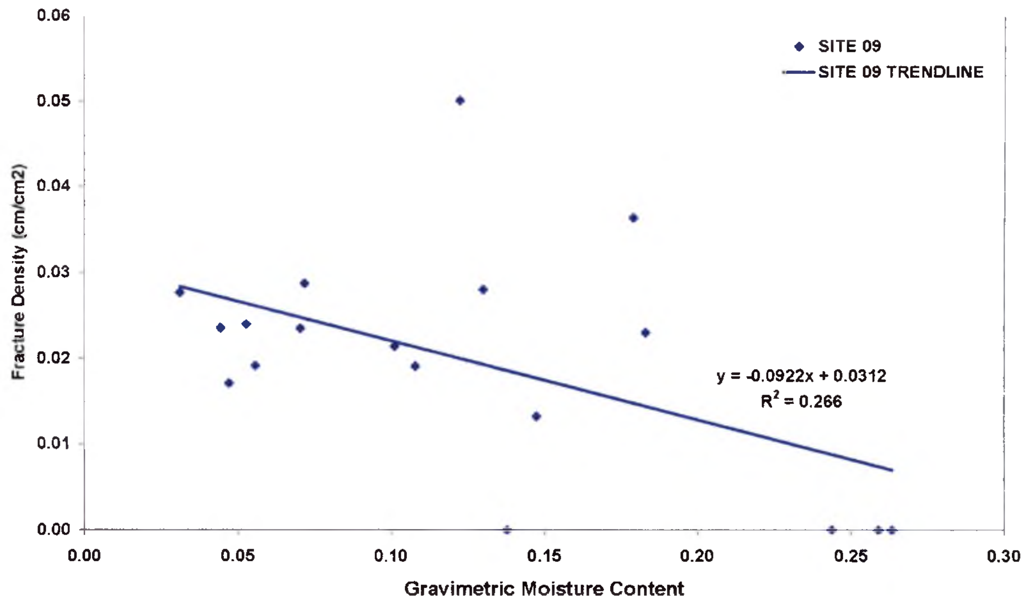

FIGURE 34. FRACTURE DENSITY VERSUS GRAVIMETRIC MOISTURE CONTENT FOR SITE 09

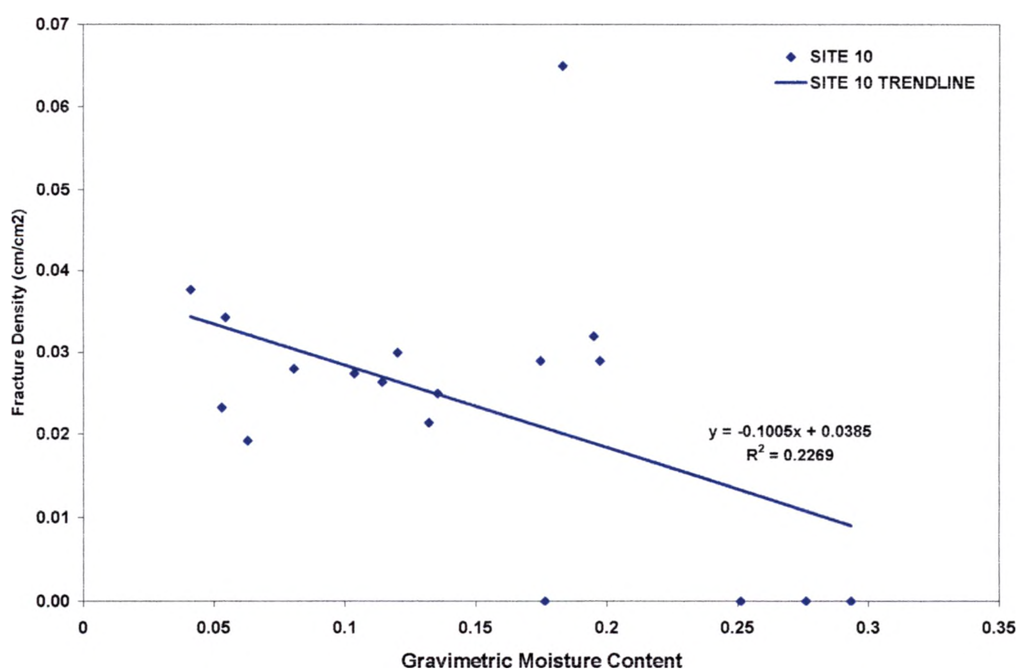

FIGURE 35. FRACTURE DENSITY VERSUS GRAVIMETRIC MOISTURE CONTENT FOR SITE 10

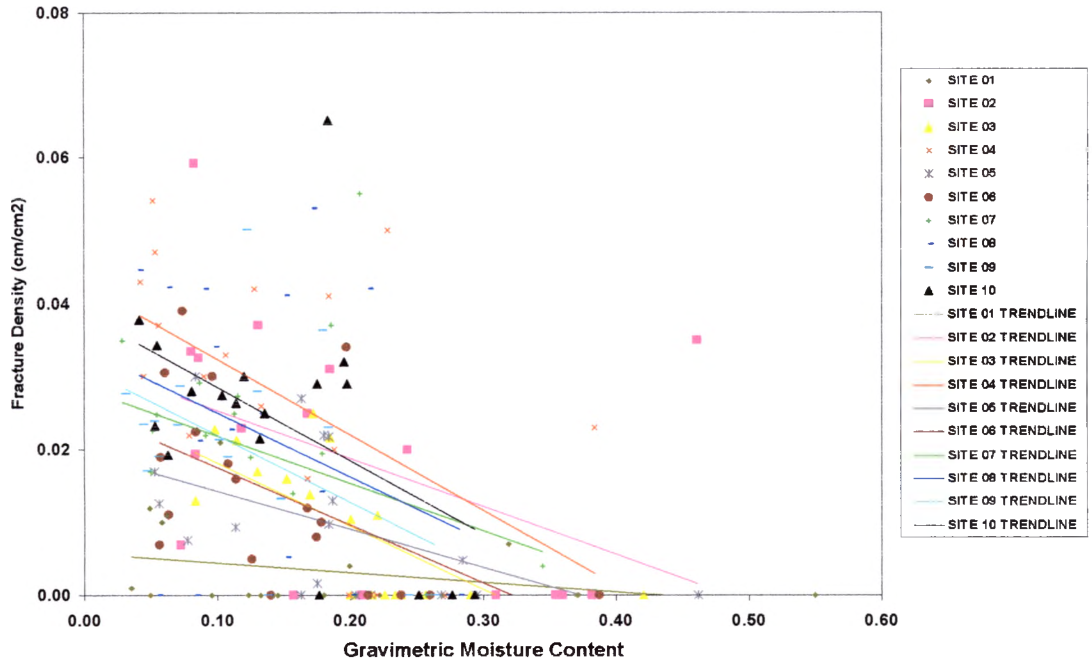

FIGURE 36. FRACTURE DENSITY VERSUS GRAVIMETRIC MOISTURE CONTENT FOR ALL SITES

FRACTURE DENSITY VERSUS GRAVIMETRIC MOISTURE CONTENT SAMPLED ON A WEEKLY BASIS

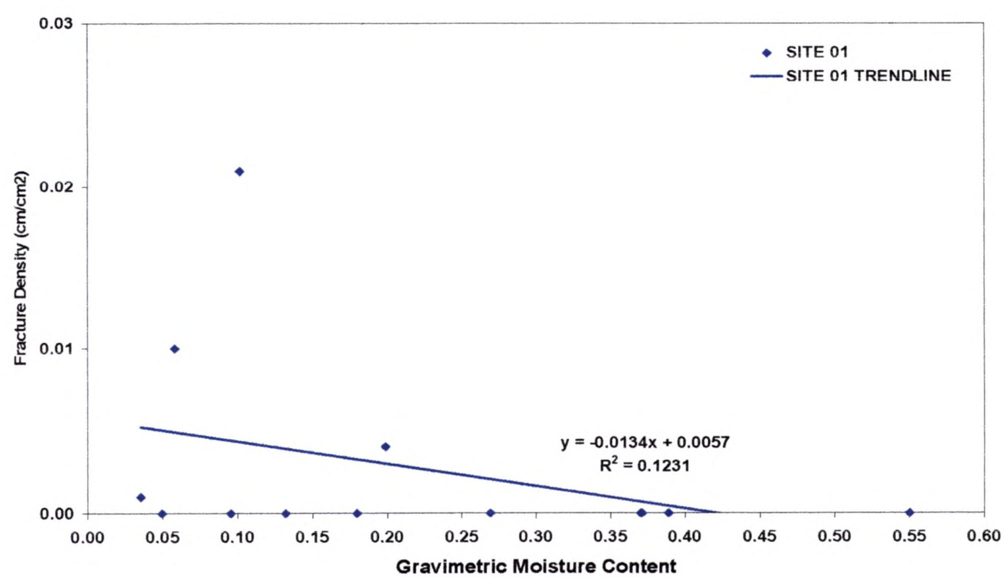

FIGURE 37. FRACTURE DENSITY VERSUS GRAVIMETRIC MOISTURE CONTENT FOR SITE 01

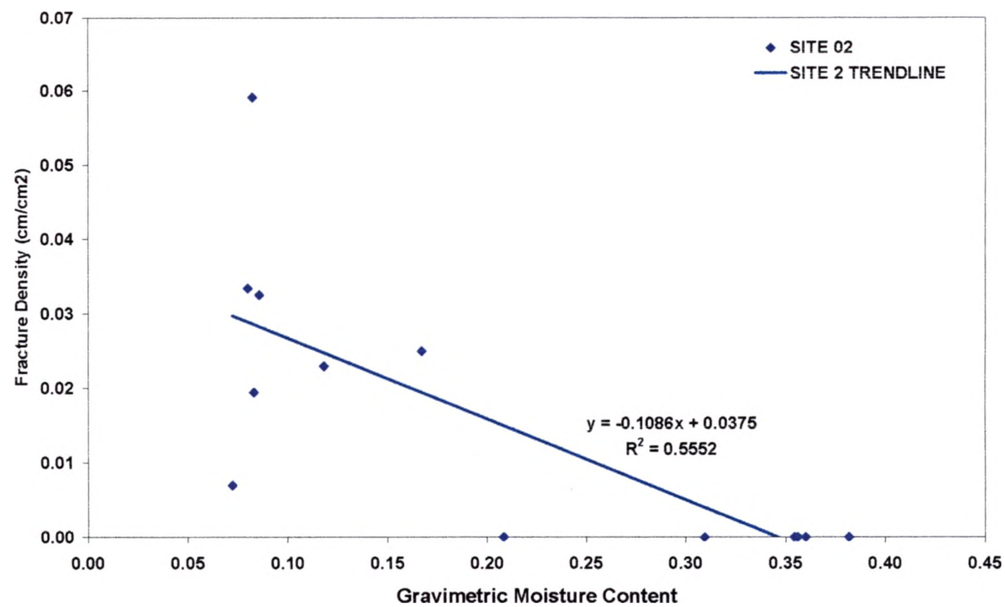

FIGURE 38. FRACTURE DENSITY VERSUS GRAVIMETRIC MOISTURE CONTENT FOR SITE 02

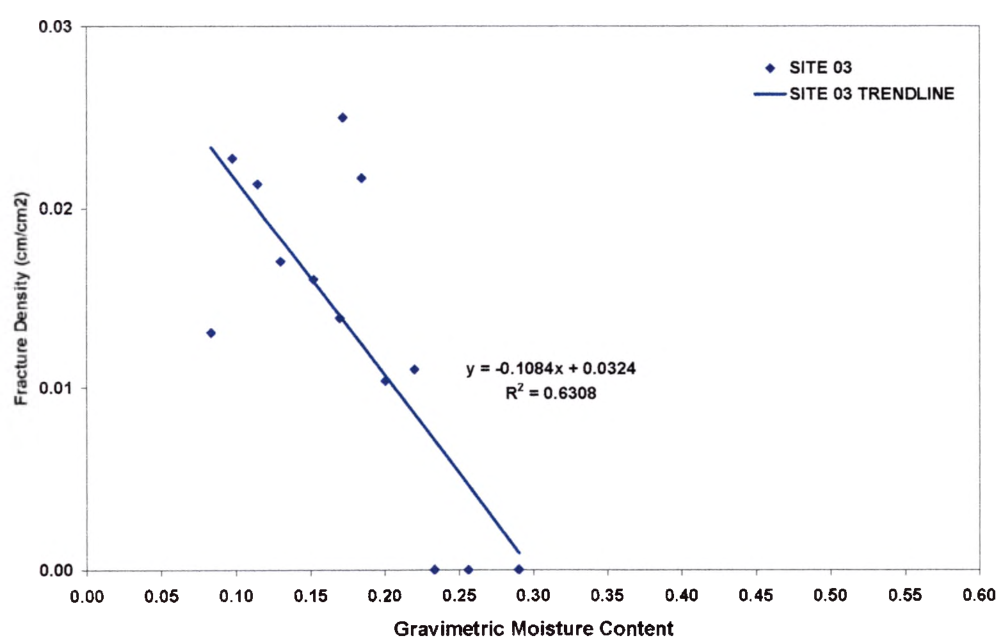

FIGURE 39. FRACTURE DENSITY VERSUS GRAVIMETRIC MOISTURE CONTENT FOR SITE 03

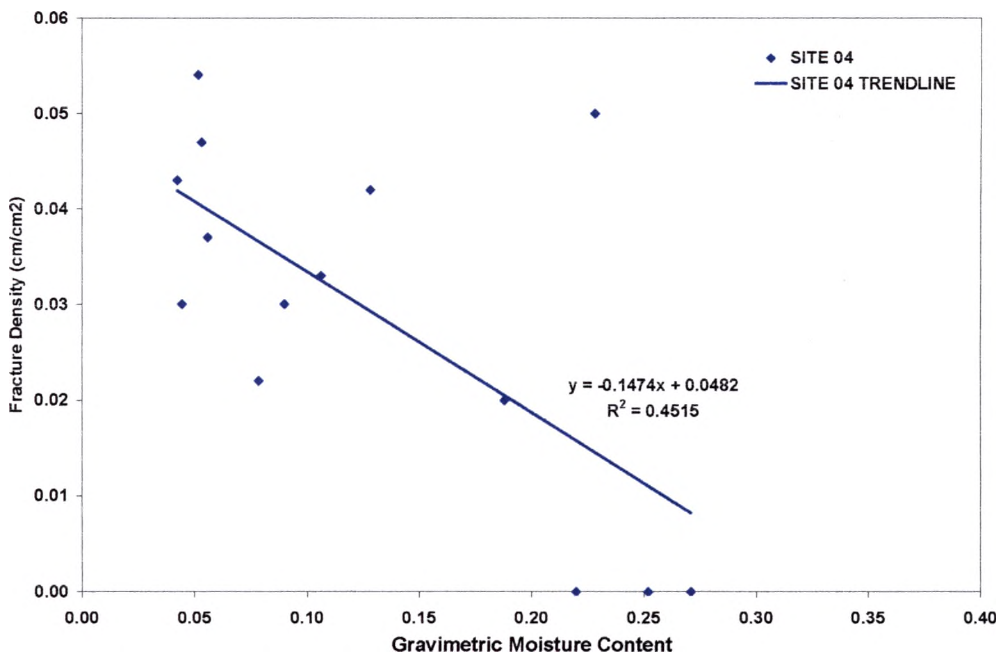

FIGURE 40. FRACTURE DENSITY VERSUS GRAVIMETRIC MOISTURE CONTENT FOR SITE 04

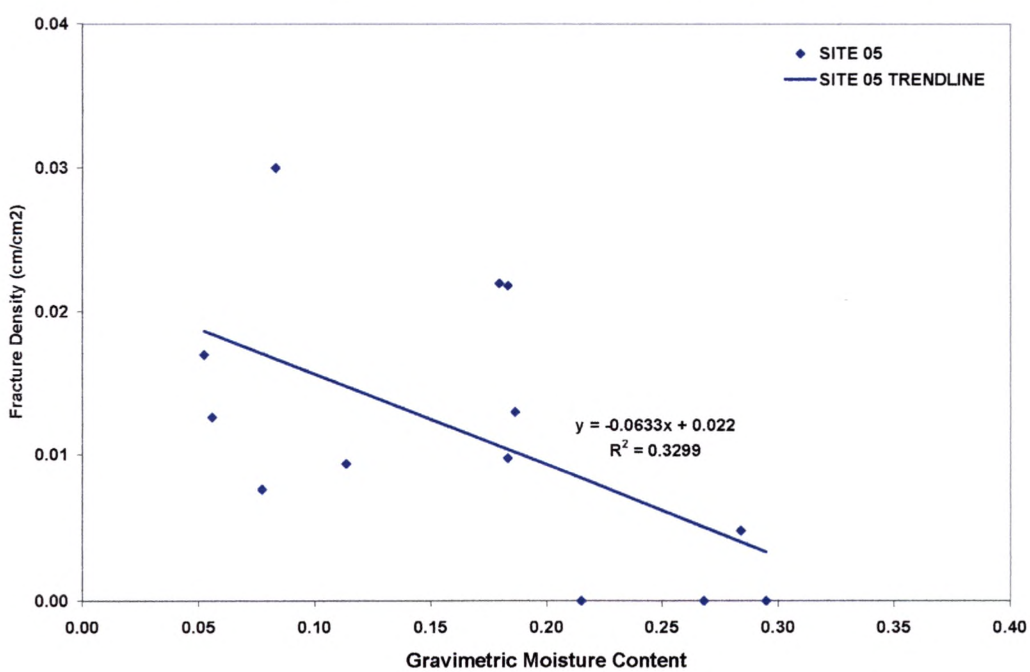

FIGURE 41. FRACTURE DENSITY VERSUS GRAVIMETRIC MOISTURE CONTENT FOR SITE 05

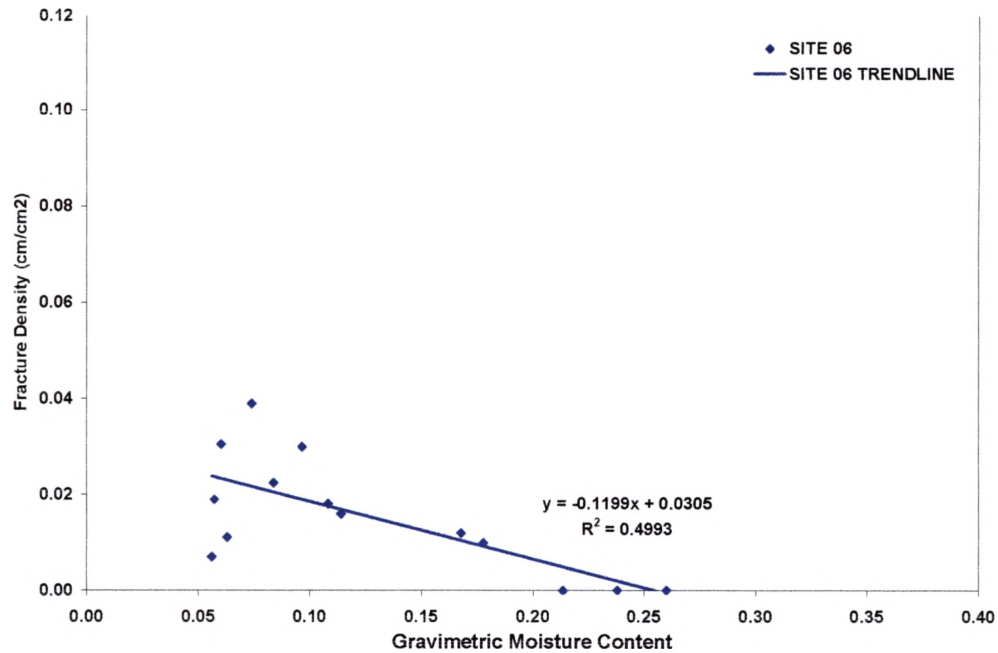

FIGURE 42. FRACTURE DENSITY VERSUS GRAVIMETRIC MOISTURE CONTENT FOR SITE 06

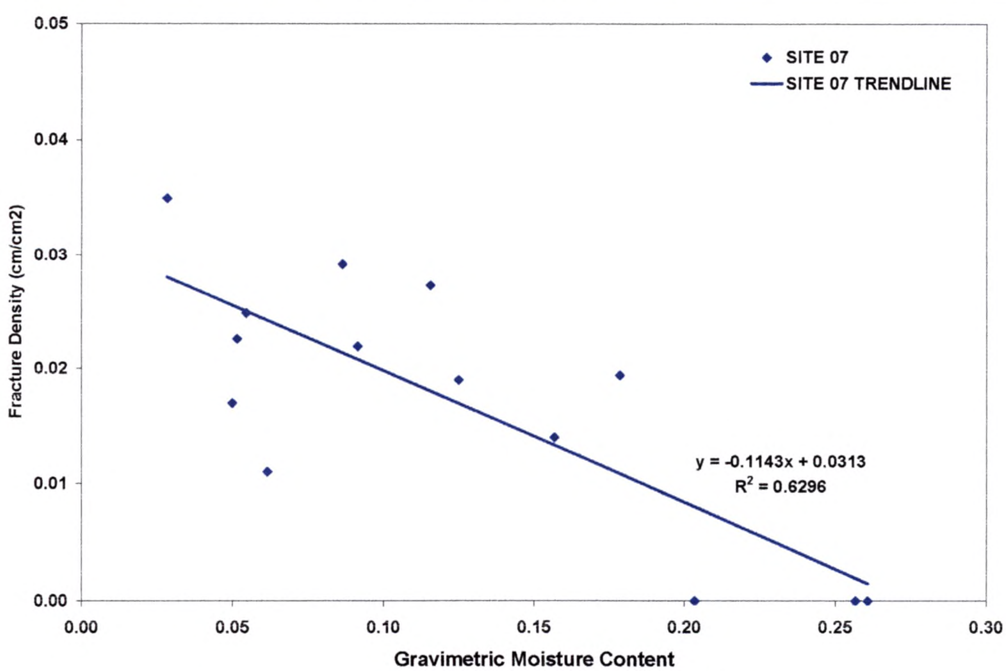

FIGURE 43. FRACTURE DENSITY VERSUS GRAVIMETRIC MOISTURE CONTENT FOR SITE 07

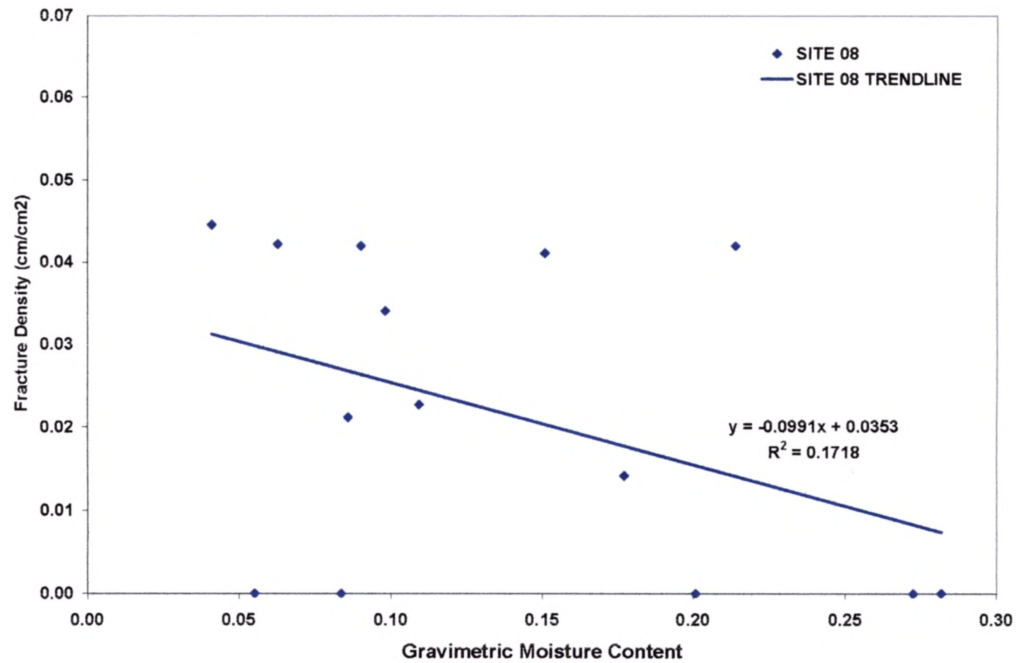

FIGURE 44. FRACTURE DENSITY VERSUS GRAVIMETRIC MOISTURE CONTENT FOR SITE 08

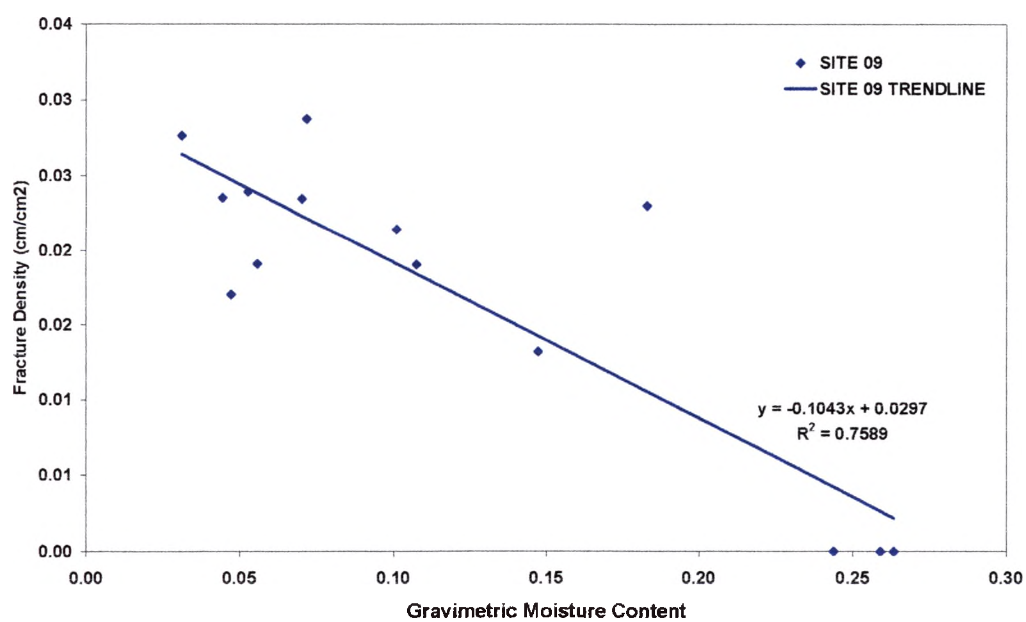

FIGURE 45. FRACTURE DENSITY VERSUS GRAVIMETRIC MOISTURE CONTENT FOR SITE 09

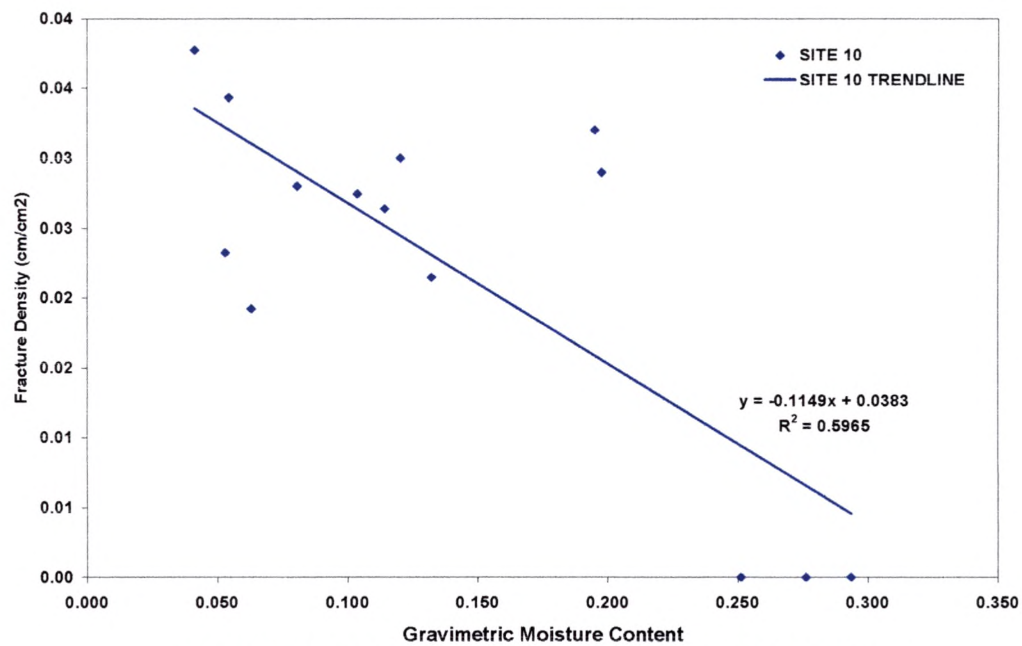

FIGURE 46. FRACTURE DENSITY VERSUS GRAVIMETRIC MOISTURE CONTENT FOR SITE 10

MOISTURE CONTENT RANGES THROUGHOUT STUDY PERIOD

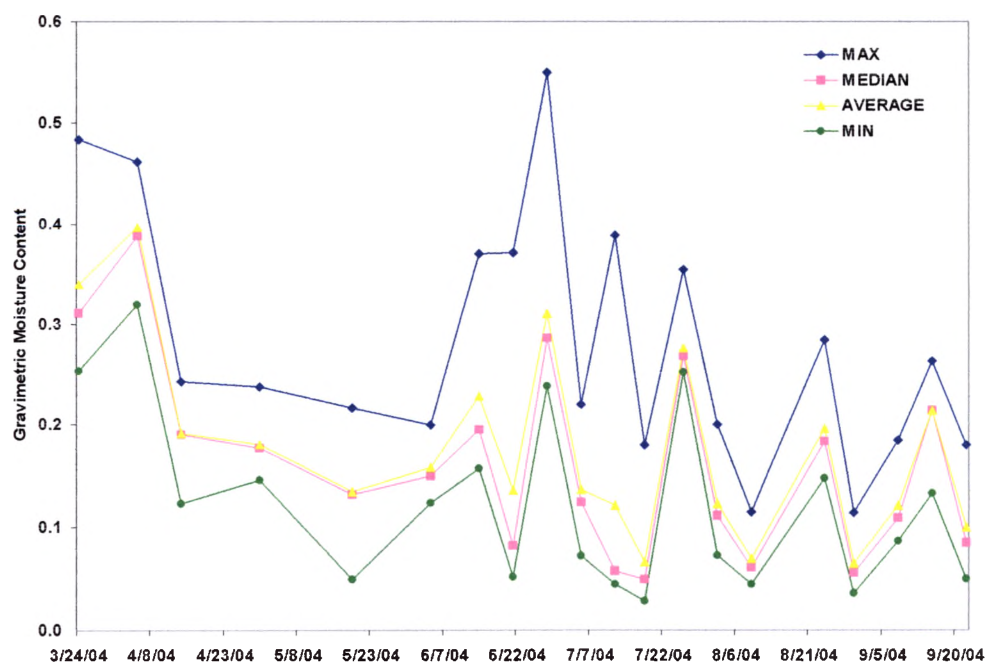

FIGURE 47. MOISTURE CONTENT RANGES THROUGHOUT STUDY PERIOD

DAILY TEMPERATURE VERSUS GRAVIMETRIC MOISTURE CONTENT

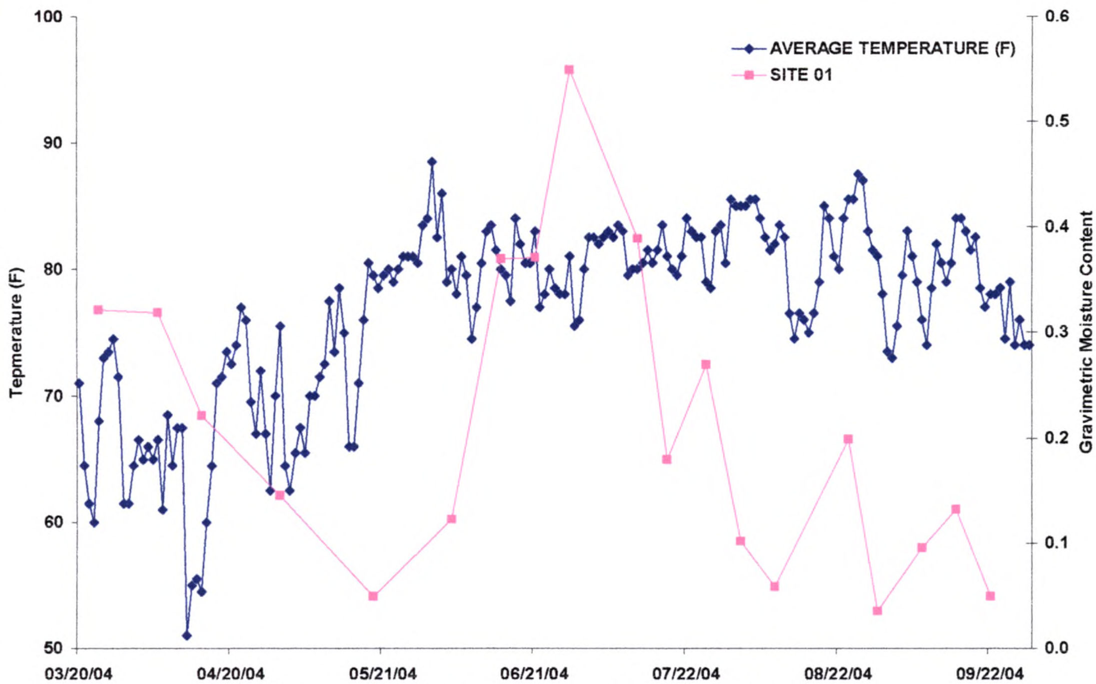

FIGURE 48. TEMPERATURE VERSUS GRAVIMETRIC MOISTURE CONTENT FOR SITE 01

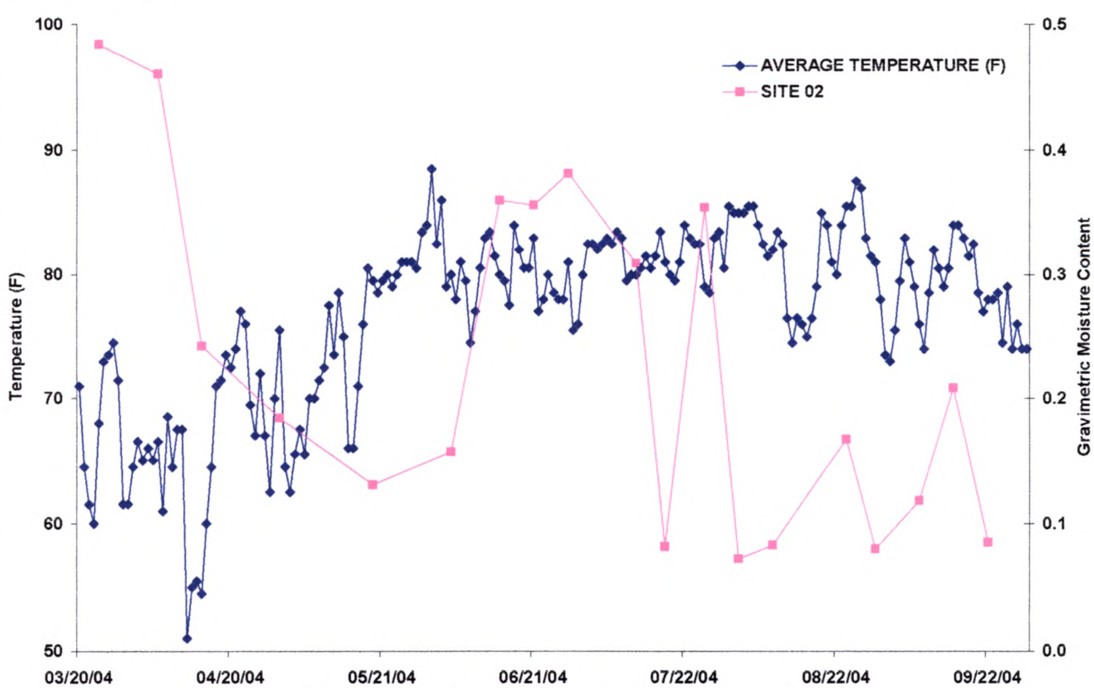

FIGURE 49. TEMPERATURE VERSUS GRAVIMETRIC MOISTURE CONTENTS FOR SITE 02

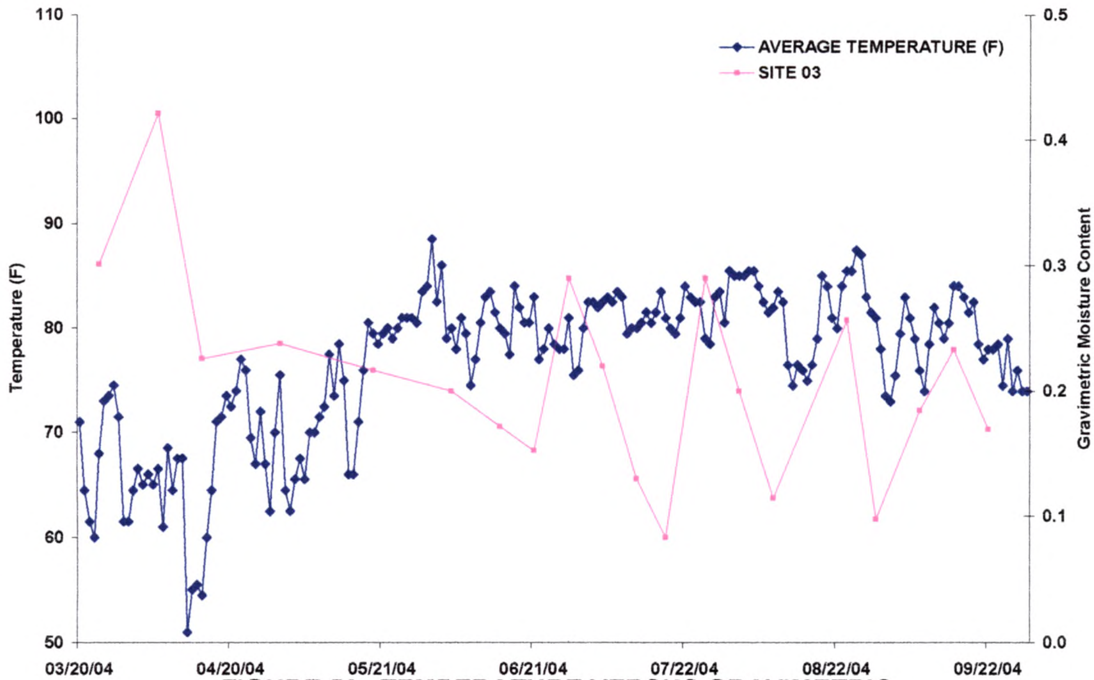

FIGURE 50. TEMPERATURE VERSUS GRAVIMETRIC MOISTURE CONTENTS FOR SITE 03

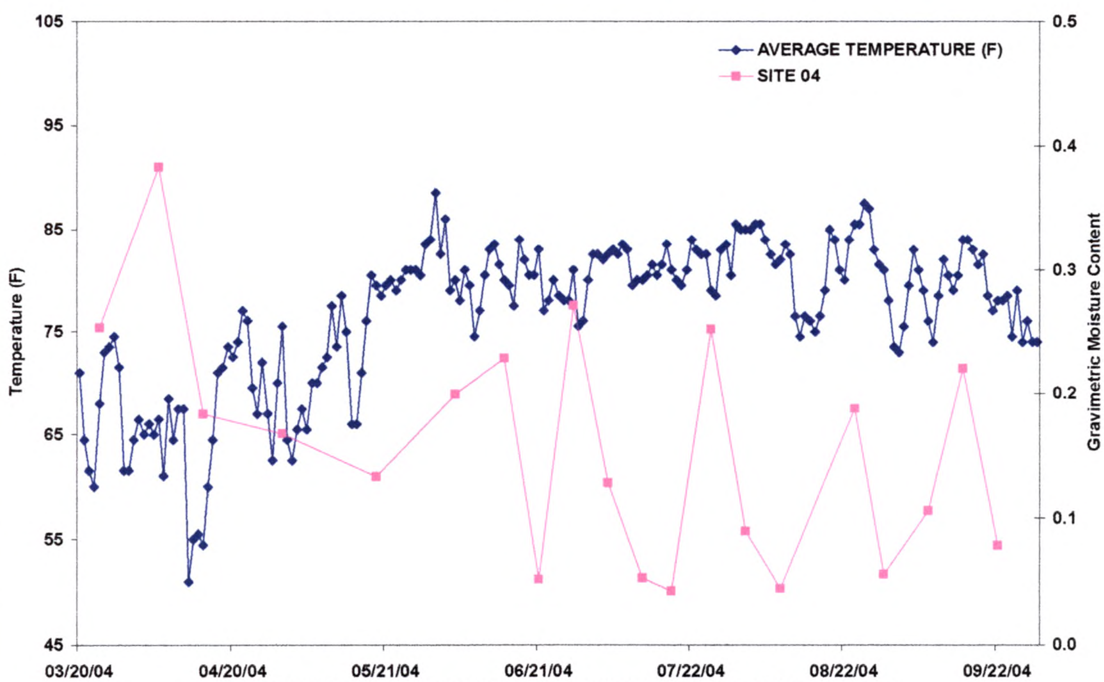

FIGURE 51. TEMPERATURE VERSUS GRAVIMETRIC MOISTURE CONTENTS FOR SITE 04

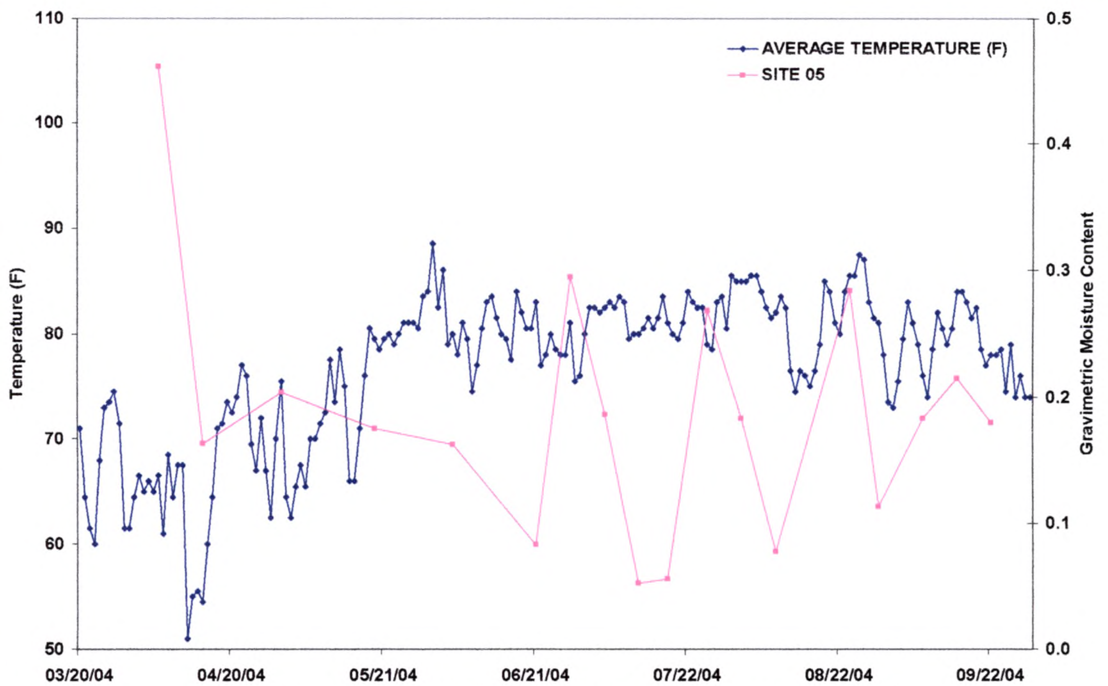

FIGURE 52. TEMPERATURE VERSUS GRAVIMETRIC MOISTURE CONTENTS FOR SITE 05

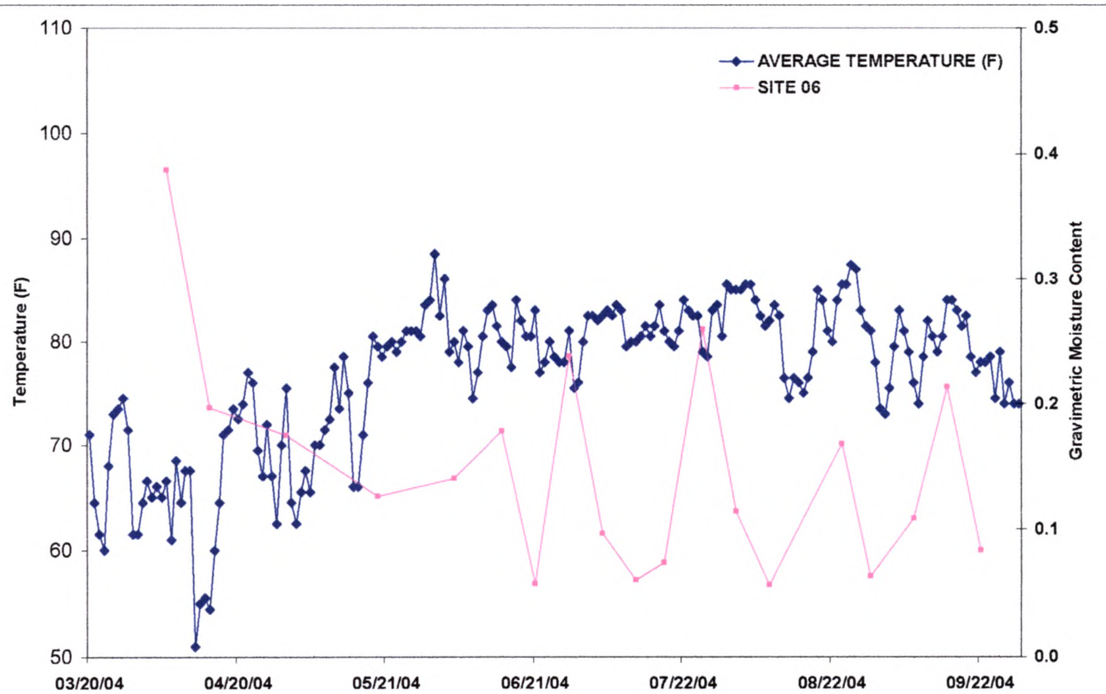

FIGURE 53. TEMPERATURE VERSUS GRAVIMETRIC MOISTURE CONTENTS FOR SITE 06

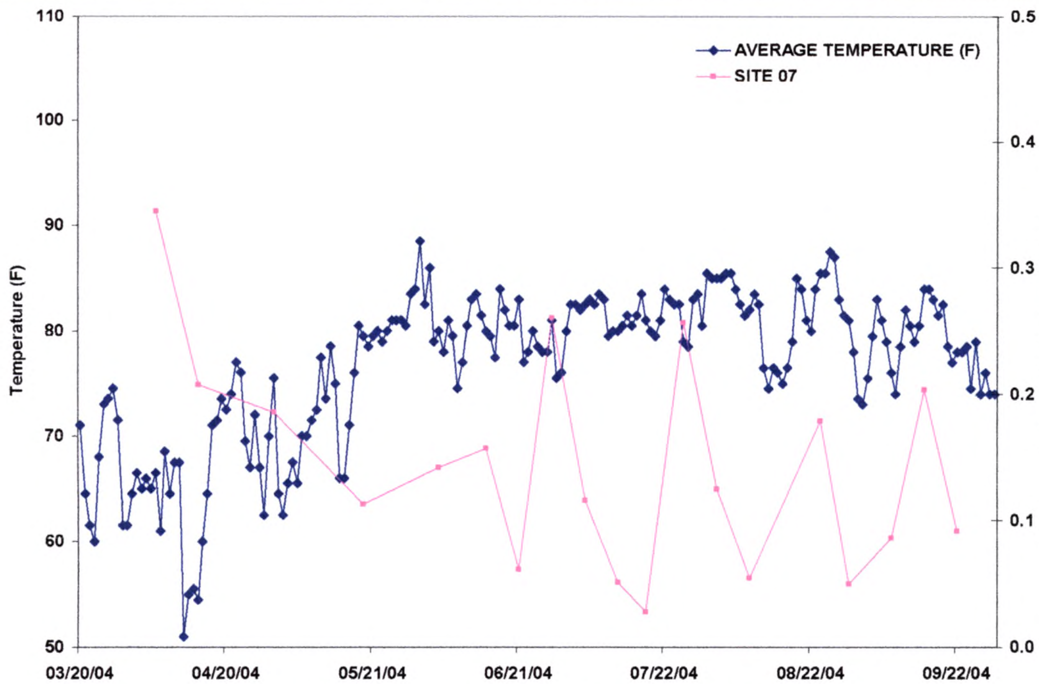

FIGURE 54. TEMPERATURE VERSUS GRAVIMETRIC MOISTURE CONTENTS FOR SITE 07

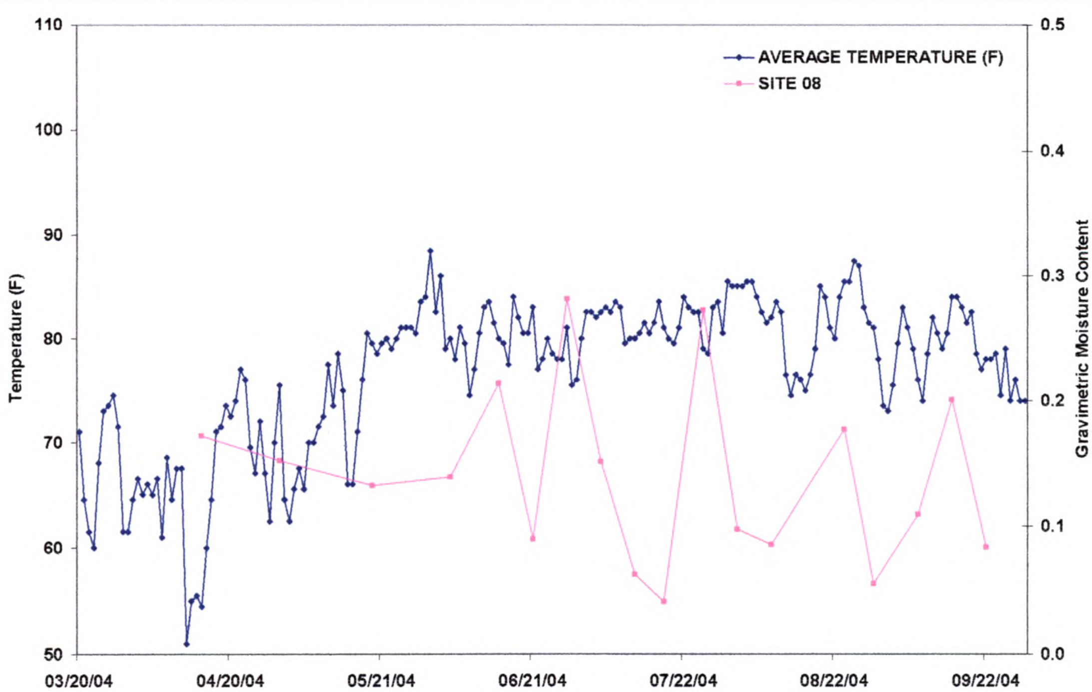

FIGURE 55. TEMPERATURE VERSUS GRAVIMETRIC MOISTURE CONTENTS FOR SITE 08

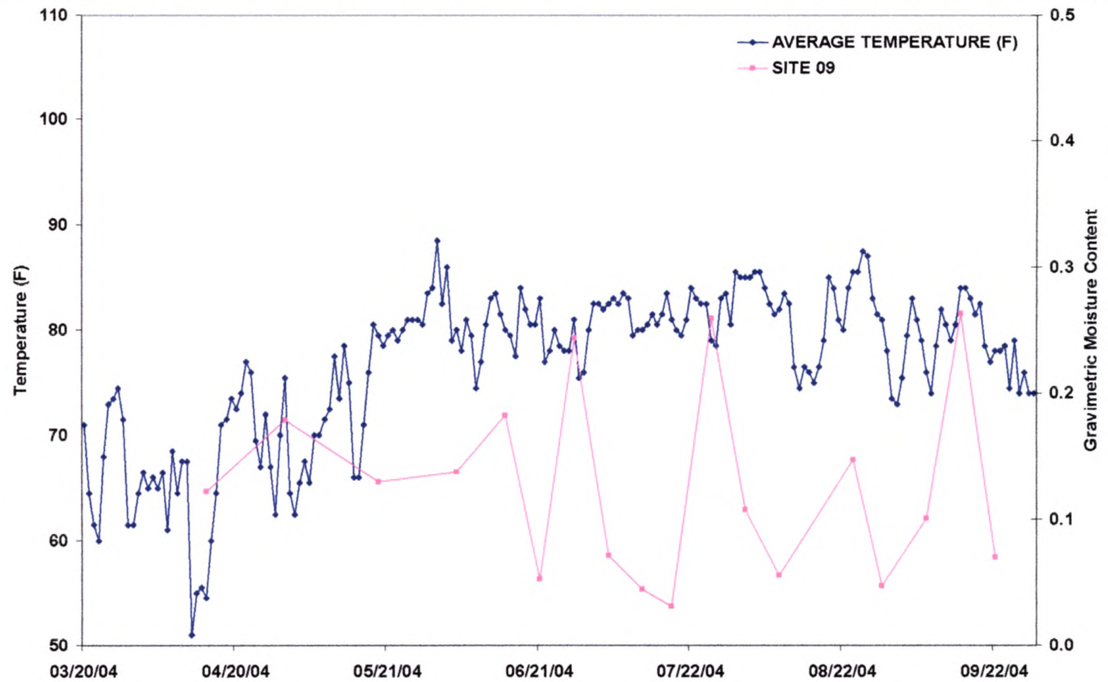

FIGURE 56. TEMPERATURE VERSUS GRAVIMETRIC MOISTURE CONTENT FOR SITE 09

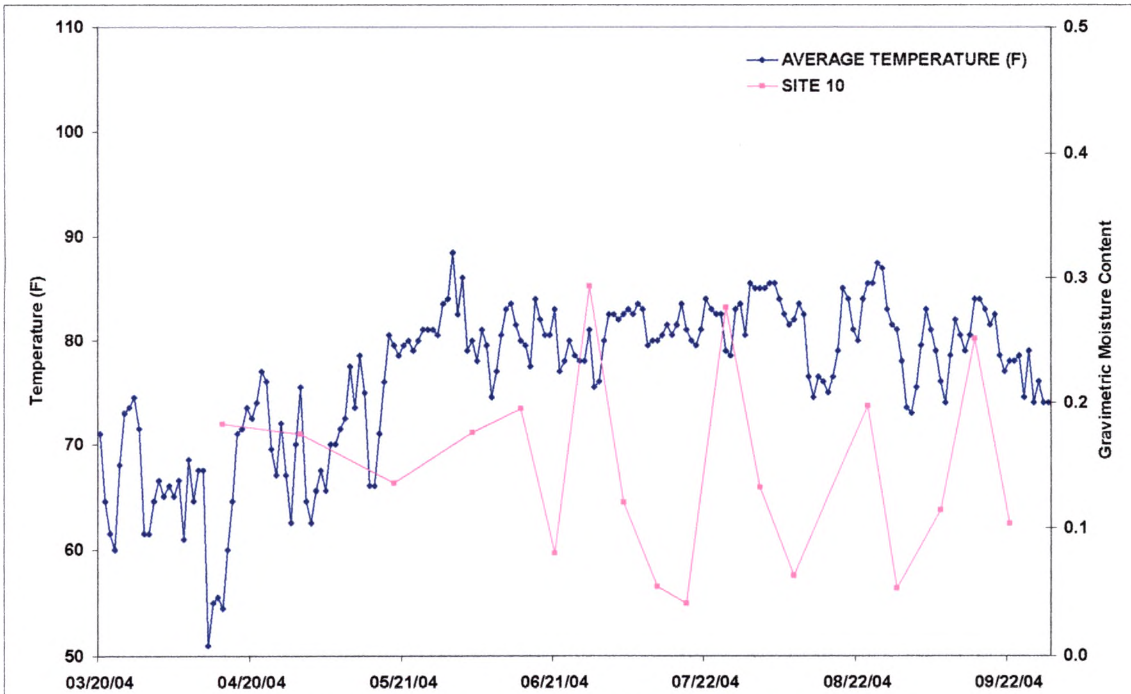

FIGURE 57. TEMPERATURE VERSUS GRAVIMETRIC MOISTURE CONTENTS FOR SITE 10

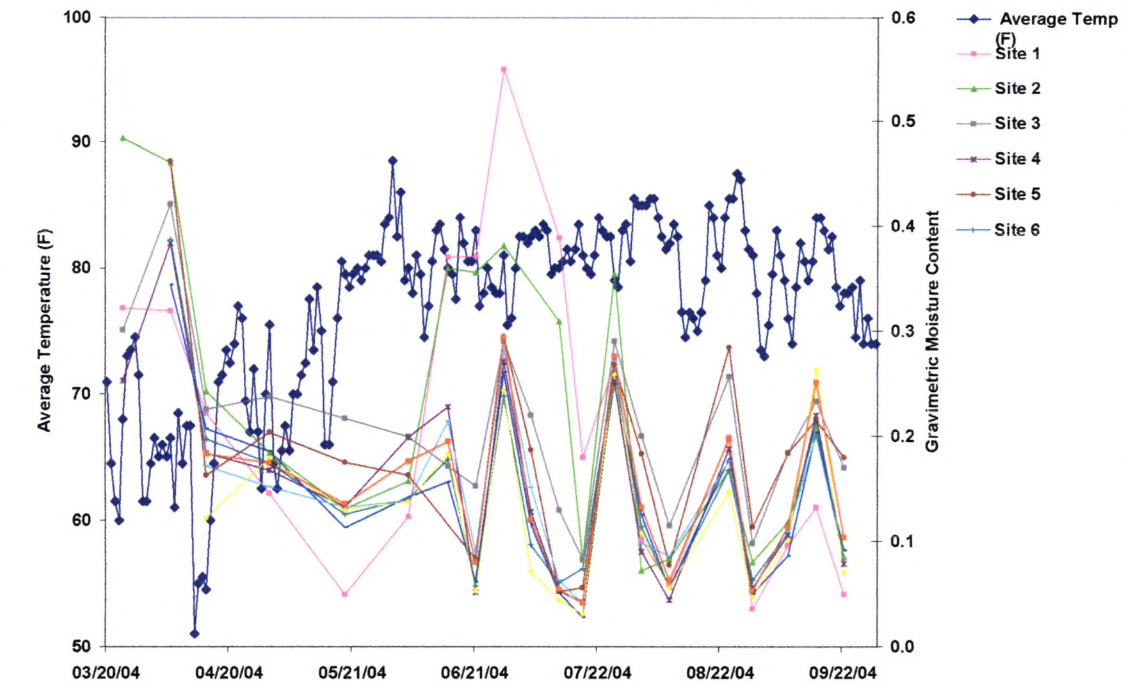

Figure 58. TEMPERATURE VERSUS GRAVIMETRIC MOISTURE CONTENTS FOR ALL SITES

DAILY PRECIPITATION VERSUS GRAVIMETRIC MOISTURE CONTENT

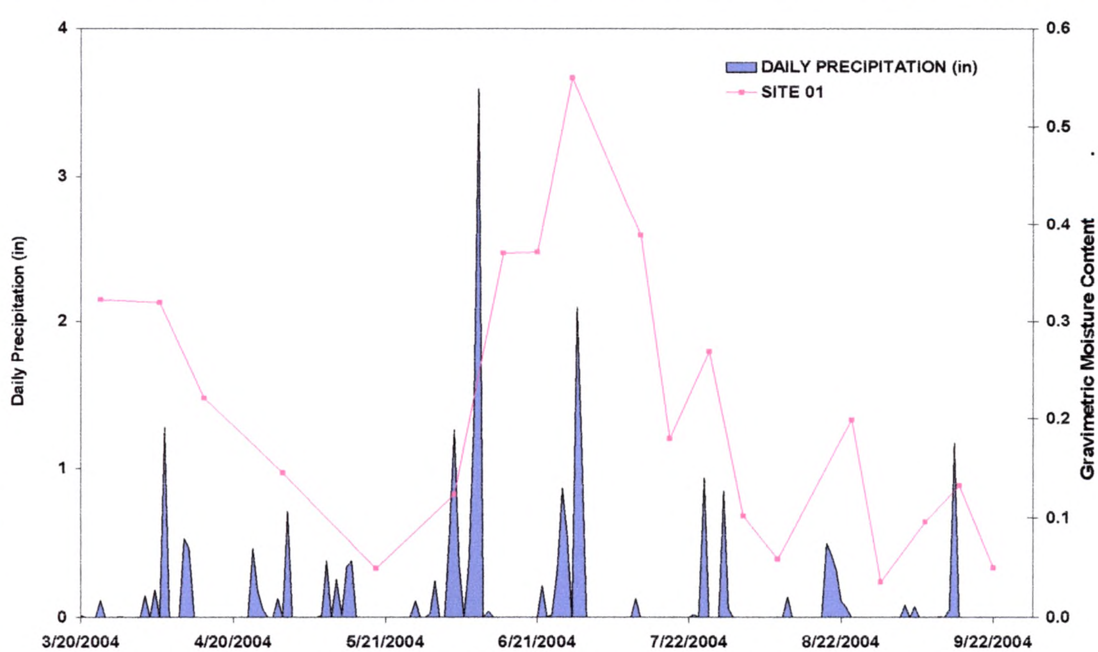

FIGURE 59. DAILY PRECIPITATION VERSUS GRAVIMETRIC MOISTURE CONTENTS FOR SITE 01

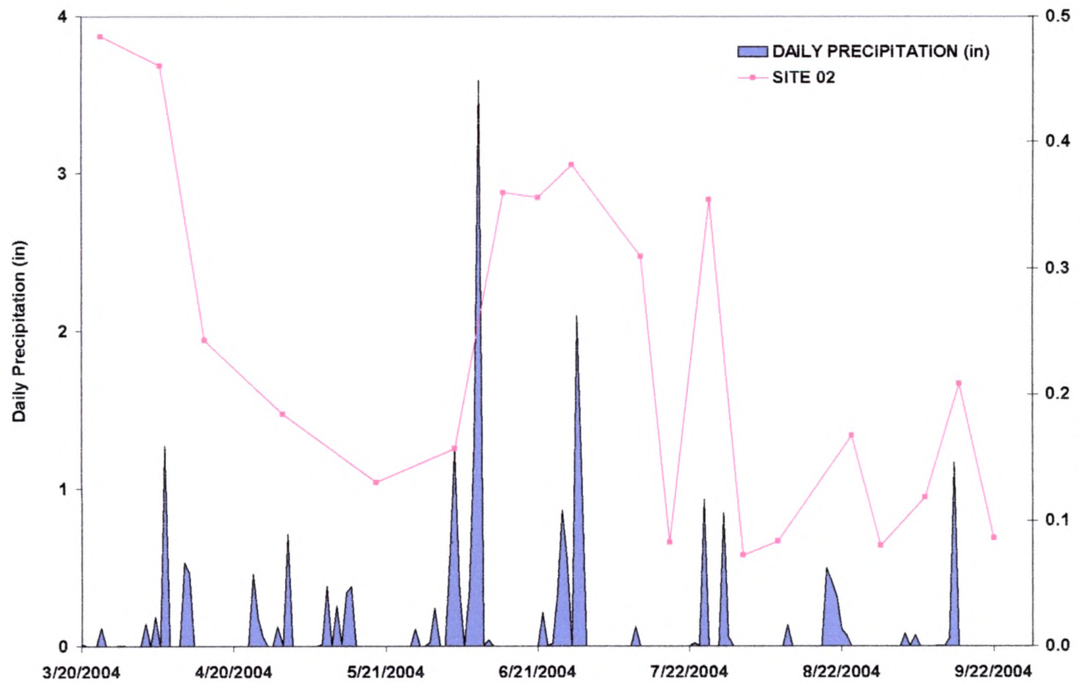

FIGURE 60. DAILY PRECIPITATION VERSUS GRAVIMETRIC MOISTURE CONTENTS FOR SITE 02

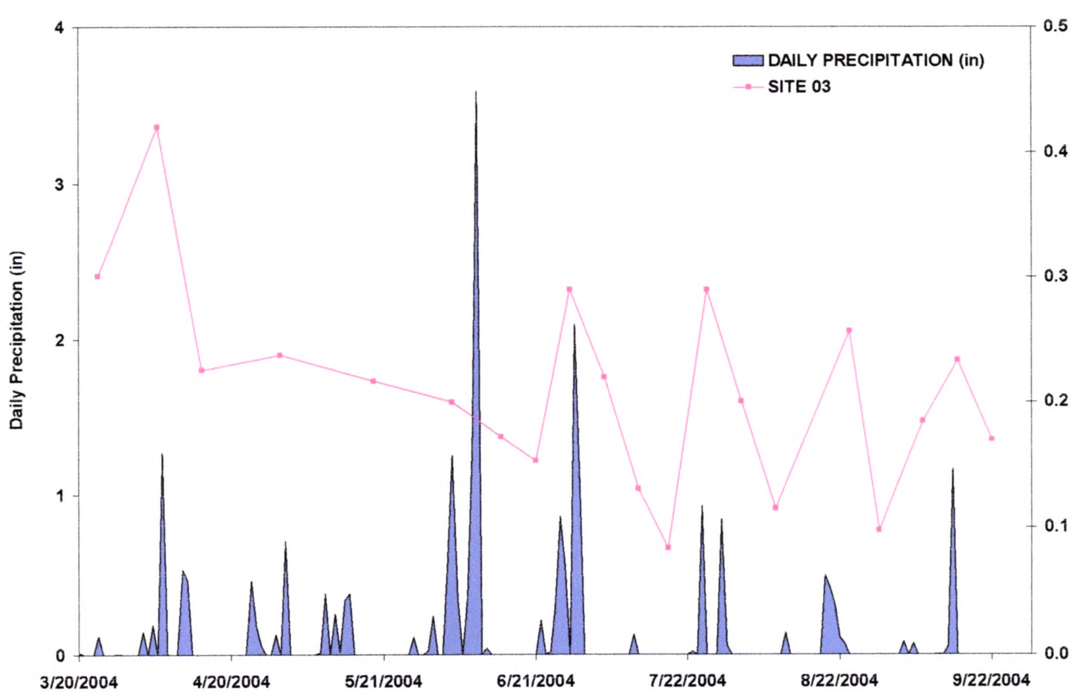

FIGURE 61. DAILY PRECIPITATION VERSUS GRAVIMETRIC MOISTURE CONTENTS FOR SITE 03

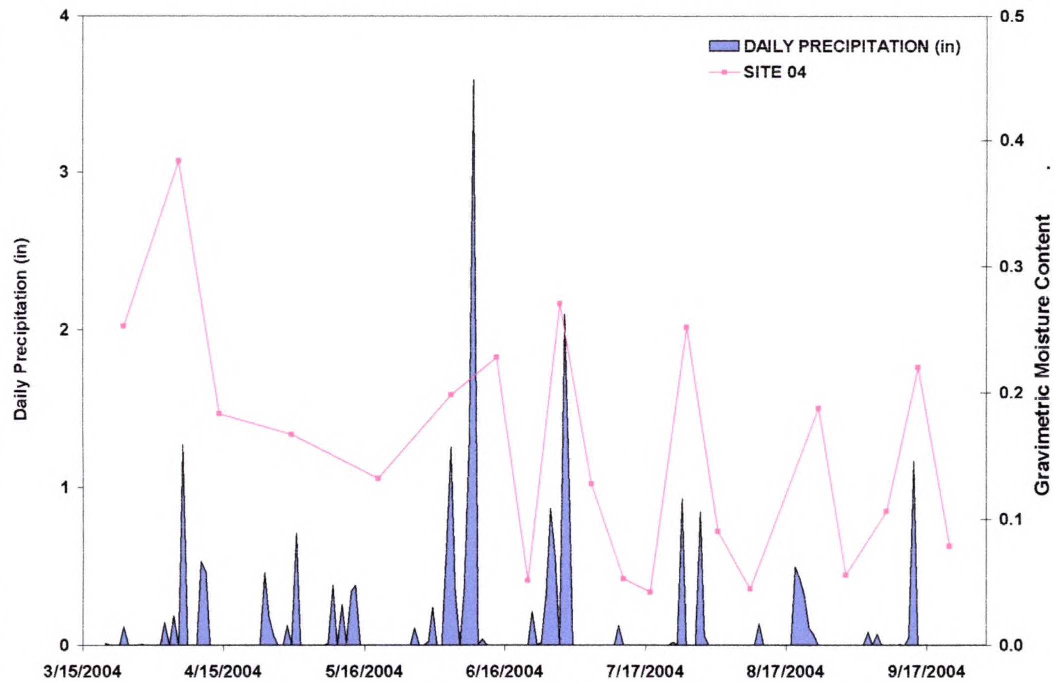

FIGURE 62. DAILY PRECIPITATION VERSUS GRAVIMETRIC MOISTURE CONTENTS FOR SITE 04

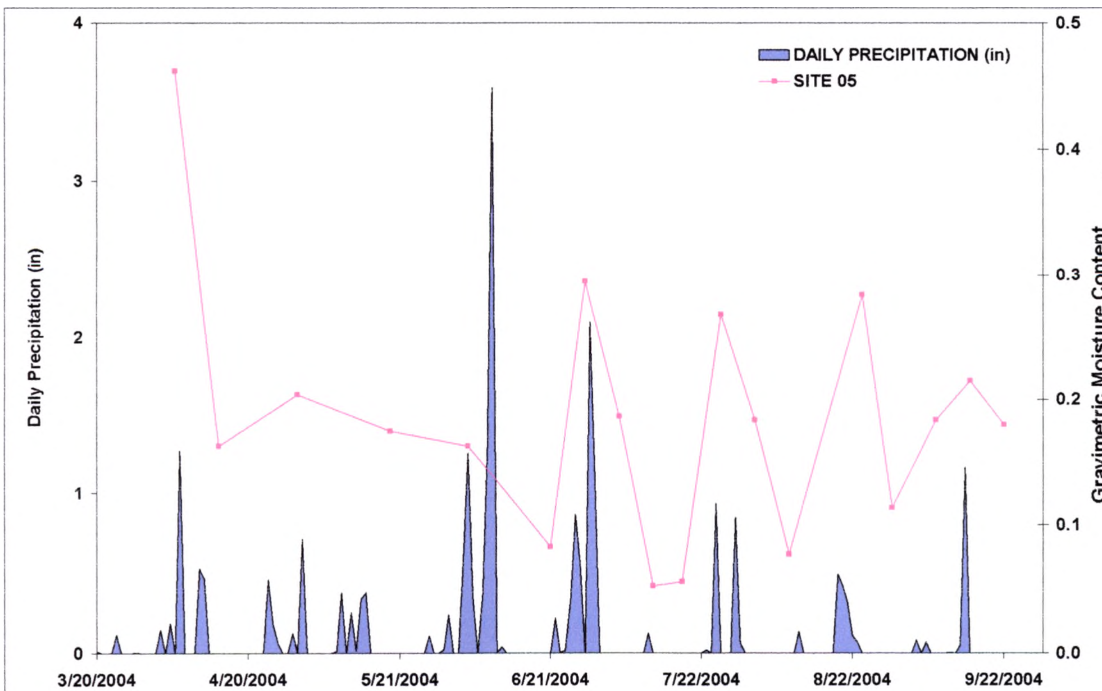

FIGURE 63. DAILY PRECIPITATION VERSUS GRAVIMETRIC MOISTURE CONTENTS FOR SITE 05

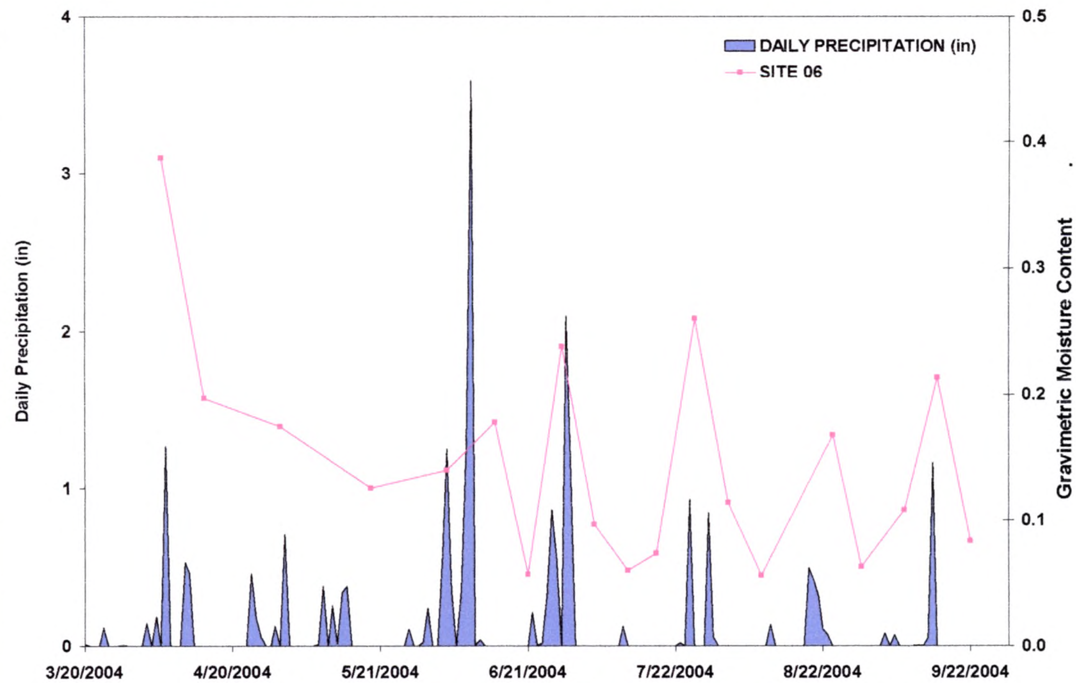

FIGURE 64. DAILY PRECIPITATION VERSUS GRAVIMETRIC MOISTURE CONTENTS FOR SITE 06

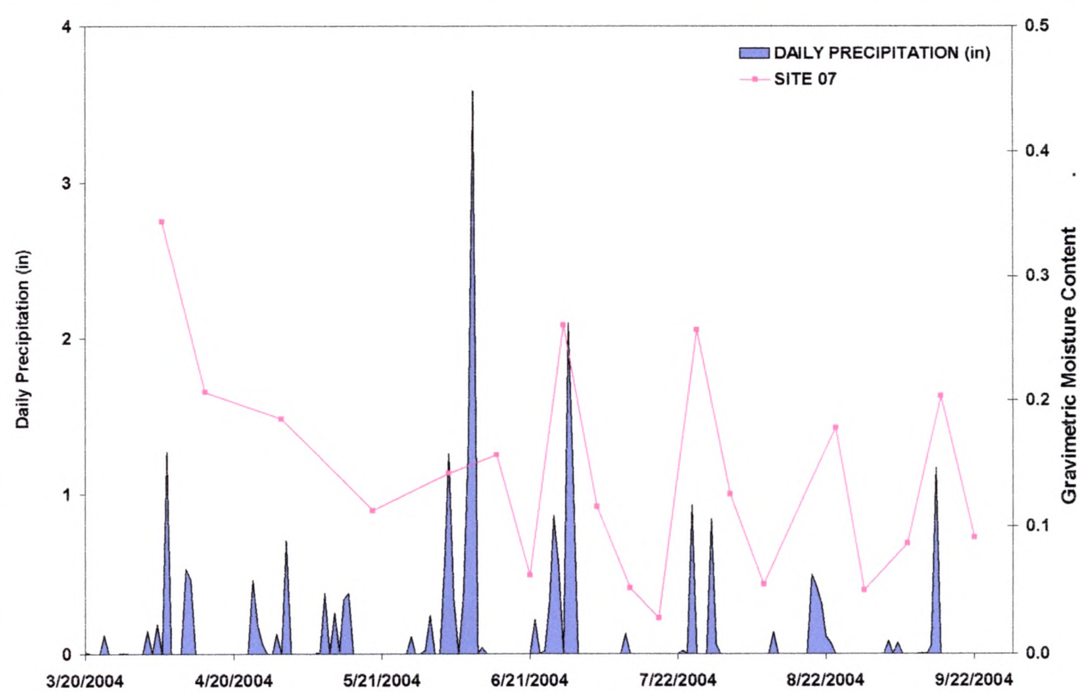

FIGURE 65. DAILY PRECIPITATION VERUS GRAVIMETRIC MOISTURE CONTENTS FOR SITE 07

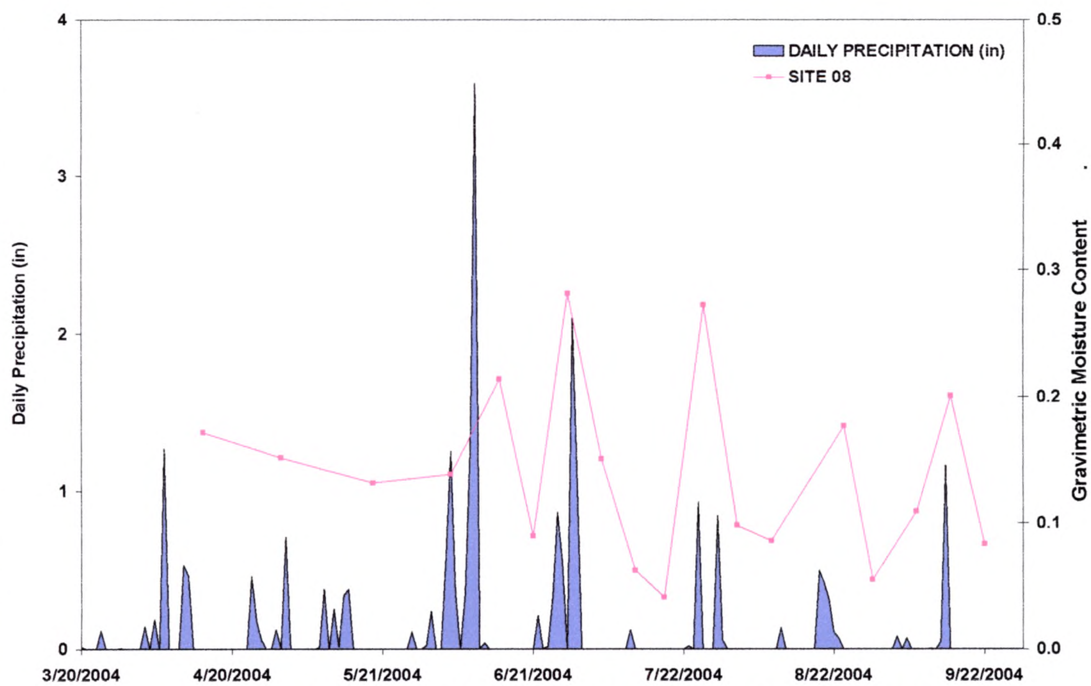

FIGURE 66. DAILY PRECIPITATION VERSUS GRAVIMETRIC MOISTURE CONTENTS FOR SITE 08

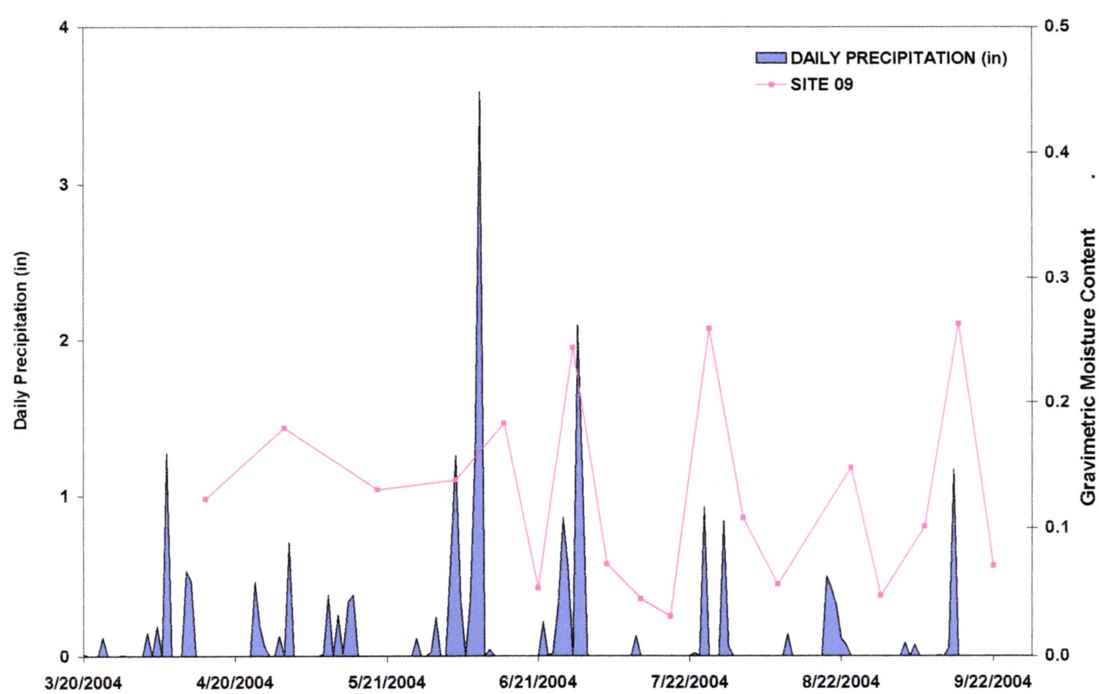

FIGURE 67. DAILY PRECIPITATION VERSUS GRAVIMETRIC MOISTURE CONTENTS FOR SITE 09

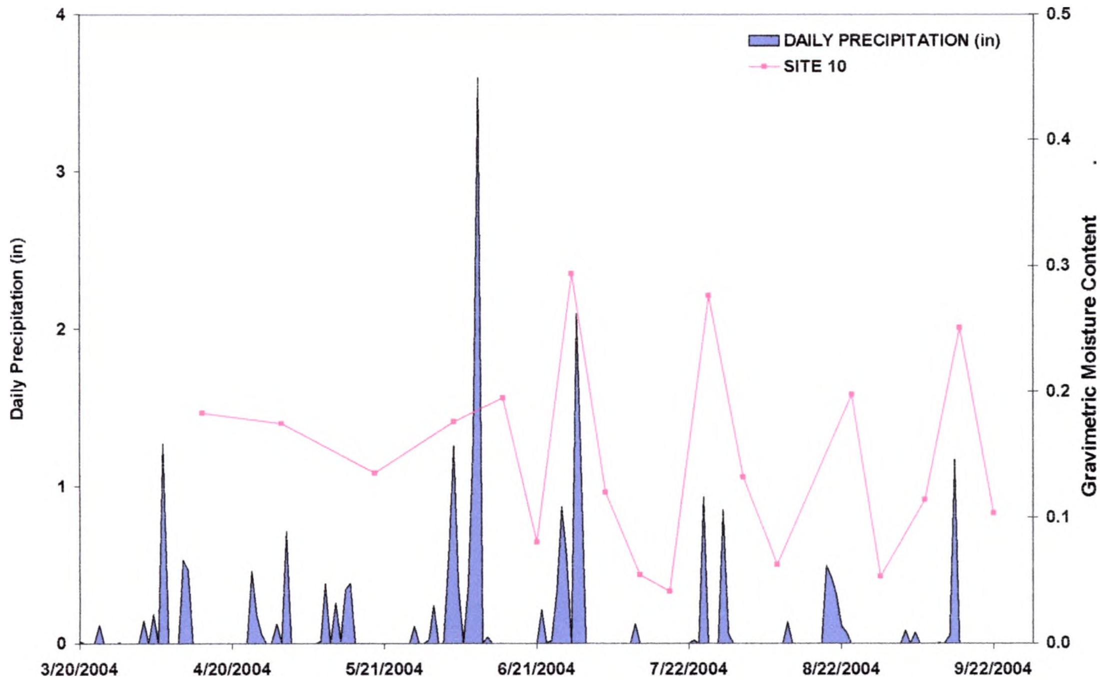

FIGURE 68. DAILY PRECIPITATION VERSUS GRAVIMETRIC MOISTURE CONTENTS FOR SITE 10

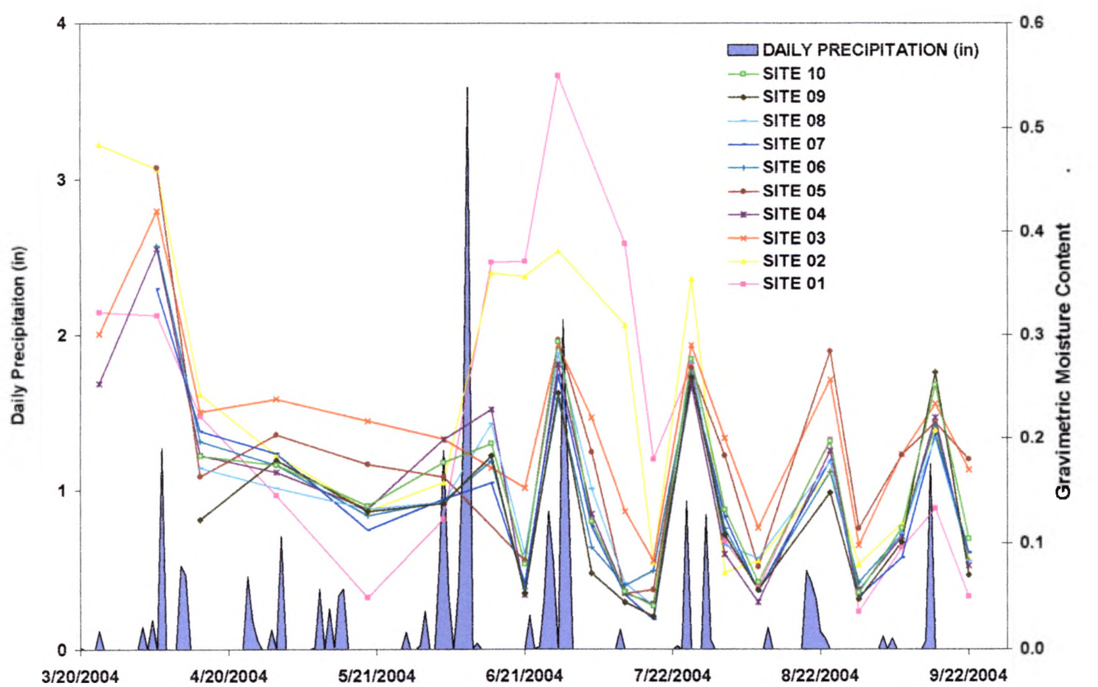

FIGURE 69. DAILY PRECIPITATION VERSUS GRAVIMETRIC MOISTURE CONTENTS FOR ALL SITES

APERTURE WIDTH VERSUS FRACTURE DEPTH

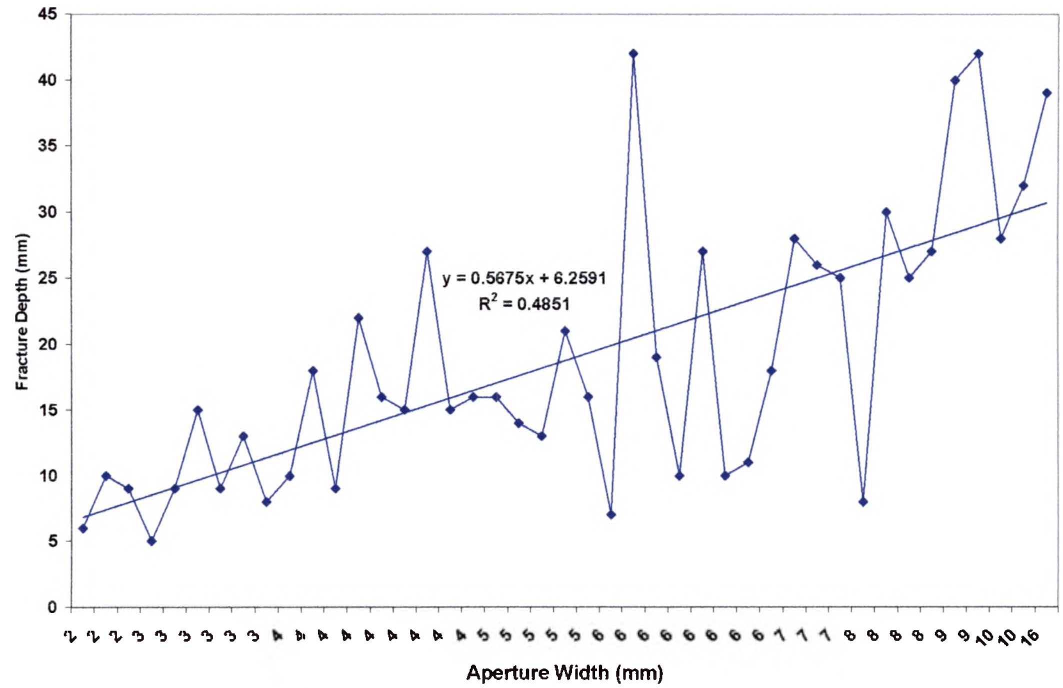

FIGURE 70. APERTURE WIDTH VERSUS FRACTURE DEPTH FOR SITE 02

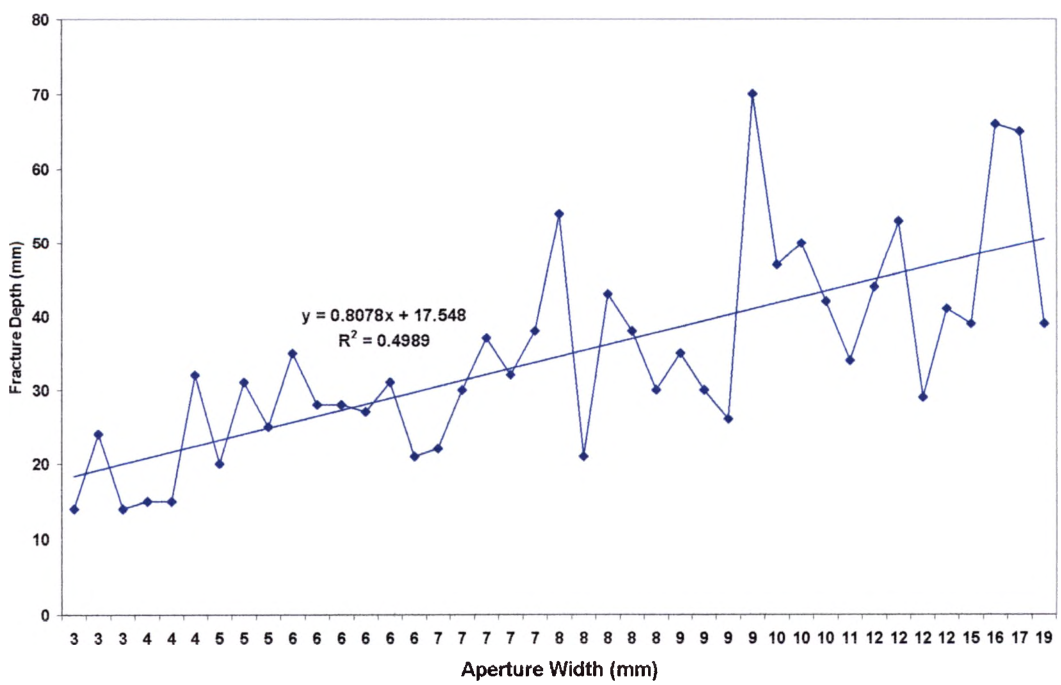

FIGURE 71. APERTURE WIDTH VERSUS FRACTURE DEPTH FOR SITE 03

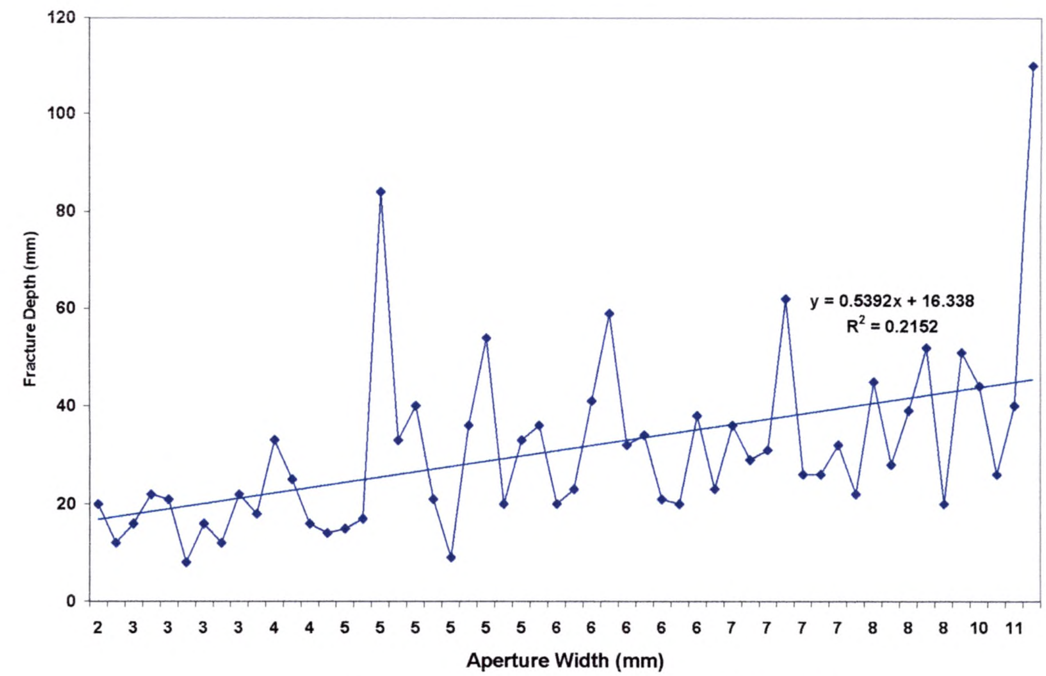

FIGURE 72. APERTURE WIDTH VERSUS FRACTURE DEPTH FOR SITE 04

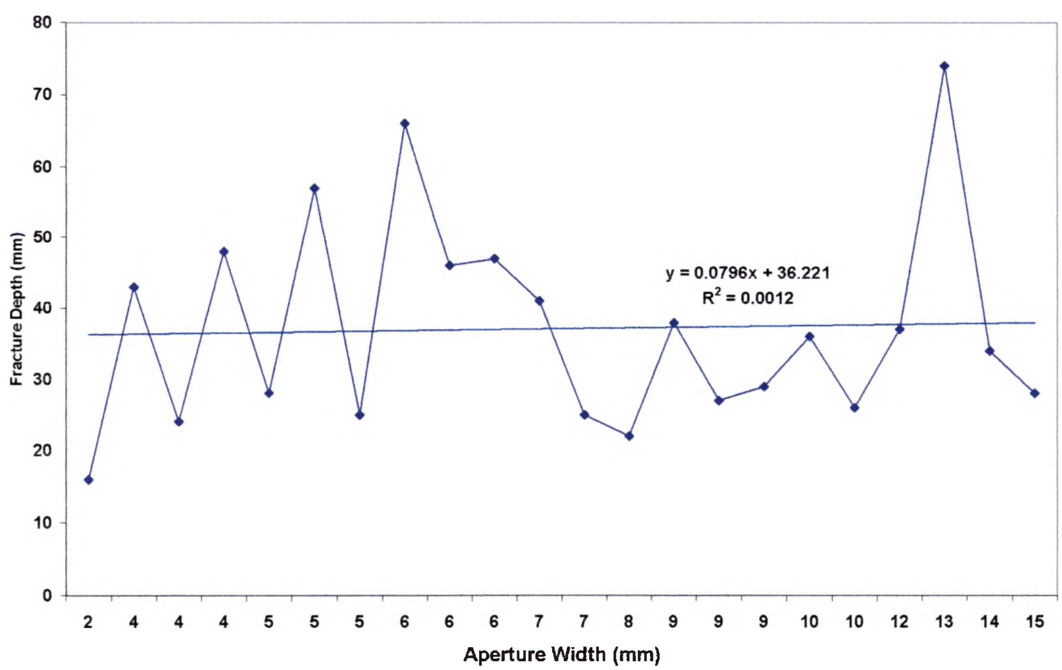

FIGURE 73. APERTURE WIDTH VERSUS FRACTURE DEPTH FOR SITE 05

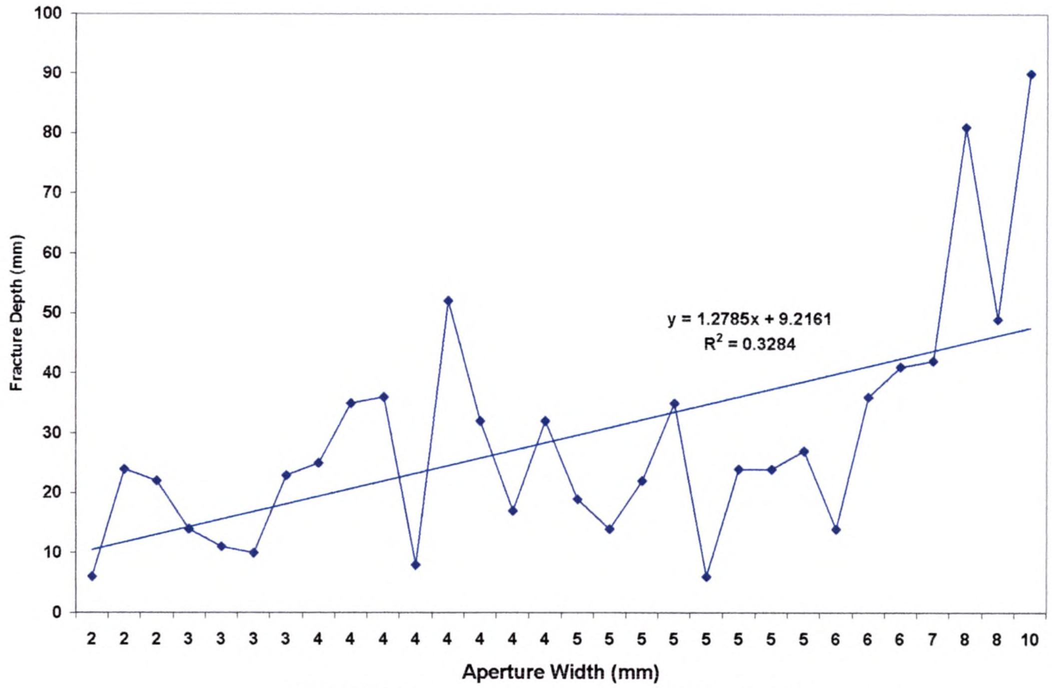

FIGURE 74. APERTURE WIDTH VERSUS FRACTURE DEPTH FOR SITE 06

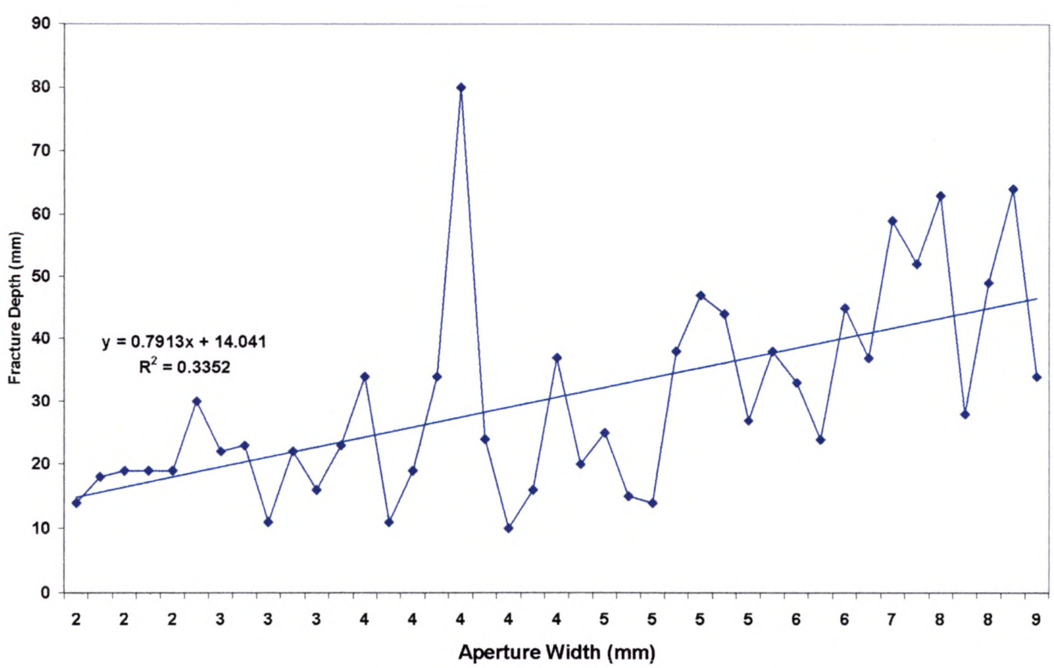

FIGURE 75. APERTURE WIDTH VERSUS FRACTURE DEPTH FOR SITE 07

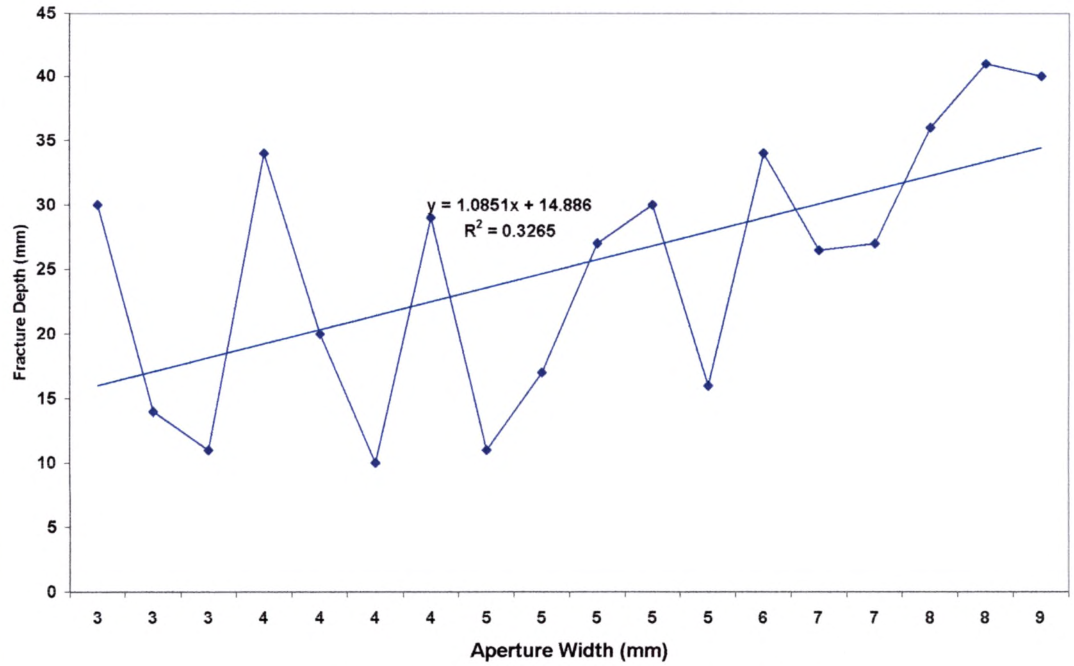

FIGURE 76. APERTURE WIDTH VERSUS FRACTURE DEPTH FOR SITE 08

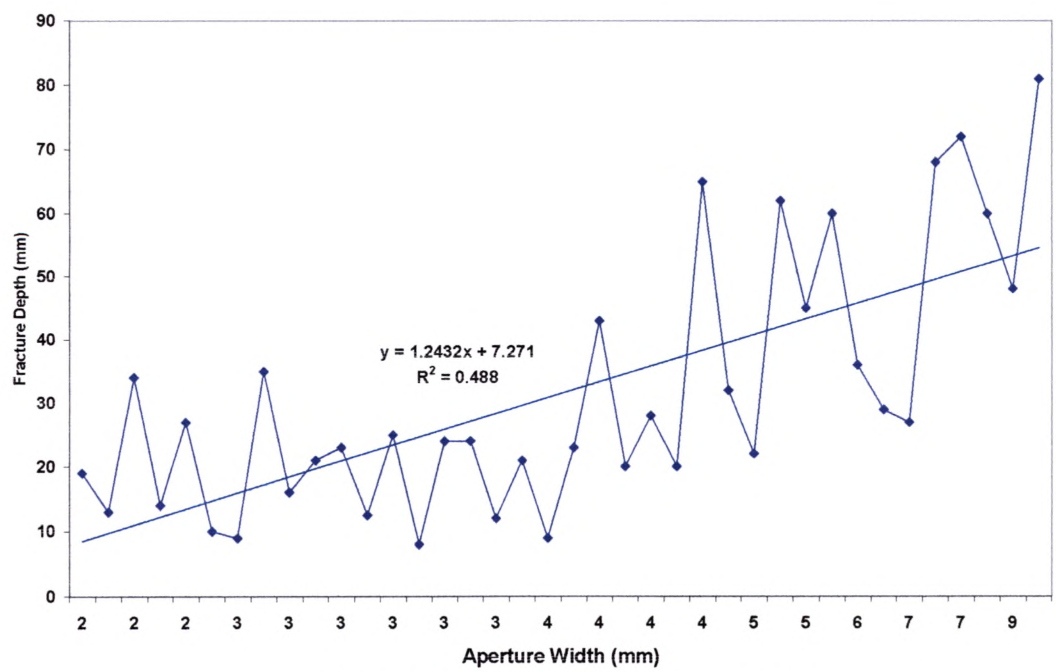

FIGURE 77. APERTURE WIDTH VERSUS FRACTURE DEPTH FOR SITE 09

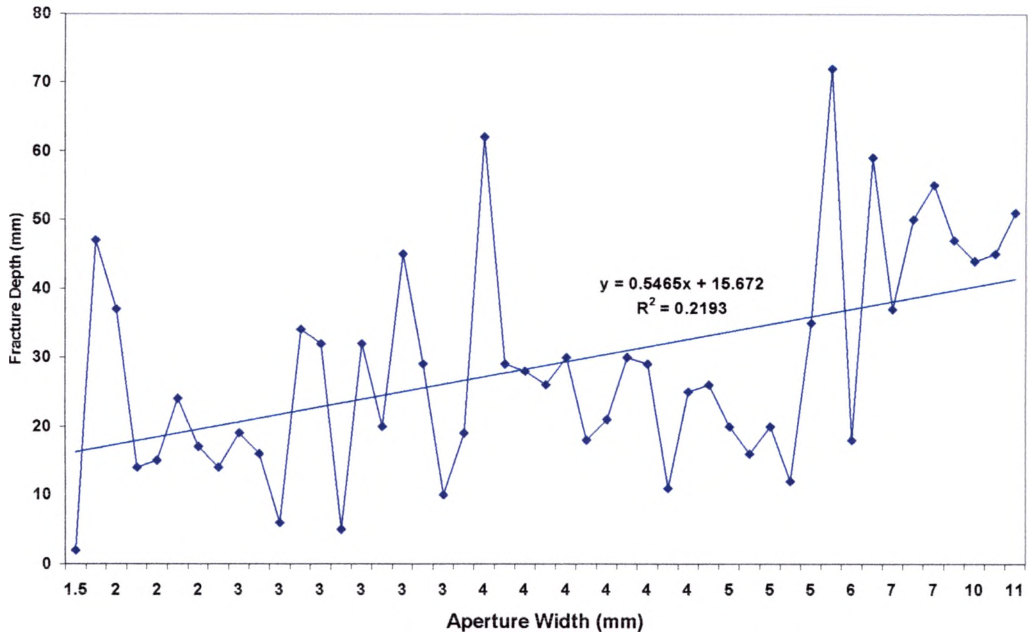

FIGURE 78. APERTURE WIDTH VERSUS FRACTURE DEPTH FOR SITE 10

APERTURE DISTRIBUTION HISTOGRAMS

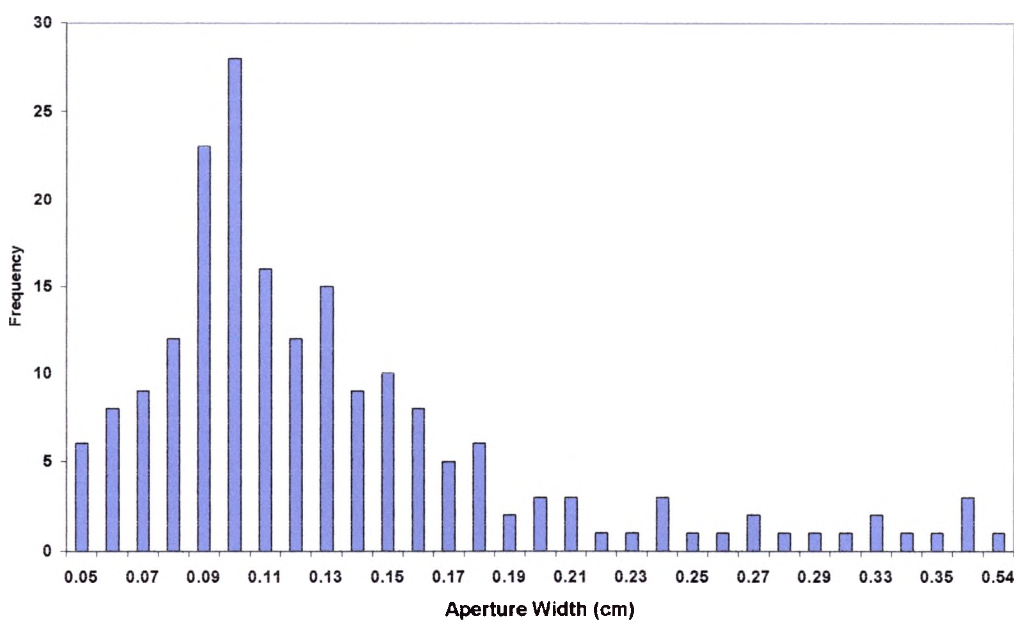

FIGURE 79. APERTURE DISTRIBUTION HISTOGRAM FOR SITE 01

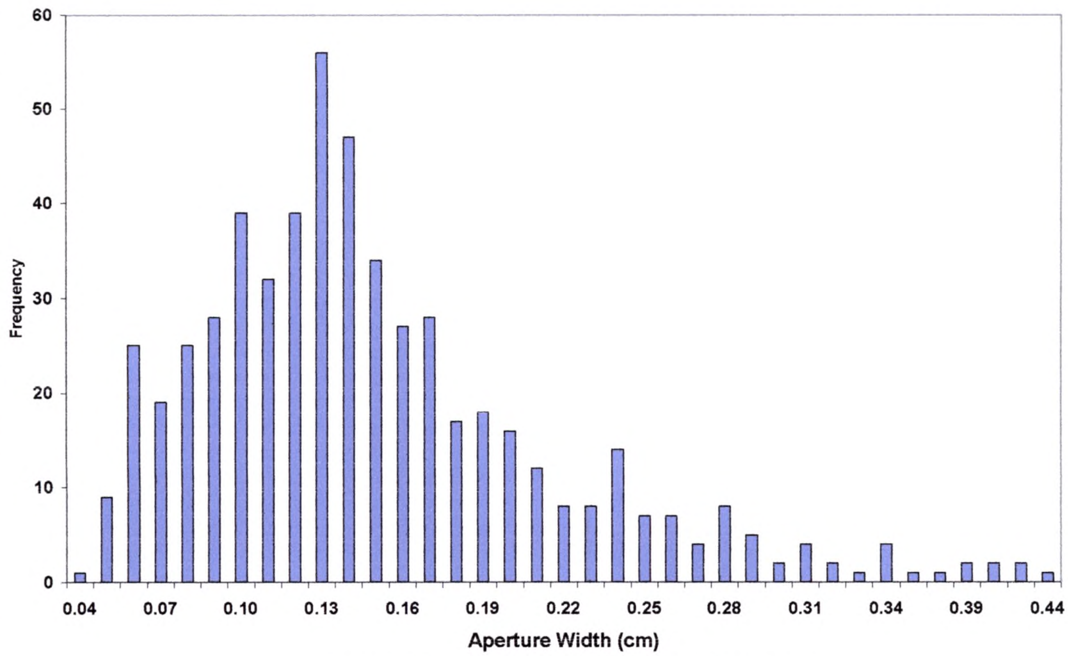

FIGURE 80. APERTURE DISTRIBUTION HISTOGRAM FOR SITE 02

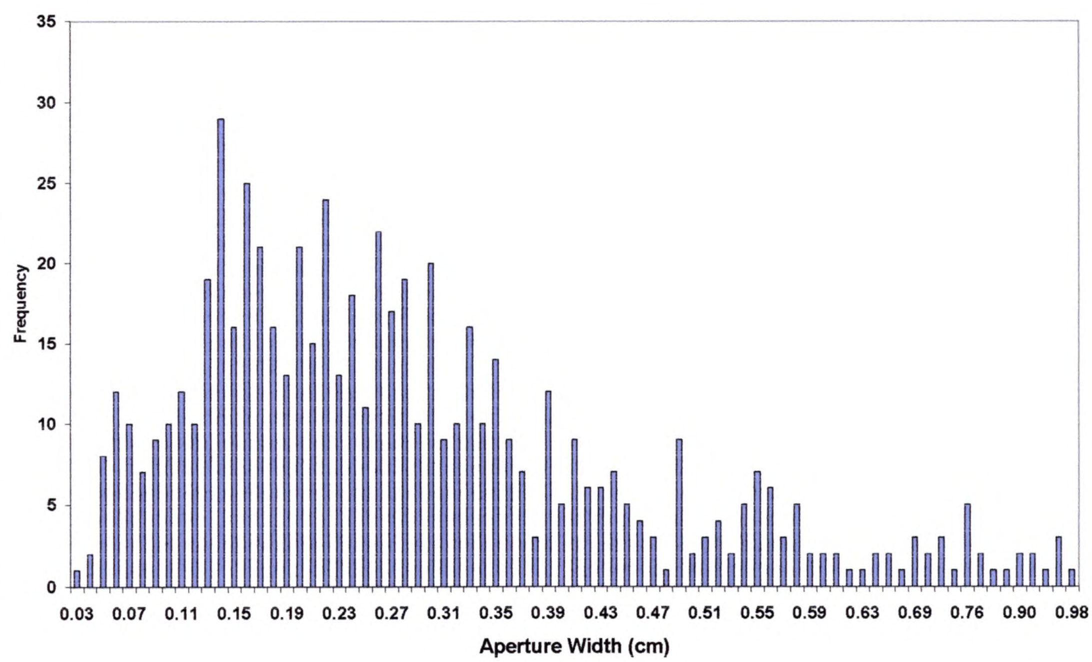

FIGURE 81. APERTURE DISTRIBUTION HISTOGRAM FOR SITE 03

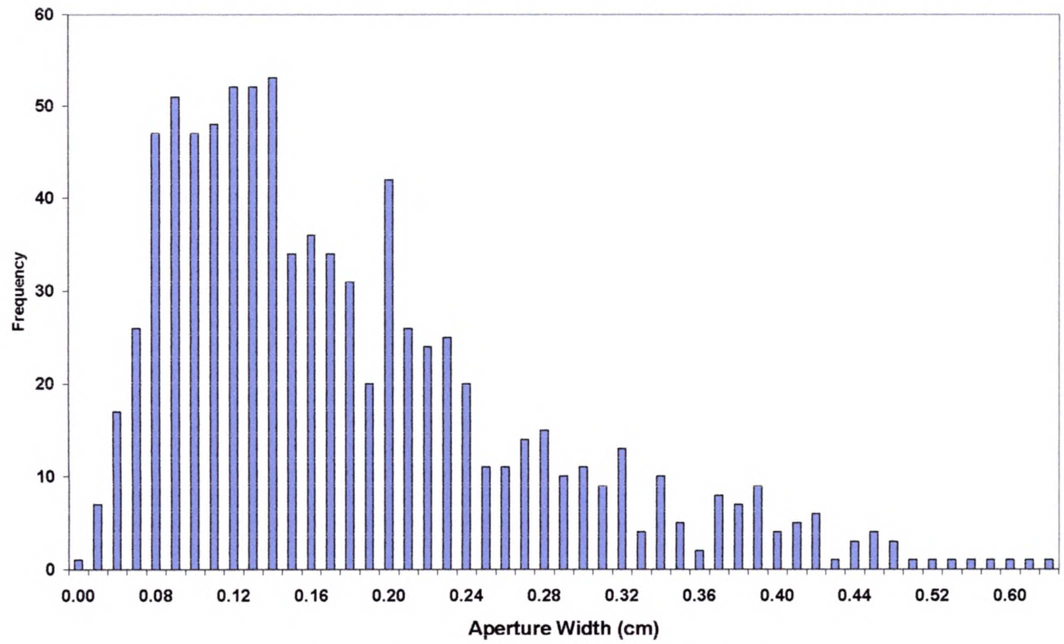

FIGURE 82. APERTURE DISTRIBUTION HISTOGRAM FOR SITE 04

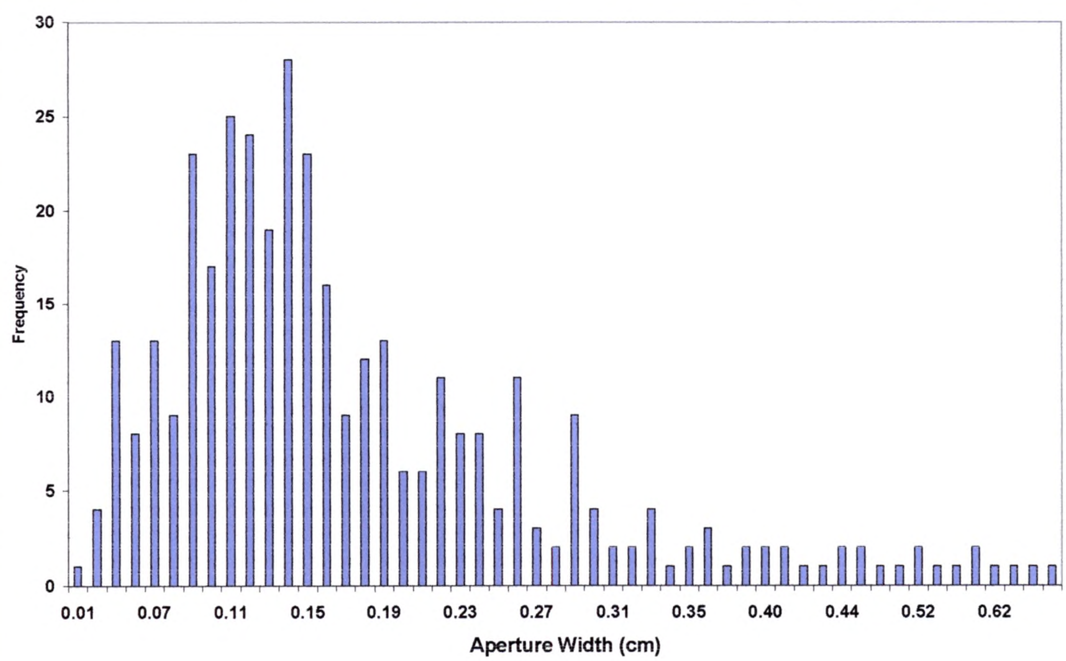

FIGURE 83. APERTURE DISTRIBUTION HISTOGRAM FOR SITE 05

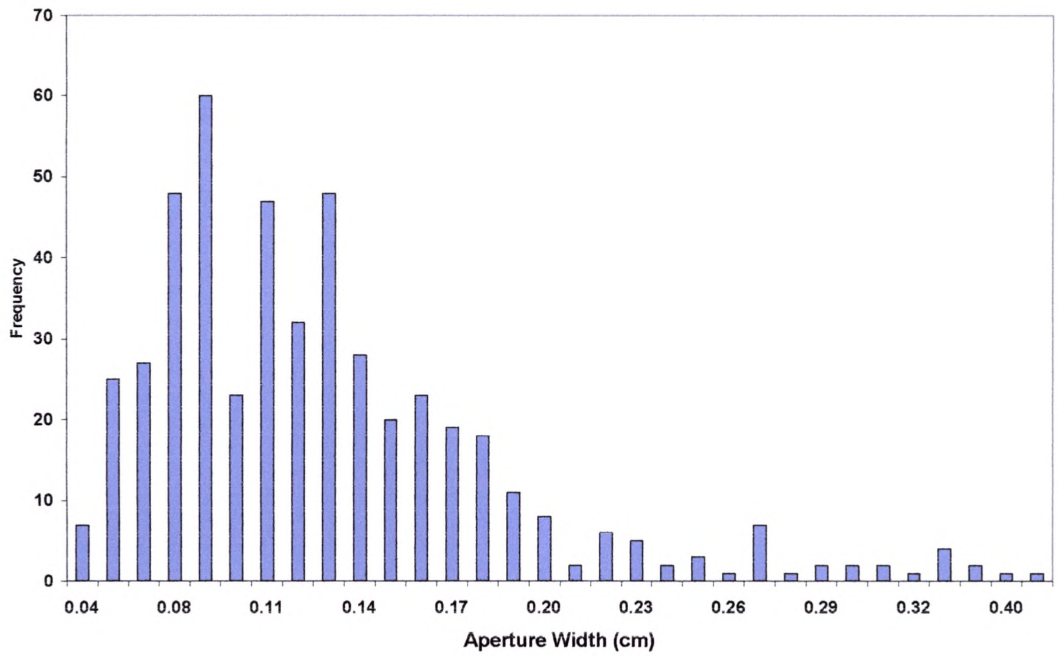

FIGURE 84. APERTURE DISTRIBUTION HISTOGRAM FOR SITE 06

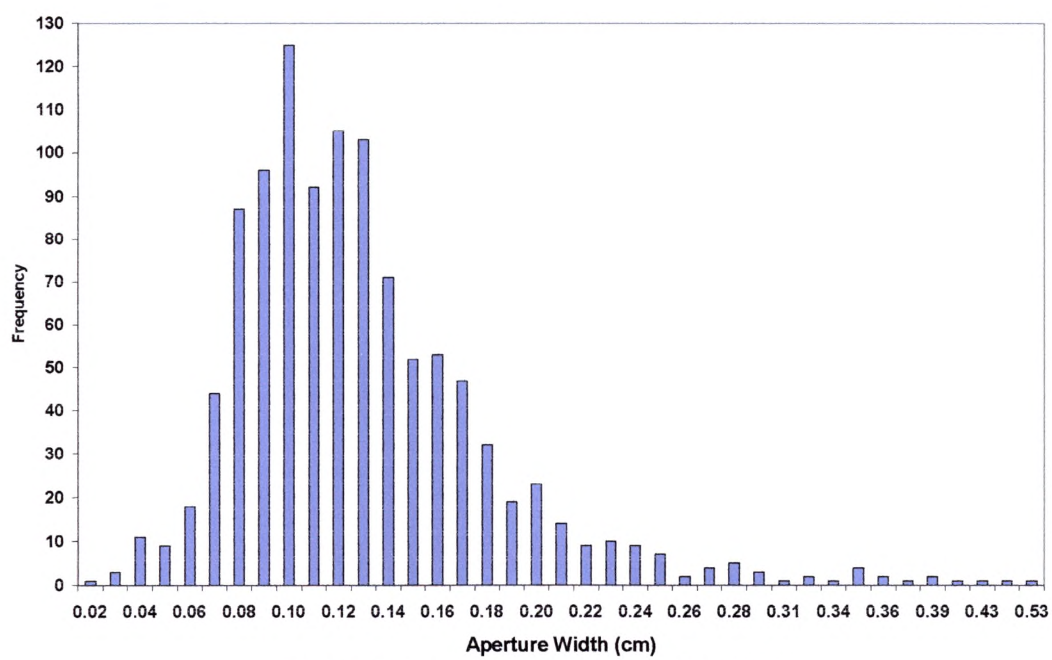

FIGURE 85. APERTURE DISTRIBUTION HISTOGRAM FOR SITE 07

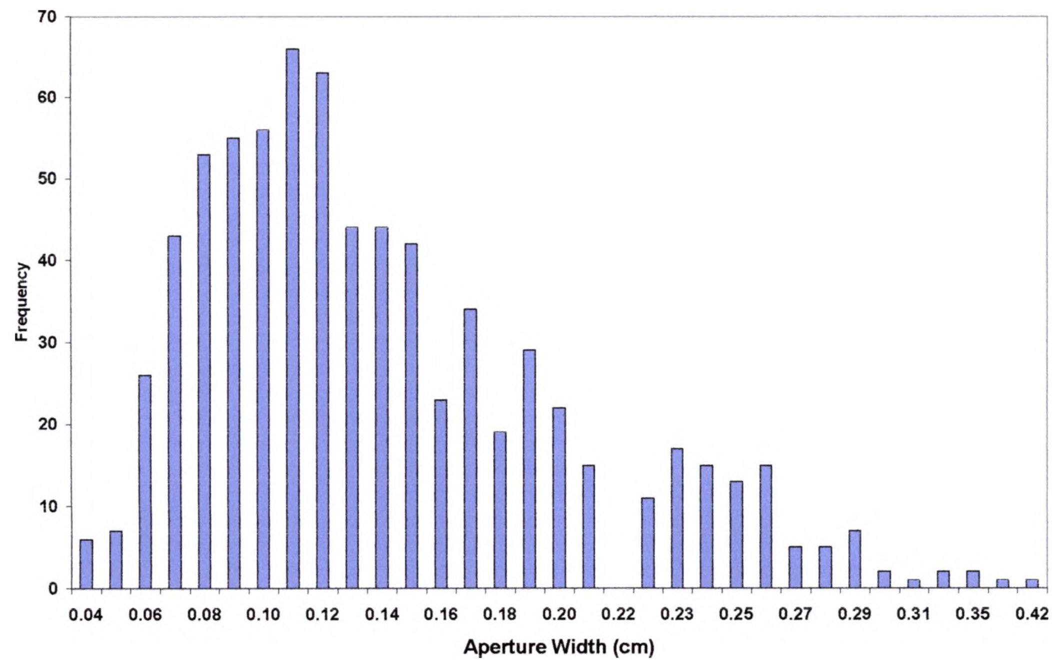

FIGURE 86. APERTURE DISTRIBUTION HISTOGRAM FOR SITE 08

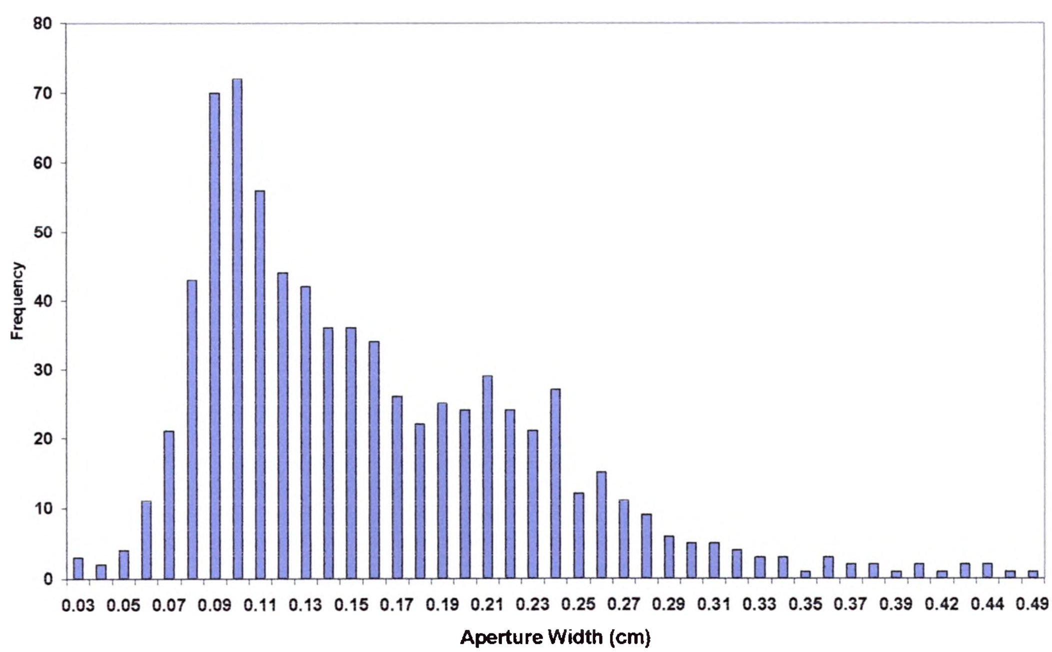

FIGURE 87. APERTURE DISTRIBUTION HISTOGRAM FOR SITE 09

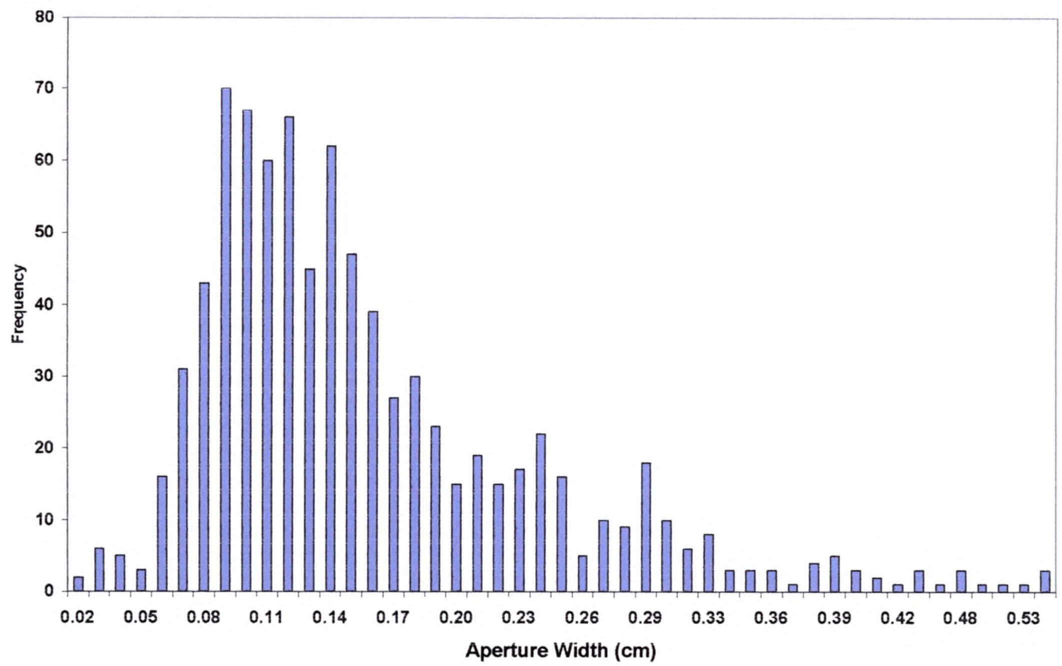

FIGURE 88. APERTURE DISTRIBUTION
HISTOGRAM FOR SITE 10

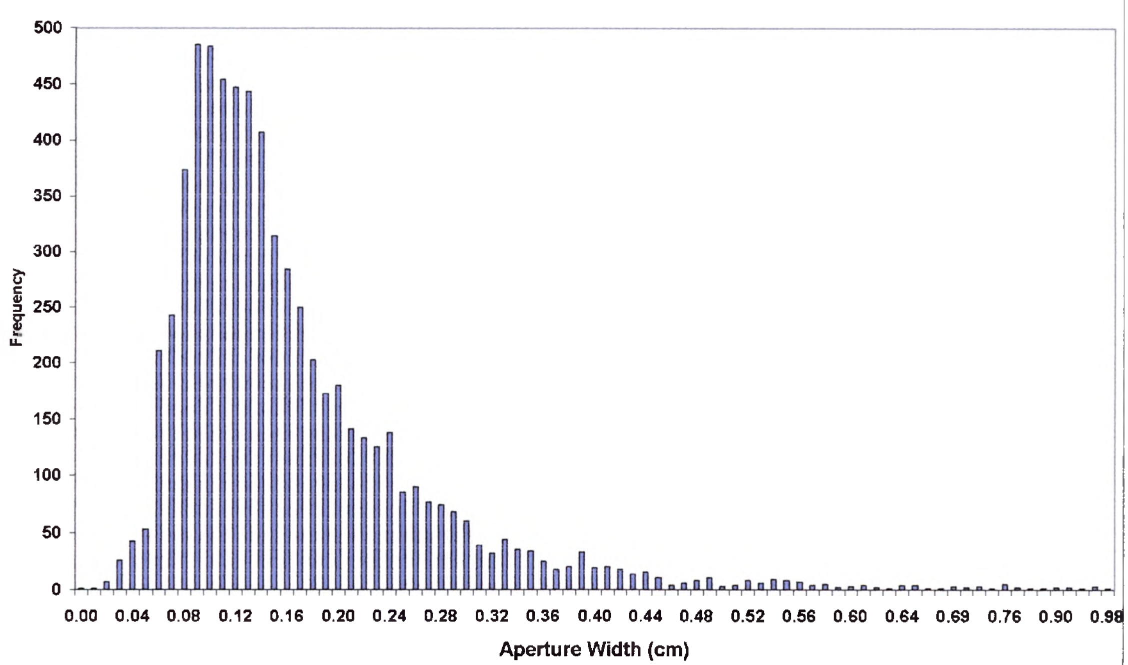

FIGURE 89. APERTURE DISTRIBUTION
HISTOGRAM FOR ALL SITES

Table 4. Grain Sizes for D_{20}, D_{50}, and D_{80} Retention Weights

PLOT ID	d_{20}			d_{50}			d_{80}			AVERAGES		
	1	2	3	1	2	3	1	2	3	d_{20}	d_{50}	d_{80}
01		0.47	0.73		0.23	0.28		0.09	0.15	**0.600**	**0.255**	**0.120**
02	1.5		1.6	0.61		0.49	0.27		0.2	**1.550**	**0.550**	**0.235**
03	0.9		1.5	0.56		0.74	0.23		0.29	**1.200**	**0.650**	**0.260**
04	0.81	0.81	0.94	0.37	0.41	0.43	0.15	0.2	0.2	**0.853**	**0.403**	**0.183**
05		0.7	0.95		0.38	0.56		0.16	0.19	**0.825**	**0.470**	**0.175**
06	0.64		0.38	0.37		0.06	0.65		0.005	**0.510**	**0.215**	**0.328**
07		0.51	0.56		0.32	0.32		0.15	0.14	**0.535**	**0.320**	**0.145**
08	0.76		0.79	0.44		0.43	0.21		0.19	**0.775**	**0.435**	**0.200**
09	0.68	0.8	2	0.39	0.39	1	0.17	0.17	0.34	**1.160**	**0.593**	**0.227**
10	0.97		0.7	0.54		0.4	0.23		0.17	**0.835**	**0.470**	**0.200**

GRAIN SIZE DISTRIBUTION AT EACH SITE

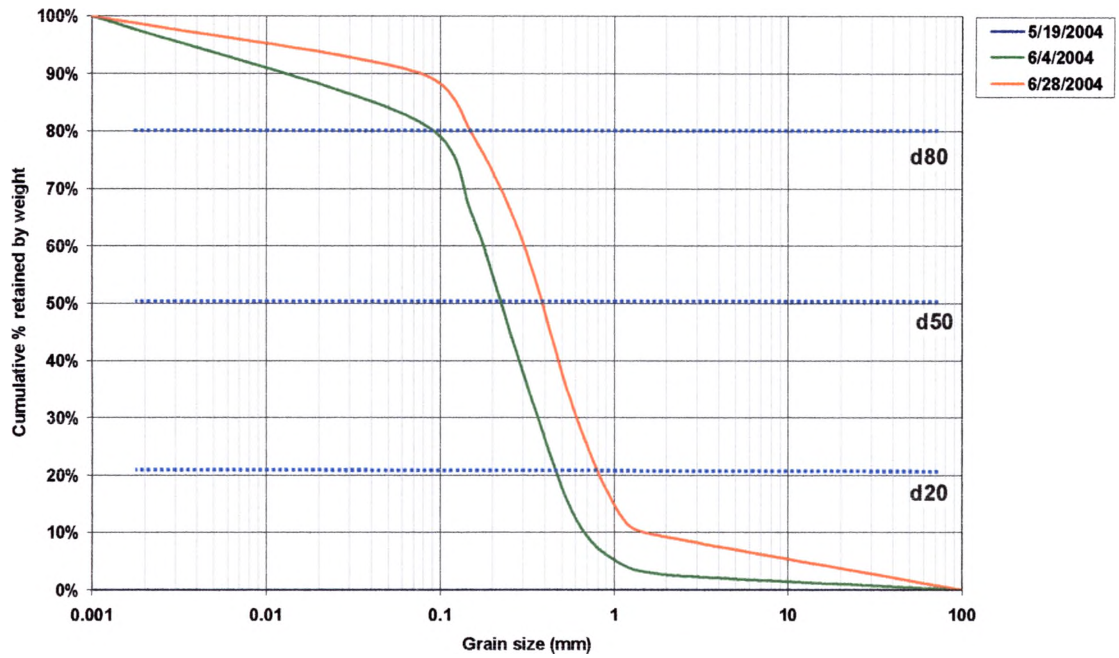

FIGURE 90. GRAIN SIZE VERSUS CUMULATIVE PERCENT FOR SITE 01

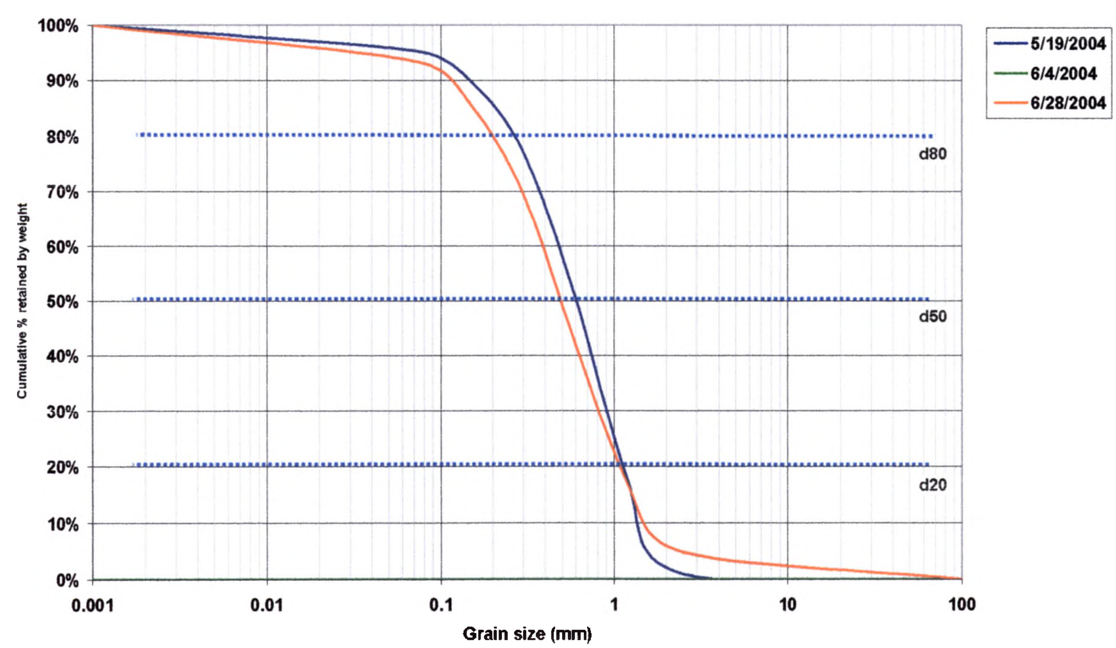

FIGURE 91. GRAIN SIZE VERSUS CUMULATIVE PERCENT FOR SITE 02

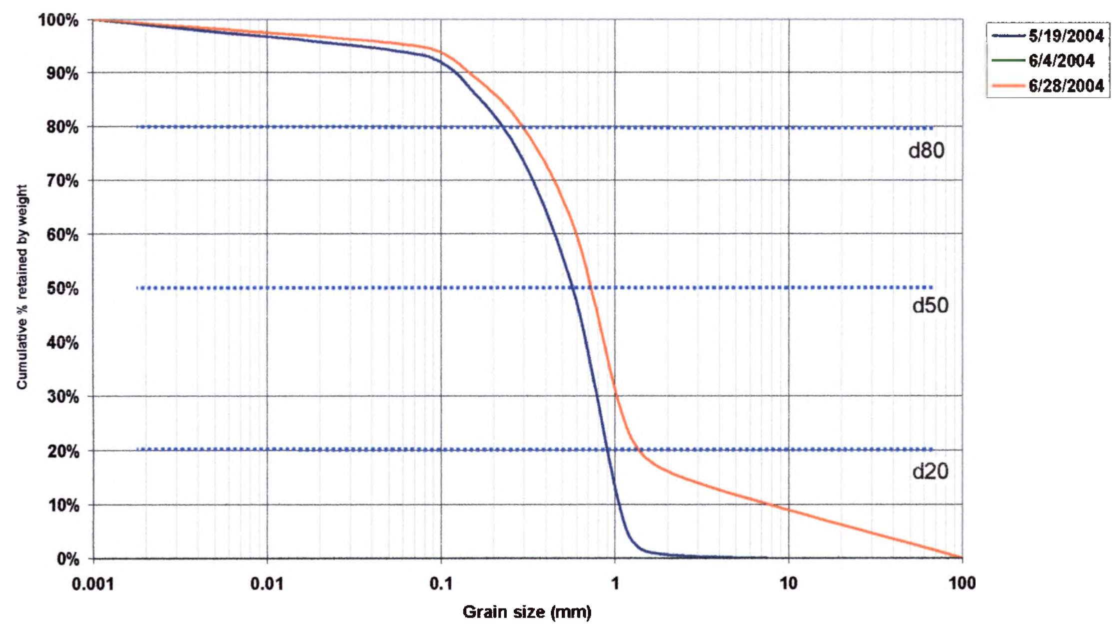

FIGURE 92. GRAIN SIZE VERSUS CUMULATIVE PERCENT FOR SITE 03

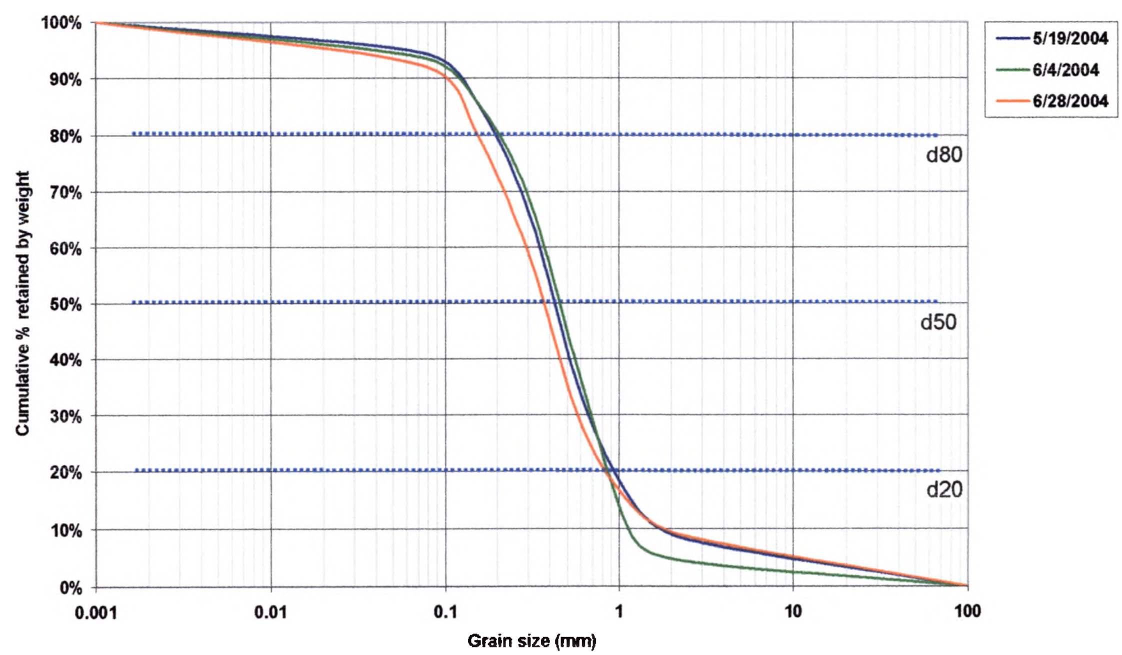

FIGURE 93. GRAIN SIZE VERSUS CUMULATIVE PERCENT FOR SITE 04

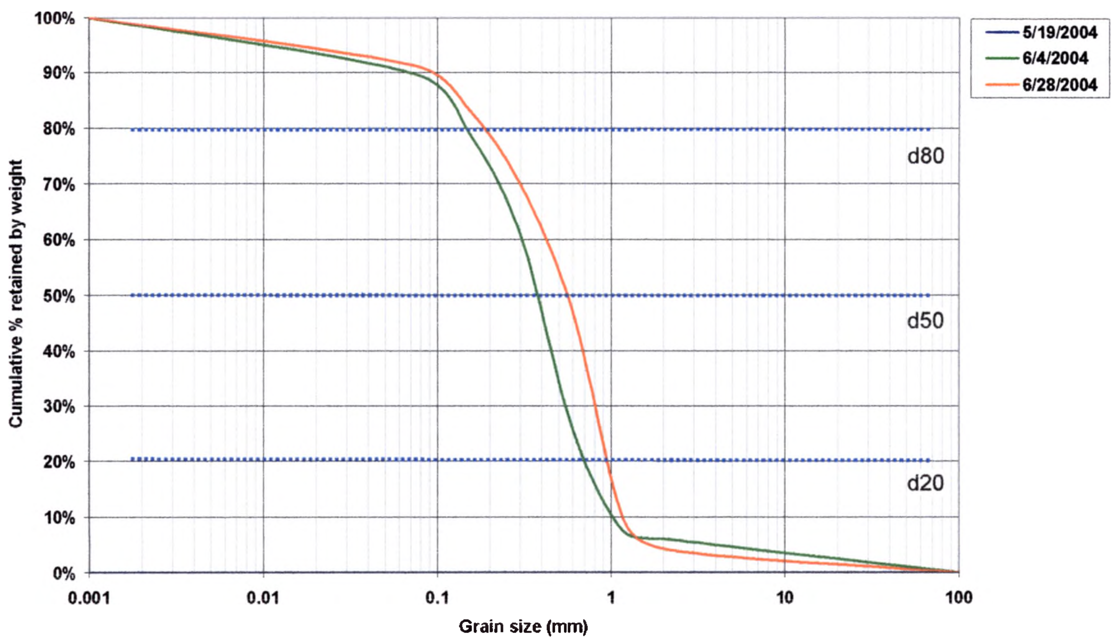

FIGURE 94. GRAIN SIZE VERSUS CUMULATIVE PERCENT FOR SITE 05

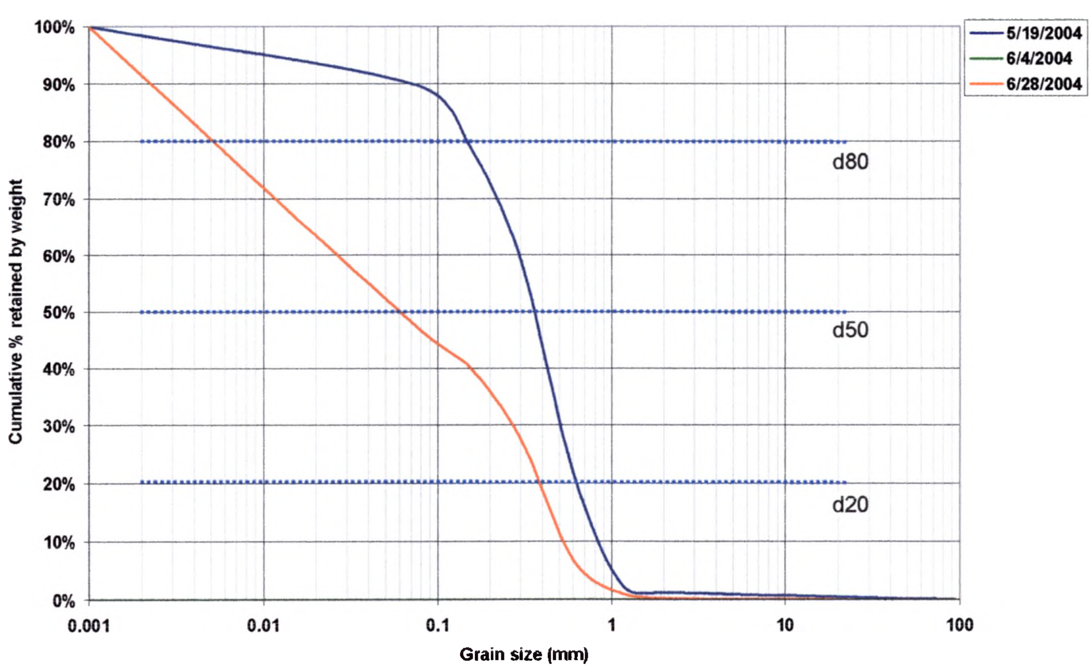

FIGURE 95. GRAIN SIZE VERSUS CUMULATIVE PERCENT FOR SITE 06

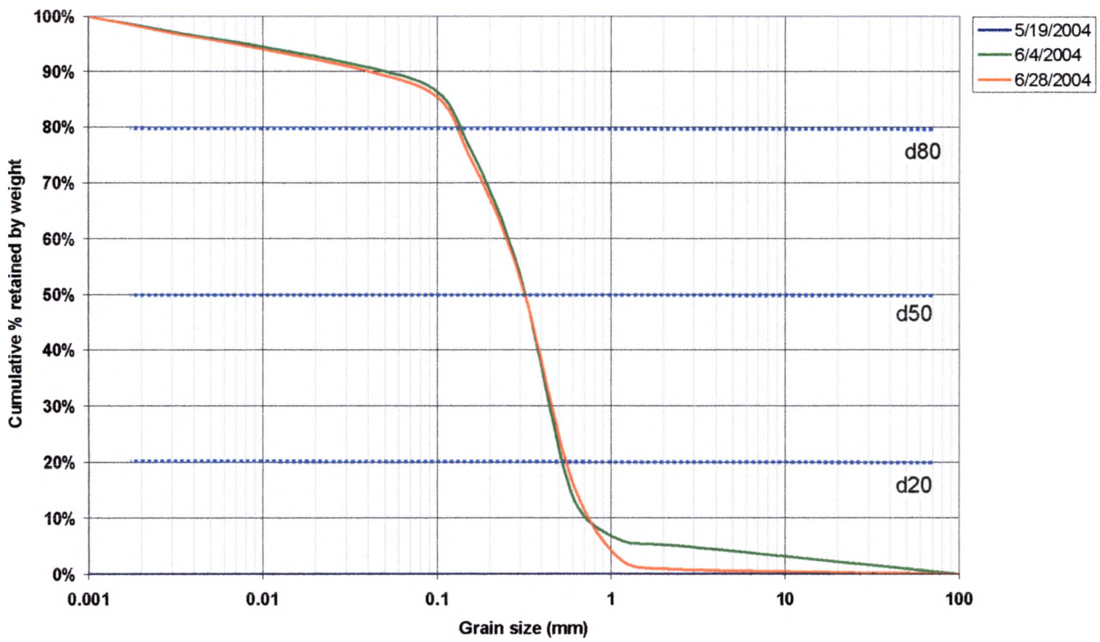

FIGURE 96. GRAIN SIZE VERSUS CUMULATIVE PERCENT FOR SITE 07

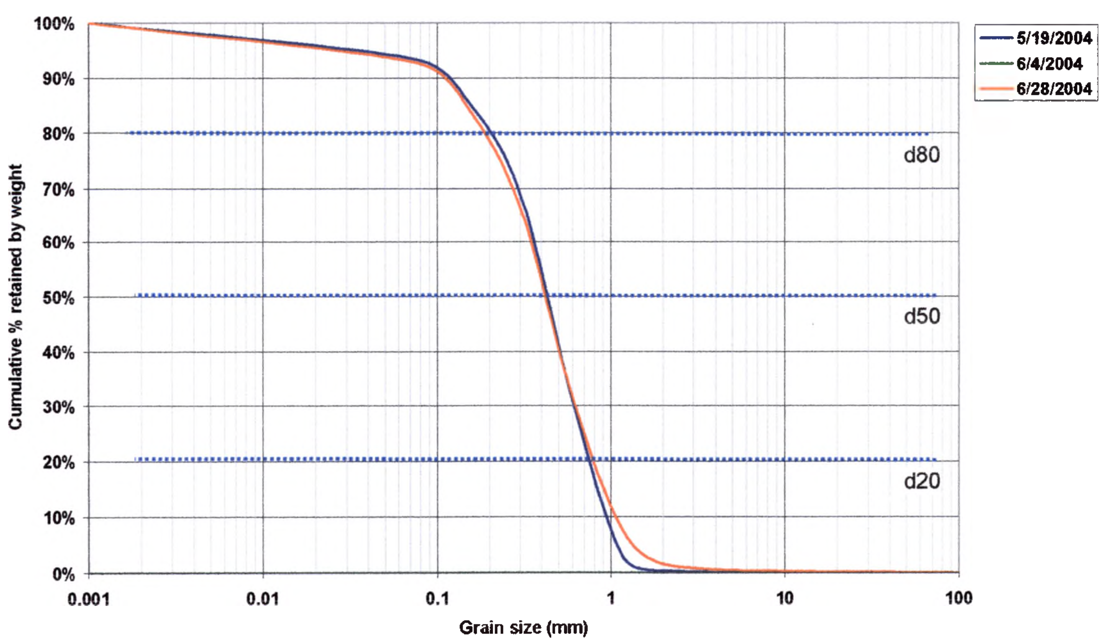

FIGURE 97. GRAIN SIZE VERSUS CUMULATIVE PERCENT FOR SITE 08

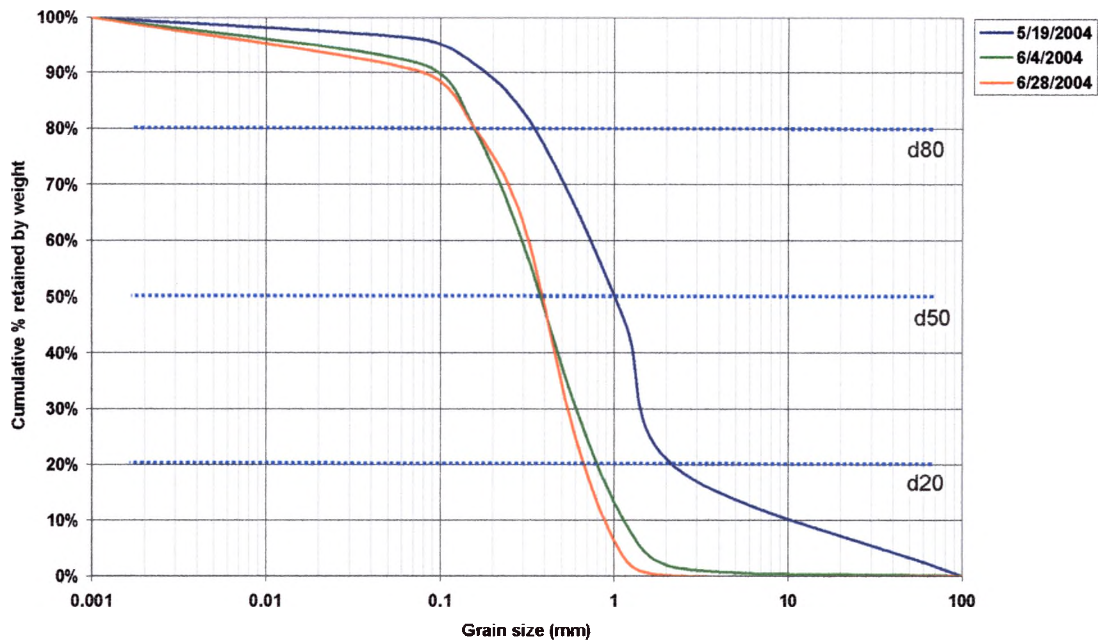

FIGURE 98. GRAIN SIZE VERSUS CUMULATIVE PERCENT FOR SITE 09

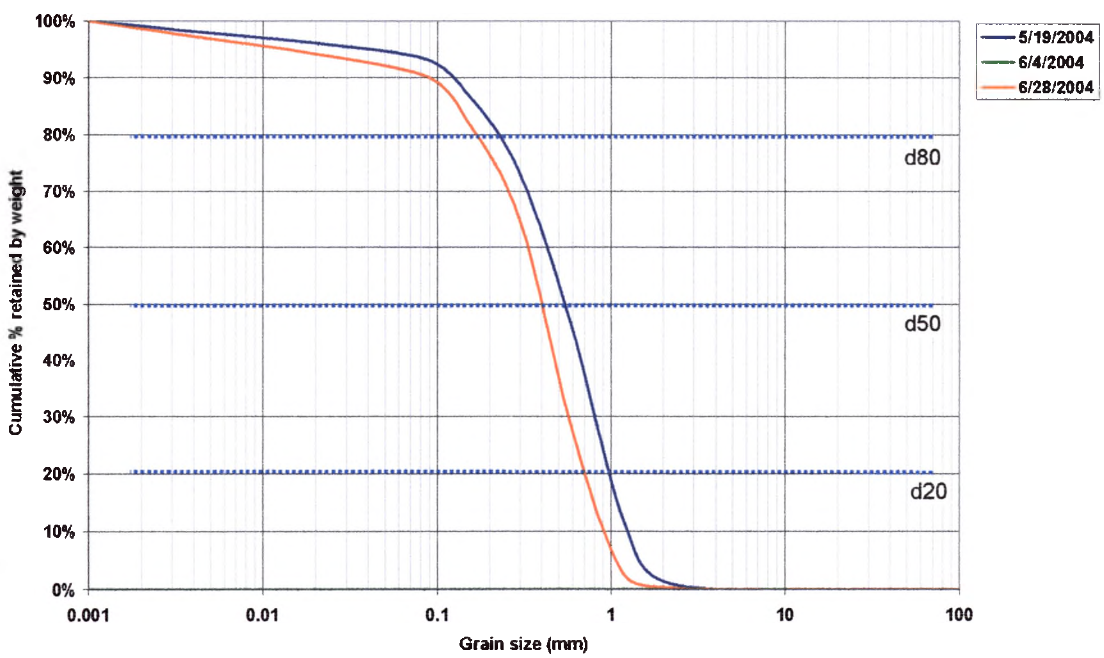

FIGURE 99. GRAIN SIZE VERSUS CUMULATIVE PERCENT FOR SITE 10

GRAIN SIZE DISTRIBUTION AVERAGES VERSUS FRACTURE GROWTH RATE

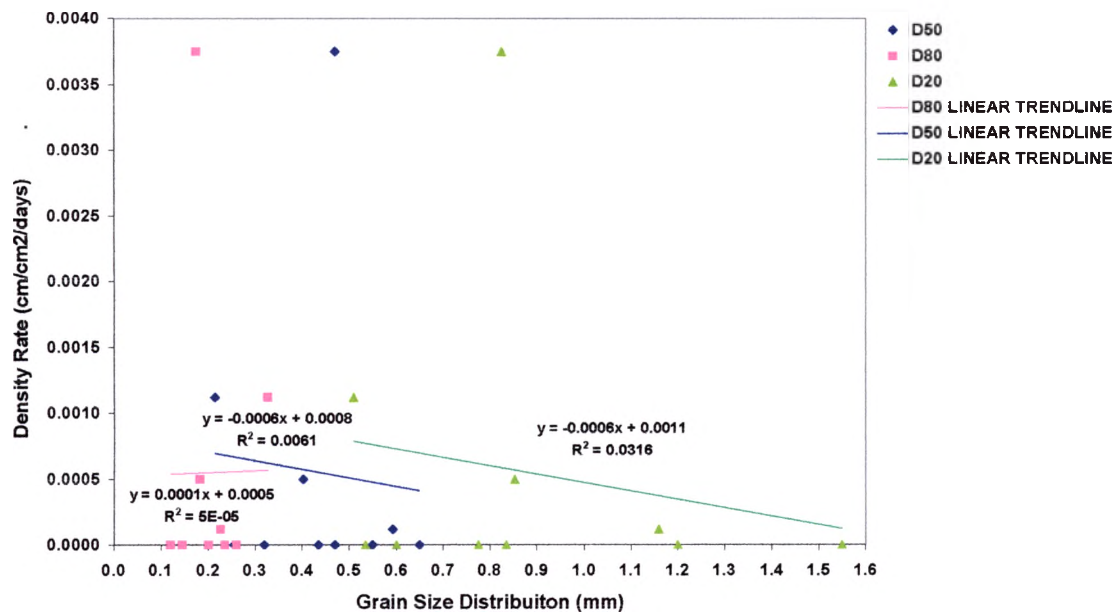

FIGURE 100. DENSITY RATE VERSUS GRAIN SIZE DISTRIBUTION IN JUNE

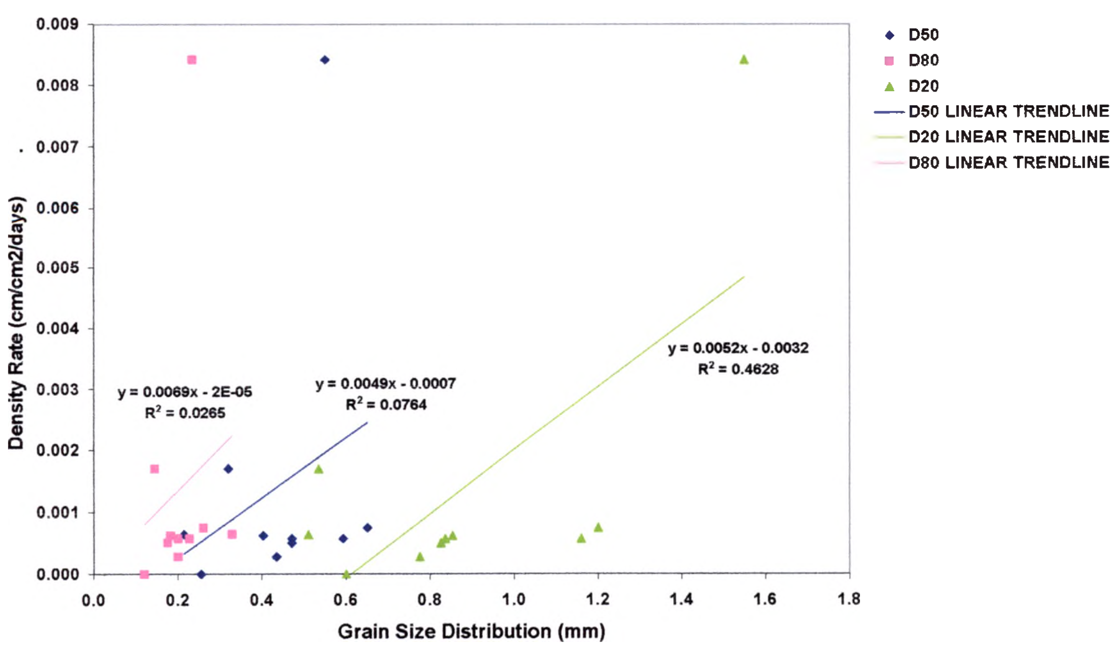

FIGURE 101. DENSITY RATE VERSUS GRAIN SIZE DISTRIBUTION IN JULY

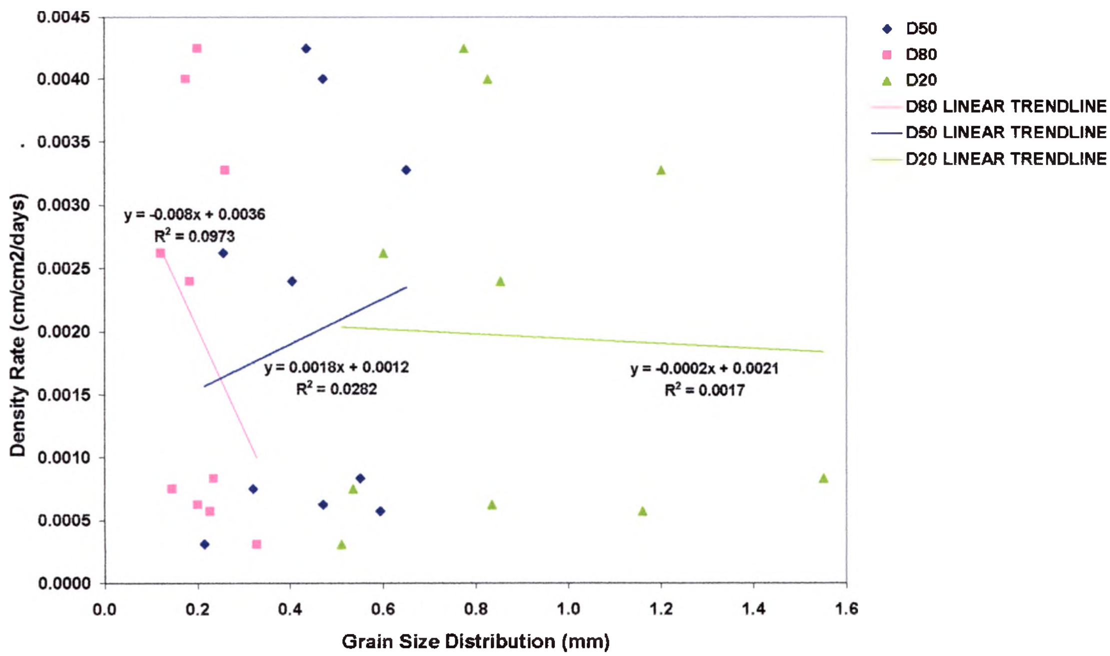

FIGURE 102. DENSITY RATE VERSUS GRAIN SIZE DISTRIBUTION IN AUGUST

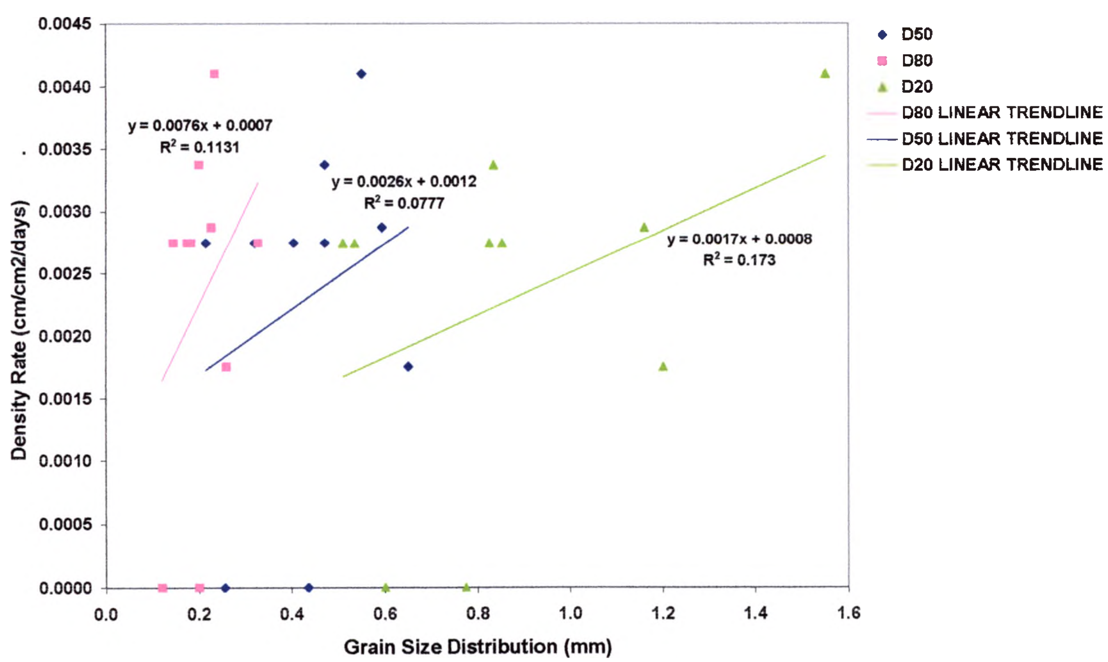

FIGURE 103. DENSITY RATE VERSUS GRAIN SIZE DISTRIBUTION IN SEPTEMBER

INFILTRATION OF WATER INTO THE SOIL

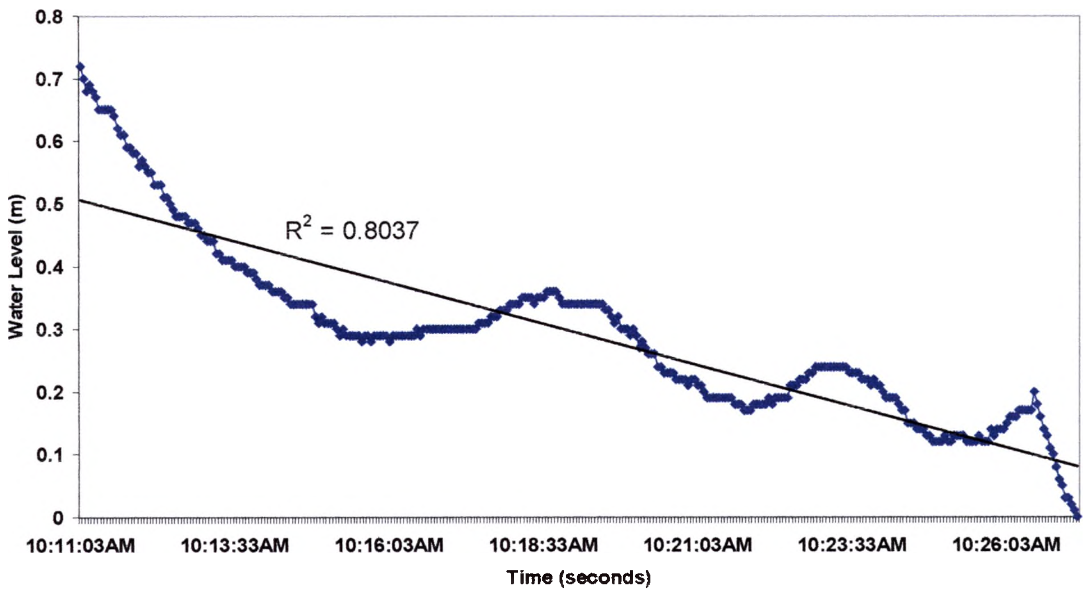

FIGURE 104. INFILTRATION OF WATER INTO THE SOIL OVER TIME

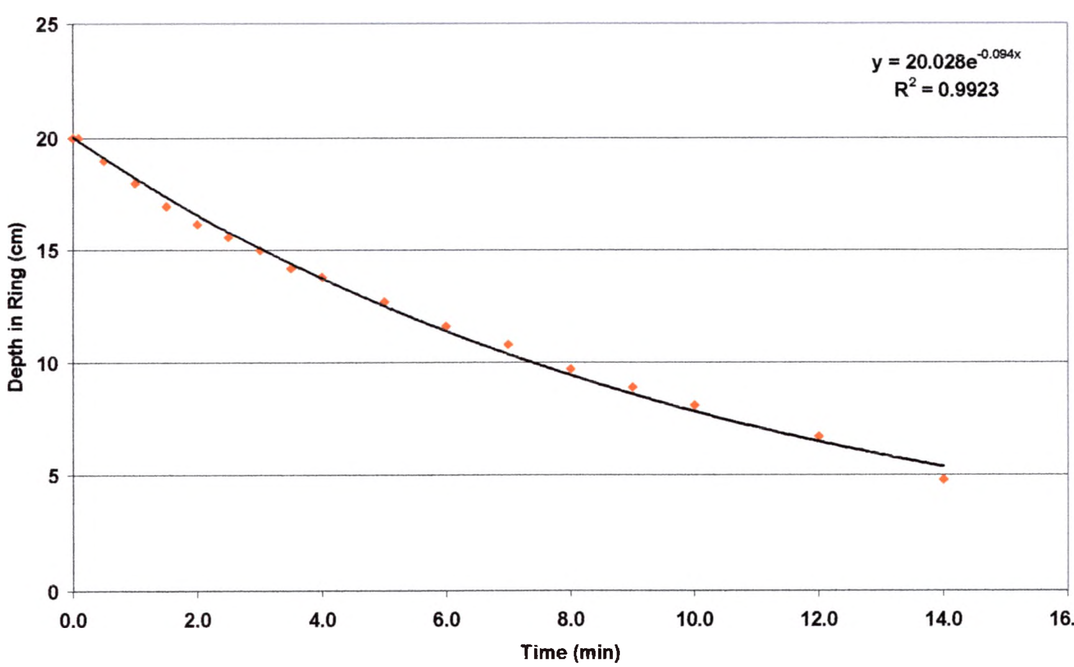

FIGURE 105. TELECOM INFILTRATION EXPERIMENT

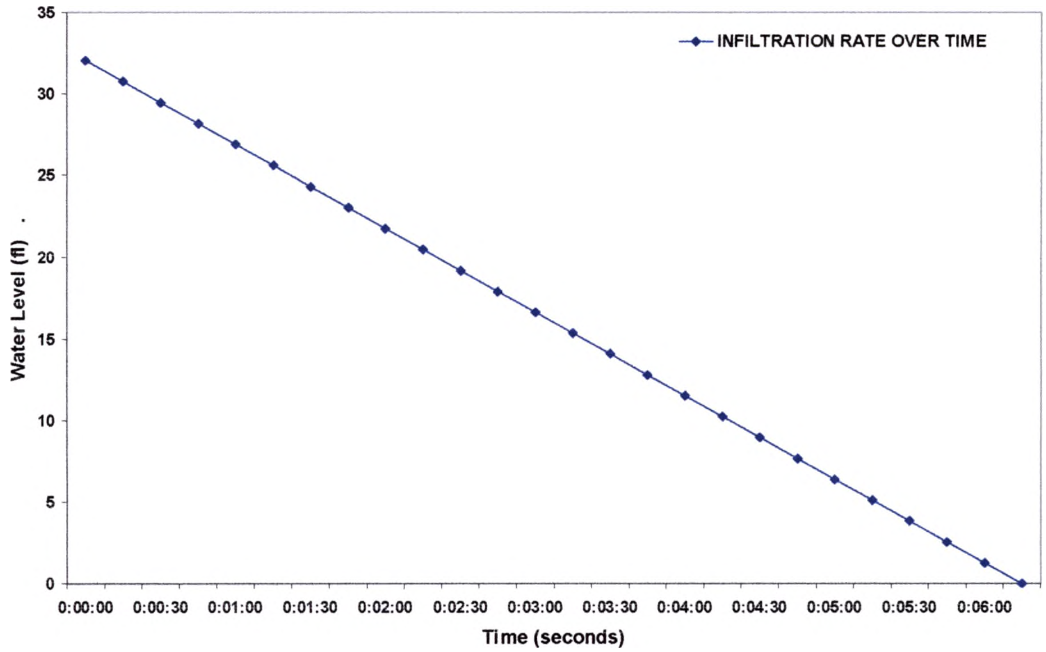

FIGURE 106. INFILTRATION RATE OVER TIME ON DECEMBER 03

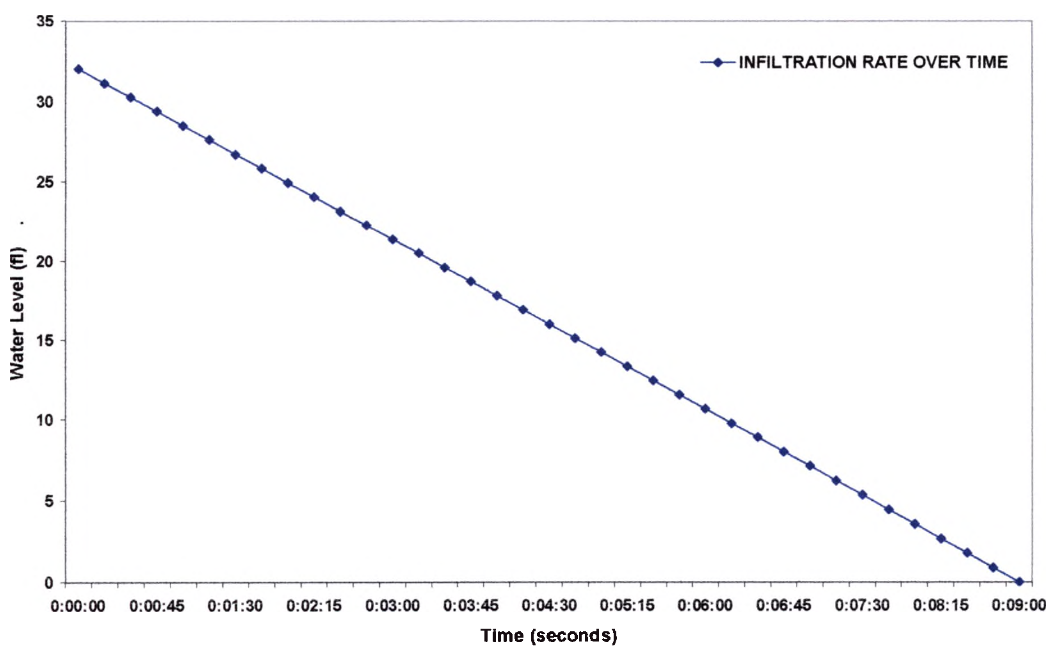

FIGURE 107. INFILTRATION RATE OVER TIME ON DECEMBER 15

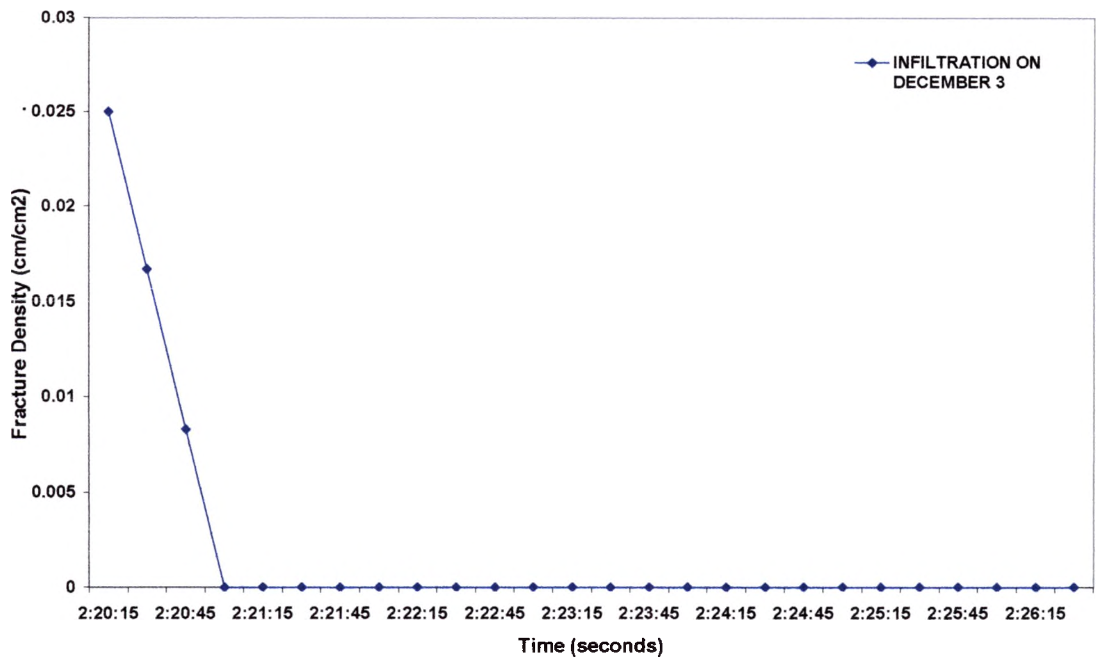

FIGURE 108. FRACTURE DENSITY VERSUS INFILTRATION TIME ON DECEMBER 3

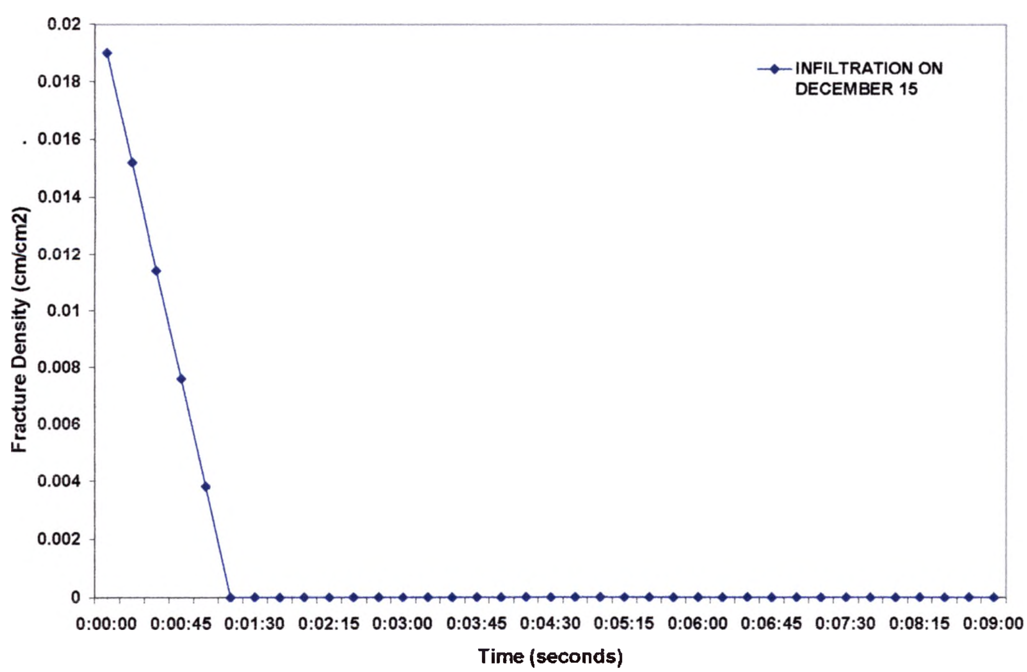

FIGURE 109. FRACTURE DENSITY VERSUS INFILTRATION TIME ON DECEMBER 15

INFILTRATION RATE VERSUS FRACTURE PROPERTIES

TABLE 5

Model Summary[b]

Model	R	R Square	Adjusted R Square	Std. Error of the Estimate	Change Statistics				
					R Square Change	F Change	df1	df2	Sig. F Change
1	996[a]	.992	984	.34873	992	124 743	3	3	.001

a. Predictors (Constant), Fracture Depth (mm), Aperture Width (cm), density of fractures

b. Dependent Variable: infiltration rate (fl oz)

TABLE 6

ANOVA[b]

Model		Sum of Squares	df	Mean Square	F	Sig.
1	Regression	45 510	3	15.170	124 743	.001[a]
	Residual	365	3	.122		
	Total	45.875	6			

a Predictors. (Constant), Fracture Depth (mm), Aperture Width (cm), density of fractures

b Dependent Variable: infiltration rate (fl oz)

TABLE 7

Coefficients[a]

Model		Unstandardized Coefficients		Standardized Coefficients			95% Confidence Interval for B		Correlations		
		B	Std Error	Beta	t	Sig.	Lower Bound	Upper Bound	Zero-order	Partial	Part
1	(Constant)	9.191	1 132		8.118	.004	5.588	12.794			
	density of fractures	-192 032	39.466	-.702	-4.866	.017	-317.630	-66.434	-.977	-.942	-.251
	Aperture Width (cm)	-3.824	3.443	-.134	-1.111	348	-14.780	7.133	-.492	-.540	- 057
	Fracture Depth (mm	-.341	.118	-.337	-2.882	.063	-.718	.036	-.712	-.857	- 148

a Dependent Variable: infiltration rate (fl oz)

CHAPTER 4

IMPLICATIONS AND CONCLUSIONS

I have spent the last year measuring fracture properties and soil characteristics in an attempt to define which independent variables control fracture density and infiltration rates the most. The following paragraphs summarize my findings, state the implications of these findings, offer future suggestions, and give my conclusions.

Summary and Implications

Gravimetric moisture content is the main variable affecting fracture densities. The graphs depicting gravimetric moisture content versus fracture density data measured in weekly installments show moderate to strong linear relationships. Figures 38 through 46 depict these data. This relationship means that a change in one variable changes the state of the other variable. The negative correlation implies that high moisture content will correspond to a low fracture density and vice versa. The gravimetric moisture content value of 0.029 is the point where fracture densities cannot sustain themselves, so they heal until the moisture content of the soil decreases. Fracture growth commences once the moisture content reaches below this value. Precipitation also has a strong influence on fracture densities. Figures 15 through 25 show that precipitation events cause a decrease or termination in fracture densities, while dry periods show an increase in the amount of fractures at each site. Temperature did not affect fracture densities significantly. Fracture density did increase slightly with increases in temperature and vice versa, but precipitation events were more effective at altering fracture densities.

Precipitation is the main variable affecting gravimetric moisture contents. Rain events were followed by increases in soil moisture while dry days created lower gravimetric moisture contents in the soil. Small discrepancies in this relationship are caused by temperature. Small changes in temperature led to modifications in the reaction to precipitation events by the moisture content of the soil. These temperature changes do not affect the strong relationship between moisture content and precipitation sufficiently to become the main motive for moisture content changes.

The implications for fracture growth are important. The length of time a plot of soil takes to reach maximum fracture density was one of the questions I set out to answer. The time it takes an area to reach maximum fracture density depends on the gravimetric moisture content of the soil. Since gravimetric moisture content is dependent on precipitation events, the number of dry days, and to some extent temperature, fracture density reaches a maximum in variable time periods. For example, site 02 went from a fracture density of zero to a maximum fracture density of $0.59cm^{-1}$ in six days. Over the same time period, a 0.227 decrease in gravimetric moisture content was observed. At the same time, no precipitation episodes were recorded during these six days, and the average temperature increased only slightly. In contrast, site 06 reached its maximum fracture density of $0.039cm^{-1}$ in twenty-one days. This time period included a moderately sized precipitation event which slowed down the decrease in gravimetric moisture content in the first seven days. Even so, fracture density increased the most in the first seven days because the average temperature increased about 4° C (7° F). These examples illustrate the complexity in answering the question of what amount of time is required for an area to reach maximum fracture density.

Increasing aperture width tends to correspond positively with increasing fracture depths. This relationship is moderate at best because of the methods of measurement. Nevertheless, water flowing into a larger aperture fracture has a greater probability of flowing through a deeper crack than water into a smaller fracture. These deeper fractures deliver the water into the subsoil faster and for longer periods, since swelling clay particles heal in smaller fractures first. This reasoning implies that infiltration into the subsoil and underlying aquifers occurs in areas composed of fractures with larger apertures. Larger apertures increase the chance for successful infiltration into underlying aquifers.

Width and depth of fractures are not the only characteristics that affect rates of infiltration. The frequency of aperture widths influences water penetration as well. The aperture distribution histograms provide clues to this analysis. All the graphs depict a log normal distribution; in other words, most aperture widths measured are small with a few large apertures in any given area. Certain sites, such as site 07 in figure 85, demonstrated a greater frequency of fractures less than 0.12 cm in width. The probability of faster infiltration through fractures increases as these higher frequency fractures are distributed over a large spread of aperture widths, such as in figure 82. The larger distribution of high frequencies enables more water to infiltrate into the subsurface at a faster rate before fracture healing occurs. Ultimately, aperture distribution histograms are another approach to measuring fracture density of a soil.

The grain size distribution has a similar pattern at all ten sites. The majority of grains are between 0.15 mm and 0.6 mm, with few grains larger or smaller that these sizes. Each site has a unique percentage of grains retained within each sieve, and some sites are uniformly composed of larger grains, such as site 02. These differences in grain sizes do not appear to correlate with fracture density growth rate, so it is concluded that this soil property is not an essential variable to consider when developing a quantitative analysis of recharge rates in smectite clay soils.

The field infiltration experiment clearly shows water infiltrating in an exponential manner. Faster infiltration occurs at the start of the experiment and slowly decreases over time. As the clay grains heal together, pathways to the subsurface begin to vanish, slowing the downward movement, and delaying recharge to the subsurface.

The laboratory experiments show fracture density decreasing to zero in the first minutes of infiltration. These results lead me to conclude that the first minutes in a precipitation event are when the infiltration through clay soils is greatest. The statistical analysis illustrated the importance of fracture density in affecting infiltration rates while downplaying fracture depth and aperture width. These results imply that clay soils with higher fracture densities will increase infiltration regardless of the widths or depths of these fractures.

Future Suggestions and Conclusions

The field work for this project took place over the spring and summer months of 2004. In the future, I believe data collected in the fall and winter months should be incorporated into this type of study. These data could change the context through which results are analyzed. For instance, seasonality might be shown as a factor in fracture growth, thus affecting infiltration rates. In addition, data was collected on a weekly basis. Data collected on a daily basis or even twice daily will give more information about the changes in fracture density over time. Such data could increase the accuracy in measuring changes in soil moisture contents.

Fracture depth should be measured by a variety of different methods. I was unable to create a mold of the fracture network at depth, but I believe this idea holds promise for future studies. This mold can be created either by a cement mixture, as I proposed, or by filling the fractures with small glass beads. These beads will not compact the soil as much as they descend, unlike cement, since they are less dense than the cement. Once they are bonded together by epoxy, the mold can be brought to the surface. Another viable method for measuring fracture depth is by using light refracting technology. A light could be directed into the fracture and once the delay in time that this light refracts upward is calculated, the depth of the fracture can be accurately measured. Although this method is not very accurate if the fractures are convoluted, it can give some information about fracture depth.

Another area that I would like to see different methods used is with the infiltration experiments. It would be advantageous to have field tests conducted with a pressure transducer and data logger at different sites under different soil conditions. Such a set-up could illustrate how slight changes in fracture densities and soil moisture contents change the infiltration rate. From such an analysis, it would be possible to find the optimal fracture properties and soil conditions to maximize infiltration in smectite clays.

I believe more can be accomplished in the infiltration lab experiments as well. These experiments might provide more information on differences in infiltration rates if performed under a variety of soil moisture content values. Also, differences in the light source used to dry the soil might change the length of time the soil takes to reach maximum fracture density.

I would also like to perform this study at a site with a different grain structure in conjunction with the site used in this study. For example, a site with thin clay soil layers underlain by layers of limestone is likely to supply different results from a site with a sand and clay mixture. I would like to see how diverse these results would be and how these changes affect infiltration.

Recharge into an aquifer has historically been a difficult variable to calculate. Many parameters control recharge into the soil. This study focused on fracture properties and the soil characteristics of smectite clay soils and how these variables influence infiltration into the subsurface. Gravimetric moisture content and precipitation have the most control over changes in fracture density. Without a change in these two variables, fracture density would remain constant indefinitely. These changes in density, in turn, control infiltration rates. Smectite clay soils with greater fracture density have faster infiltration into the soil than areas with lower density. Groundwater modelers should incorporate these findings into their calculations in order to achieve the most accurate results possible.

BIBLIOGRAPHY

Adams, John E., and R. J. Hanks. 1964. Evaporation from soil shrinkage cracks. *Soil Science Society of America Proceedings*. pp. 281-84.

Baer, J. U., and S. H. Anderson. 1997. Landscape effects on desiccation cracking in an aqualf. *Soil Science Society of America Journal* 61: 1497-502.

Beven, K. and P. Germann. 1982. Macropores and water flow in soils. *Water Resource Research* 18, no. 5: 1311-25.

Blake, G., E. Schlichting, and U. Zimmermann. 1973. Water recharge in a soil with shrinkage cracks. *Soil Science Society of America Proceedings* 37: 669-72.

Bouma, J., and L. W. Dekker. 1978. A case study on infiltration into dry clay soil I. Morphological observations. *Geoderma* 20: 27-40.

Bouma, J., and P. J. M. de Laat. 1981. Estimation of the moisture supply capacity of some swelling soils in the Netherlands. *Journal of Hydrology* 49, no. 3-4: 247-59.

Bouma J., A. Jongerius, O. Boersma, A. Jager, and D. Schoonderbeek. 1977. The function of different types of macropores during saturated flow through four swelling soil horizons. *Soil Science Society of America Journal* 41: 945-50.

Bouma J., A. Jongerius, and D. Schoonderbeek. 1979. Calculation of saturated hydraulic conductivity of some pedal clay soils using micromorphometric data. *Soil Science Society of America Journal* 43: 261-64.

Bouma, J., and J. H. M. Wösten. 1979. Flow patterns during extended saturated flow in two, undisturbed swelling clay soils with different macrostructures. *Soil Science*

Society of America Journal 43: 16-22.

Bronswijk, J. J. B. 1988. Modeling of water balance, cracking and subsidence of clay soils. *Journal of Hydrology* 97: 199-212.

_______. 1991. Relation between vertical soil movements and water-content changes in cracking clays. *Soil Science Society of America Journal* 55: 1220-26.

Brown, S. R. 1987. Fluid flow through rock joints: The effect of surface roughness. *Journal of Geophysical Research* 92, no. B2: 1337-47.

Brush, David J., and Thomson, Neil R. 2003. Fluid flow in synthetic rough-walled fractures: Navier-Stokes, Stokes, and local cubic law simulations. *Water Resources Research* 39, no. 4: SBH5-1-15.

Chertkov, V. Y., and Ravina, I. 2001. Effect of interaggregate capillary cracks on the hydraulic conductivity of swelling clay soil. *Water Resources Research* 37, no. 5: 1245-53.

Choi, J. W., and D. W. Oscarson. 1996. Diffusive transport through compacted Na- and Ca-bentonite. *Journal of Contaminant Hydrology* 22: 189-202.

Compton, Robert. 1985. *Geology in the field.* New York: John Wiley and Sons, Inc.

D'Astous, A. Y., W. W. Ruland, J. R. G. Bruce, J. A. Cherry, and R. W. Gillham. 1989. Fracture effects in the shallow groundwater zones in weathered Sarnia-area clay. *Canadian Geotechnical Journal* 26: 43-56.

Dutt, G. R., and P. F. Low. 1962. Relationship between the activation energies for deuterium oxide diffusion and exchangeable ion conductance in clay systems. *Soil Science* 93: 195-203.

Fenneman, Nevin M. 1938. *Physiography of the eastern United States.* New York:

McGraw-Hill.

Haines, W. G. 1923. The volume changes associated with variations of water content in soil. *Journal of Agricultural Science* 13, no. 4: 296-311.

Hardy, David, Deanna Osmond, and Richard Reich. 2003. *Soil facts: Deep soil sampling for nutrient management*. Raleigh, NC: North Carolina State University Extension Service. Available from http://www.soil.ncsu.edu/publications /Soilfacts/AGW-439-40/deepsoil_1003.pdf; Internet; accessed 5 March 2004.

Harrison, B., E. A. Sudicky, and J. A. Cherry. 1992. Numerical Analysis of solute migration through fractured clayey deposits into underlying aquifers. *Water Resources Research* 28, no. 2: 515-26.

Holmes, J. W., E. L. Greacen, and C. G. Gurr. 1960. The evaporation of water from bare soils with different tilths. *Transactions of the International Congress of Soil Science 7th Madison* 1: 188-94.

Hoogmoed, W. B., and J. Bouma. 1980. A simulation model for predicting infiltration into cracked clay soil. *Soil Science Society of America Journal* 44: 458-61.

Jamison, V. C., and G. A. Thompson. 1967. Layer thickness changes in a clay-rich soil in relation to soil water content changes. *Soil Science Society of America Proceedings* 31, no. 4: 441-44.

Johnston, J. R., and H. O. Hill. 1945. A study of the shrinking and swelling properties of Rendzina soils. *Soil Science Society of America Proceedings* 9: 24-29.

Kachigan, Sam. 1991. *Multivariate statistical analysis*. New York: Radius Press.

Keen, B. A. 1931. *The Physical properties of the soil*. London: Longmans, Green, and

Co.

Kloprogge, J. T., S. Komarneni, and J. E. Amonette. 1999. Synthesis of smectite clay minerals: A critical review. *Clays and Clay Minerals* 47, no. 5: 529-54.

Lamont-Doherty Earth Observatory. 2003. *Darcy's Law*. New York, NY: Columbia University. Available from http://www.ldeo.columbia.edu/; Internet; Accessed October 14, 2004.

Mason, D. D., J. F. Lutz, and R. G. Petersen. 1957. Hydraulic conductivity as related to certain soil properties in a number of Great Soil Groups-sampling errors involved. *Soil Science Society of America Proceedings* 21: 554-60.

Mauch, James E., and Jack W. Birch. 1983. *Guide to the successful thesis and dissertation, conception to publication: A handbook for students and faculty*. New York: Marcel Dekker, Inc.

McKay, L. D., J. A. Cherry, and R. W. Gillham. 1993. Field experiments in a fractured clay till. 1. Hydraulic conductivity and fracture aperture. *Water Resources Research* 29, no. 4: 1149-62.

McMahon, C. A., Fry, R. G., and Brown, K. L. 1984. *The vegetation types of Texas*. Austin, TX: Texas Parks and Wildlife Department.

Mesri, G., and R. E. Olson. 1971. Mechanisms controlling the permeability of clays. *Clays and Clay Minerals* 19: 151-58.

Morari, F., and W. G. Knisel. 1997. Modifications of the GLEAMS model for crack flow. *American Society of Agricultural Engineers* 40, no. 5: 1337-48.

Oostindie, K., and J. J. B. Bronswijk. 1995. Consequences of preferential flow in cracking clay soils for contamination-risk of shallow aquifers. *Journal of*

Environmental Management. 43: 359-73.

Oron, Assaf P., and Berkowitz. 1998. Flow in rock fractures: The local cubic law assumption reexamined. *Water Resources Research* 34, no. 11: 2811-2825.

Oscarson, D. W. 1994. Surface diffusion: Is it an important transport mechanism in compacted clays? *Clays and Clay Minerals* 42, no. 5: 534-43.

Pyrczak, Fred, and Randall R. Bruce. 1998. *Writing empirical research reports.* 2d ed. Los Angeles: Pyrczak Publishing.

Renard, F., D. Dysthe, J. Feder, B. Jamtveit, T. Jøssang and P. Meakin. 2004. *Experimental study of the dynamics of crack healing.* [on-line]. Oslo, Norway: University of Oslo; available from http://www.fys.uio.no/faststoff/sup/Meetings/AbsKongsberg00/; Internet. Accessed 9 February 2004.

Reynolds, W. D., B. T. Bowman, R. R. Brunke, C. F. Drury, and C. S. Tan. 2000. Comparison of tension infiltrometer, pressure infiltrometer, and soil core estimates of saturated hydraulic conductivity. *Soil Science Society of America Journal* 64: 478-84.

Ritchie, J. T., D. E. Kissel, and Earl Burnett. 1972. Water movement in undisturbed swelling clay soil. *Soil Science Society of America Proceedings* 36, no. 6: 874-79.

Rosenberg, Matt. 2005. *Koppen Climate Map.* [on-line]. Available from http://geography.about.com/library/weekly/aa011700a.htm; Internet. Accessed March 30, 2005.

Rudestan, Kjell Erik, and Rae R. Newton. 1992. *Surviving your dissertation.* Newbury Park, CA: Sage Publications, Inc.

Rudolph, D. L., J. A. Cherry, and R. N. Farvolden. 1991. Groundwater flow and solute transport in fractured lacrustrine clay near Mexico City. *Water Resource Research* 27, no. 9: 2187-202.

Ruland, W. W., J. A. Cherry, and S. Feenstra. 1991. The depth of active ground-water flow in a clayey till plain in southwestern Ontario. *Ground Water* 29, no. 3: 405-17.

Salkind, Neil J. 2000. *Statistics for people who (think they) hate statistics.* Thousand Oaks, CA: Sage Publications, Inc.

Shainberg, I., N. Alperovitch, and R. Keren. 1988. Effect of magnesium on the hydraulic conductivity of Na-smectite-sand mixtures. *Clays and Clay Minerals* 36: 432-38.

Snow, David T. 1969. Anisotropic permeability of fractured media. *Water Resources Research* 5, no. 6: 1273-89.

Soil Conservation Service. 1974. *Soil Survey of Travis County, Texas.* Washington, D. C.: United States Department of Agriculture.

Stirk, G. B. 1954. Some aspects of soil shrinkage and the effect of cracking upon water entry into the soil. *Australian Journal of Agricultural Research* 5, no. 3: 279-90.

Texas Department of Transportation. 1996. Travis County Texas (County Number 227, Supplementary Sheet 5355), in *Texas Department of Transportation: Texas County Highway Maps* [on-line database] (Austin, TX: University of Texas, 1999, accessed 5 January 2005); available from http://txdot.lib.utexas.edu/select.html?urn=urn:utlol:txdot.tctravd3; Internet.

Tsang, Y. W. 1984. The effect of tortuosity on fluid flow through a single fracture. *Water Resource Research* 20, no. 9: 1209-15.

US National Climate Data Center. 2004. *Record of Climatological Observations*. [on-line]; available from http://www.ncdc.noaa.gov/oa/ncdc.html; Internet. Accessed 23 November 2004.

van Schaik, J. C., W. D. Kemper, and S. R. Olsen. 1966. Contribution of absorbed cations to diffusion in clay-water systems. *Soil Science Society of America Proceedings* 30: 17-22.

van Schilfgaarde. 1970. Theory of flow to drains. In *Advanced Hydroscience*, ed. V. T. Chow, 43-106. New York: Academic Press.

Vance, David. 2002. *Anisotropic Hydrology-Part 1 Fracture Flow Systems* [on-line]. Available from http://2the4.net/anisofrac.htm; Internet. Accessed 9 February 2004.

Young, Keith. 1977. *Guidebook to the Geology of Travis County* [on-line]. Austin, Texas: University of Texas at Austin; Available from http://www.utexas.edu/ftp/student/geo/ggtc/ch2.html; Internet. Accessed 14 October 2004.

Yule, D. F., and J. T. Ritchie. 1980. Soil shrinkage relationships of Texas vertisols. I: Small cores. *Soil Science Society of America Journal* 44, no. 6: 1285-91.

Zhou, W. 2001. Numerical simulation of two-phase flow in conceptualized fractures. *Environmental Geology* 40: 797-808.

VITA

Miriam Akselrod Scoulios was born in Houston, Texas, on December 7, 1974, the daughter of Gustave and Ursula Akselrod. After completing her work at Memorial High School, Houston, Texas, in 1993, she entered Northland College in Ashland, Wisconsin. After two years, she transferred to the University of Texas at Austin. During this period, she worked at the Texas Memorial Museum's Nonvertebrate Paleontology Laboratory as an assistant conservationist. She received the degree of Bachelor of Science in Geological Sciences from the University of Texas at Austin in 2001. During the following years she was employed as a geophysicist at Schlumberger/WesternGeco in Houston, Texas. In August 2003, she entered the Graduate College of Texas State University-San Marcos.

Permanent Address: 3807 Key Hollow Way
Spring, Texas 77388

This thesis was typed by Miriam Akselrod Scoulios